

INFORMATION TO USERS

This dissertation was produced from a microfilm copy of the original document. While the most advanced technological means to photograph and reproduce this document have been used, the quality is heavily dependent upon the quality of the original submitted.

The following explanation of techniques is provided to help you understand markings or patterns which may appear on this reproduction.

1. The sign or "target" for pages apparently lacking from the document photographed is "Missing Page(s)". If it was possible to obtain the missing page(s) or section, they are spliced into the film along with adjacent pages. This may have necessitated cutting thru an image and duplicating adjacent pages to insure you complete continuity.
2. When an image on the film is obliterated with a large round black mark, it is an indication that the photographer suspected that the copy may have moved during exposure and thus cause a blurred image. You will find a good image of the page in the adjacent frame.
3. When a map, drawing or chart, etc., was part of the material being photographed the photographer followed a definite method in "sectioning" the material. It is customary to begin photoing at the upper left hand corner of a large sheet and to continue photoing from left to right in equal sections with a small overlap. If necessary, sectioning is continued again — beginning below the first row and continuing on until complete.
4. The majority of users indicate that the textual content is of greatest value, however, a somewhat higher quality reproduction could be made from "photographs" if essential to the understanding of the dissertation. Silver prints of "photographs" may be ordered at additional charge by writing the Order Department, giving the catalog number, title, author and specific pages you wish reproduced.

University Microfilms

300 North Zeeb Road
Ann Arbor, Michigan 48106

A Xerox Education Company

72-26,461

PATEL, Chandrakant, 1945-
ASYMMETRIC STEADY STATES IN CATALYST PARTICLES.

Rice University, Ph.D., 1972
Engineering, chemical

University Microfilms, A XEROX Company, Ann Arbor, Michigan

RICE UNIVERSITY

Asymmetric Steady States in Catalyst Particles


by

Chandrakant Patel

A THESIS SUBMITTED
IN PARTIAL FULFILLMENT OF THE
REQUIREMENTS FOR THE DEGREE OF

Doctor of Philosophy in Chemical Engineering

Thesis Director's Signature

_____

Houston, Texas

April, 1972

PLEASE NOTE:

Some pages may have
indistinct print.

Filmed as received.

University Microfilms, A Xerox Education Company

ACKNOWLEDGMENTS

It is with the most sincere appreciation and gratitude that I acknowledge the support and assistance of the following individuals and organizations:

My mother, brothers and sisters, for their confidence, support and encouragement throughout my studies;

My advisor, Professor Roy Jackson: I feel most fortunate in having had the opportunity of close association with such an exceptional researcher, teacher, and scholar;

Dr. Larry V. McIntire and Dr. Jerome D. Wiest for serving on the oral examination committee;

Miss Molly Pessarra for typing this manuscript in her usual flawless manner and for her constant goading;

Mr. Al Selmo for the use of his drafting equipment;

The National Science Foundation (Grant No. GK12522) for financial support and for research funds; and

Rice University for financial support.

TABLE OF CONTENTS

	Page Number
TITLE PAGE.....	i
ACKNOWLEDGMENTS.....	ii
TABLE OF CONTENTS.....	iii
 I. INTRODUCTION.....	 1
A. Symmetric Steady States.....	1
B. Asymmetric Steady States.....	4
 II. SOLUTIONS NOT INVARIANT UNDER LATERAL TRANSLATIONS.....	 8
A. Mathematical Formulation of the Problem.	8
B. Steady State Analysis.....	10
C. Stability of Steady States.....	29
 III. SOLUTIONS NOT INVARIANT UNDER REFLECTION....	 38
A. Mathematical Description of the Problem.	38
B. Steady State Analysis.....	40
C. Solution Procedure.....	42
D. Numerical Results and Discussion.....	47
 IV. STABILITY ANALYSIS FOR STEADY STATES ASYMMETRIC WITH RESPECT TO REFLECTION ACROSS THE CENTER PLANE.....	 66
A. Introduction.....	66

TABLE OF CONTENTS (Continued)

	Page Number
B. Method of Nishimura and Matsubara.....	67
C. Continuous Time Galerkin Approximation to Linearized Perturbation Equations....	72
D. Numerical Considerations and Results....	82
V. CONCLUSIONS.....	114
NOMENCLATURE.....	117
REFERENCES.....	124
APPENDIX I.....	127
APPENDIX II.....	137

I. INTRODUCTION

It is well known that catalyst pellets in a uniform environment can exhibit multiple steady states for particular combinations of kinetic, thermodynamic, and transport parameters. The desirability or otherwise of the multiple steady states depends on the circumstances and so the questions of predicting conditions under which uniqueness can be guaranteed and of the stability of the steady states have to be considered. In recent years extensive work has been carried out in these directions and several significant results have been obtained.

A. Symmetric Steady States

In an early paper, Weisz and Hicks⁴⁶ treated the case of a non-isothermal particle and discovered regions of three steady states at higher activation energies. Roberts and Satterfield⁴³ demonstrated the existence of three steady states in isothermal systems and for reactions with more than one reactant for kinetic expressions of the Langmuir-Hinshelwood type. Other workers (Hlavacek, Marek, and Kubicek,²¹ Kuo and Amundson,²⁸ Bischoff,⁵ McGreavy and Cresswell,³⁶ and Cresswell¹⁰) have analysed different geometrical shapes---slabs, cylinders, and spheres. Usually zero, first, or second order irreversible reactions were considered. Models with Newtonian resistances to heat and

mass at the catalyst faces together with diffusive resistances to heat and mass flux in the interior have also been treated, and a complete parametric study of first order reaction in an infinite slab with zero Newtonian surface resistance was performed by Drott and Aris.¹³ Five steady states were found for zero order kinetics in a spherical particle by Hlavacek and Marek,²⁰ and by Hatfield and Aris¹⁸ for a single first order exothermic reaction in an infinite slab with Newtonian boundary resistances. Computations have been reported by Copelowitz and Aris⁸ that show as many as seventeen steady states for a single first order reaction in a sphere. Many of these steady states are so close to one another as to be virtually indistinguishable in practice, but the theoretical implications are of interest in terms of what might be developed for more complex problems.

Using fixed point theory of integral operators, Gavalas¹⁶ proved that the steady state is unique when the particle shrinks to sufficiently small dimensions, and developed a procedure for estimating bounds on the particle size below which uniqueness can be guaranteed in specific cases. Luss and Amundson,³³ who considered catalyst particles of arbitrary shape with zero heat and mass transfer resistances between the particle and its environment, obtained similar uniqueness criteria using spectral theorems of Sturm-Liouville theory. The sufficient conditions for uniqueness were further sharpened by Luss.³¹ Close agreement was shown

when his predicted bounds were compared with direct numerical solutions. Recently, Jackson²⁴ using only elementary mathematical results, obtained uniqueness conditions for the steady states of a catalyst slab when there are non-negligible heat and mass transfer resistances at the boundaries. Jackson also speculates that sufficient conditions for the existence of unique solutions are sufficient for the non-existence of asymmetric solutions.

The lack of a systematic means to determine stability of systems described by non self-adjoint partial differential equations has meant that many important stability problems of the reacting catalyst remain unsolved. Amundson and Raymond² examined cases with zero and non-zero mass and heat resistances concentrated at the boundaries, and investigated stability by linearized perturbation analysis. By the use of oscillation theorems of Sturm theory (see Ince²³), Amundson¹ devised necessary and sufficient conditions for the stability of an empty tubular reactor with axial mixing. This condition is very useful since it does not require the direct calculation of eigenvalues of the eigenvalue problem related to the linearized system, but only the solution of a linear differential equation. Subsequently, Kuo and Amundson²⁸ considered the catalyst particle problem. By using Amundson's necessary and sufficient condition, they derived sufficient conditions for stability which avoids the analysis of a complicated non self-adjoint eigenvalue

problem. The Galerkin method was used for estimating the extreme eigenvalue and for a specific problem with three steady states, they showed that the upper and lower states were stable and the middle one unstable. Stability analysis via Lyapunov functionals was used by Wei⁴⁵ for a somewhat simpler model of a catalyst pellet. Berger and Lapidus,⁴ also using Lyapunov functionals, devised sufficient conditions for the stability of steady states of catalyst particles and empty adiabatic tubular reactors. Using the maximum principle for parabolic equations and topological concepts, Luss and Amundson³² devised sufficient conditions for the stability of the empty tubular reactor. The methods used are also applicable to catalyst pellets. For the case considered they showed that steady states alternate, stable and unstable. Luss and Lee³⁴ considered only perturbations which satisfied the "adiabatic" conditions, and performed transient calculations for unit Lewis number. In a subsequent paper,³⁰ they extended their work to non-unit Lewis numbers. Using Lyapunov's direct method, Nishimura and Matsubara³⁹ extended Amundson's necessary and sufficient conditions for stability in self-adjoint problems to provide a sufficient stability condition for non self-adjoint problems.

B. Asymmetric Steady States

In all the discussions of chemical reactions accompanied by heat conduction and diffusion in catalyst

particles, it has been tacitly assumed that the solutions must be invariant under the symmetry operations of the differential equations and boundary conditions describing the system; for example, it is universally assumed that the solutions in spherical catalyst particles with uniform boundary conditions are spherically symmetric. In general, this assumption is only justifiable if the solution is unique. It is certainly true that any solution satisfying the differential equations and boundary conditions must transform into another such solution under a symmetry operation of the particle, but it cannot be concluded that the transformed solution is identical with the original solution unless it is known that there is just one solution, and indeed the existence of asymmetric steady states in catalyst particles has recently been demonstrated,^{41,40,22} indicating that the already extensive literature has only uncovered a fraction of all possible steady states.

In the particular case of a nonporous catalytic heat conducting material with Newtonian resistances to heat and mass transfer at the boundaries, Pis'men and Kharkats⁴¹ demonstrated the existence of solutions unsymmetric with respect to reflection across the center plane. They also showed, by a stability analysis based on the linearized conservation equations, that some of these asymmetric states are stable. Similar asymmetric states were found by Horn et al.²² who considered an infinite porous catalyst

slab of finite thickness, again with Newtonian resistances at the boundaries. Horn and Jackson²⁶ made a theoretical study of this problem and derived conditions which must be satisfied by the boundary heat and mass transfer coefficients, the effective thermal conductivity, the diffusion coefficient in the slab, and the heat of reaction, if asymmetric solutions are to occur.

Both Pis'men and Kharkats⁴¹ and Horn et al.²² also discussed the possibility of standing wave solutions in a catalytic wire surrounded by fluid of uniform composition and temperature. Both groups suggested that this type of asymmetric state is unstable, and this has been confirmed by Erwin and Luss,¹⁴ using topological results, and recently by Jackson,²⁵ using Amundson's criterion.¹

Recently Bailey³ has shown that asymmetric steady states can be constructed in a slab with non-uniform (though symmetric) catalyst activity when multiple steady states exist in a uniform slab. However, a complete analysis of asymmetric states in a porous catalyst, comparable with the well known analyses of symmetric states, has not hitherto been carried out.

In this work two examples of asymmetric solutions in a symmetric system will be presented. For simplicity, consideration will be restricted to the infinite slab type of geometry, for which the symmetry operations are lateral translation parallel to the slab faces, and reflection

across the central plane.

For algebraic simplicity, the discussion in Chapter II will be directed to consideration of a situation in which the catalyst slab is very thin and lateral variations may occur in only one direction. Stability of the steady states is investigated by the use of Amundson's necessary and sufficient conditions.¹ The complete set of steady states, asymmetric with respect to reflection symmetry, for an infinite slab geometry in a uniform environment, with Newtonian resistances at the boundaries and a single exothermic reaction, will be presented in Chapter III. It is there shown that the asymmetric solutions contribute new branches to the familiar Thiele-Modulus effectiveness factor plot, and these branches are completely mapped for a particular example. In the subsequent chapter, stability is analysed by the sufficient condition of Nishimura and Matsubara,³⁹ and by the analysis of the linearized perturbation equations. The parabolic system of equations is solved by the Galerkin method using Hermite cubics as basis functions.

II. SOLUTIONS NOT INVARIANT UNDER LATERAL TRANSLATIONS

A. Mathematical Formulation of the Problem

The system considered is a long thin wire, impermeable to diffusion of reactants and products but with finite thermal conductivity, and with resistances to heat and mass transfer concentrated at its boundary. A single exothermic reaction with Arrhenius temperature dependence is considered. The wire is thin enough that its temperature may be assumed uniform in a cross section, but heat conduction in the longitudinal direction is taken into account. It is surrounded by fluid at uniform temperature T_b , with a uniform concentration c_b of reactant. Then the reactant concentration and temperature satisfy the equations

$$\alpha(c_b - c) = ck_o e^{-E/RT} \quad (2.1)$$

$$C \frac{\partial T}{\partial t} = \kappa S \frac{\partial^2 T}{\partial x^2} + \mu(T_b - T) + cQk_o e^{-E/RT} \quad x \in \Omega \quad (2.2)$$

where c is the bulk concentration of reactant which would be in equilibrium with the adsorbed reactant, T is the absolute temperature, α and μ are mass and heat transfer coefficients per unit length of wire, C is the heat capacity per unit length, Q is the magnitude of the heat of reaction

(considered positive for exothermic reactions), κS is the product of thermal conductivity and cross-sectional area and Ω is the x -interval occupied by the wire. Equations (2.1) and (2.2) are subject to the following boundary conditions

$$k \frac{\partial T}{\partial x} = b(T - T_b) \quad x = x_0 \quad (2.3)$$

$$k \frac{\partial T}{\partial x} = -b(T - T_b) \quad x = x_1 \quad (2.4)$$

where b is the heat transfer coefficient at the boundary and x_0 and x_1 ($x_1 > x_0$) are the terminal points of Ω .

Introducing the following dimensionless variables

$$\theta = \frac{T\mu}{\alpha Q c_b}, \quad s = x \sqrt{\frac{\mu}{\kappa S}}, \quad A = k_0/\alpha, \quad \epsilon = \frac{E\mu}{R\alpha Q c_b},$$

$$B = \frac{b}{\sqrt{k\mu}}, \quad \text{and} \quad \tau = \frac{\mu t}{c}, \quad \text{and eliminating } c \text{ between}$$

(2.1) and (2.2) gives

$$\frac{\partial \theta}{\partial \tau} = \frac{\partial^2 \theta}{\partial s^2} - F(\theta) \quad (2.5)$$

with boundary conditions

$$\frac{\partial \theta}{\partial s} = B(\theta - \theta_b) \text{ at } s = s_0 \quad (2.6)$$

$$\frac{\partial \theta}{\partial s} = -B(\theta - \theta_b) \quad \text{at } s = s_1 \quad (2.7)$$

$$\text{where } F(\theta) = \theta - \theta_b - \frac{Ae^{-\epsilon/\theta}}{1 + Ae^{-\epsilon/\theta}} \quad (2.8)$$

B. Steady State Analysis

The steady states $\bar{\theta}(s)$ are obtained by setting the left-hand side of Equation (2.5) equal to zero. The equations thus obtained can be reduced to a pair of first order equations

$$\frac{d\bar{\theta}}{ds} = \phi \quad (2.9)$$

$$\frac{d\phi}{ds} = F(\bar{\theta}) \quad (2.10)$$

The form of $F(\bar{\theta})$ depends on the relative values of A , θ_b , and ϵ . The equation $F(\bar{\theta}) = 0$ can have either one, two, or three roots. Of these the most interesting case is the one where three roots exist. Clearly the existence of two roots is just a limiting case of this one. In this work, two sets of values of the parameters A , θ_b , and ϵ are considered. These are (a) $\theta_b = 0.19$; $A = 2.86 \times 10^4$, and $\epsilon = 6.6$; and (b) $\theta_b = 0.19$, $A = 2.86 \times 10^4$, and $\epsilon = 7.2$. For both these sets, $F(\bar{\theta}) = 0$ has three roots which are denoted by θ_1 , θ_2 , and θ_3 . The corresponding shapes of $F(\bar{\theta})$ are shown in Figures 1 and 2, respectively. The area under the curve between θ_2 and θ_3 is larger in magnitude than

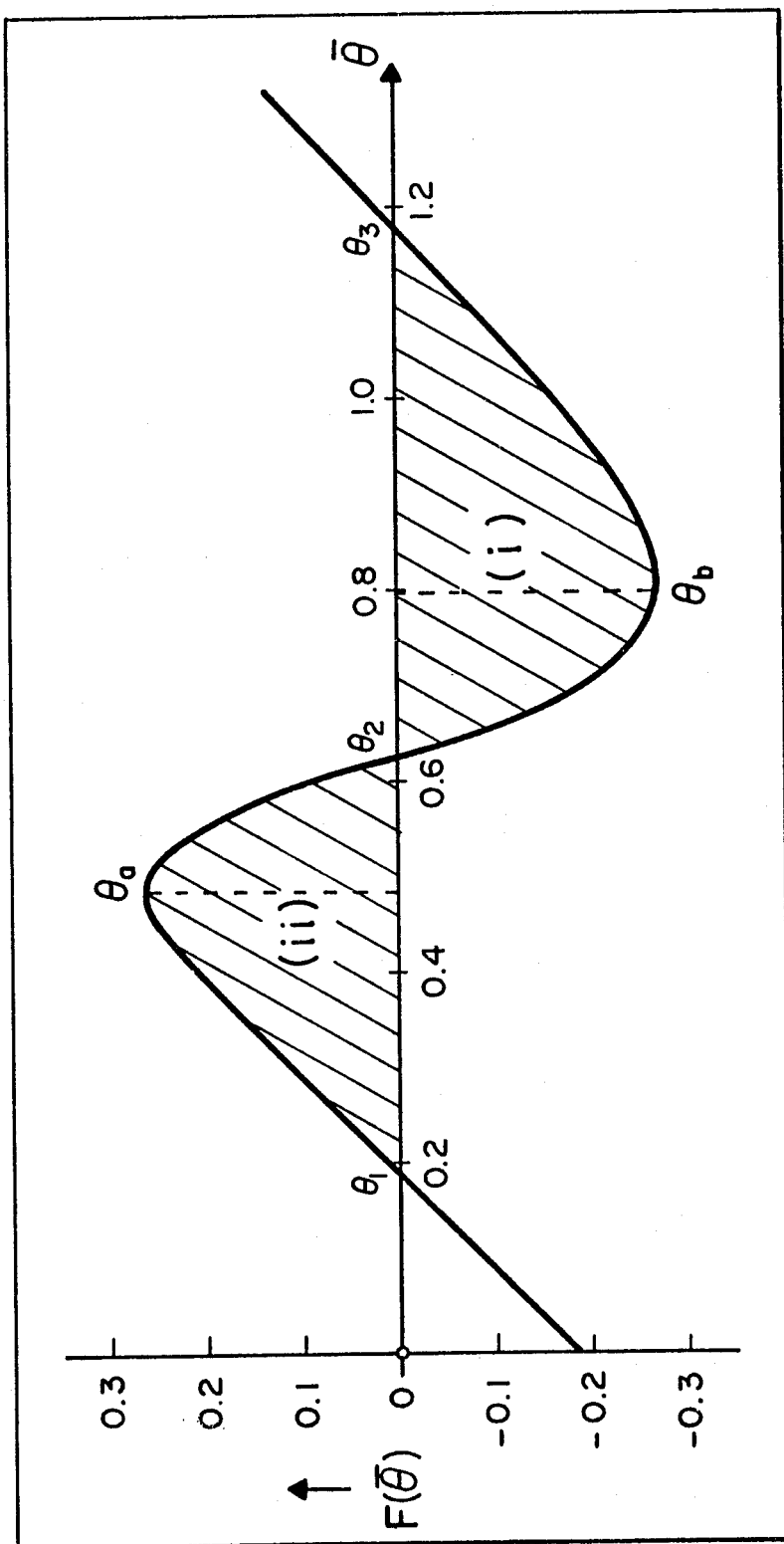


FIGURE 1: Form of the function $F(\bar{\theta})$ for $\theta_b = 0.19$, $A = 2.86 \times 10^4$ and $\epsilon = 6.6$

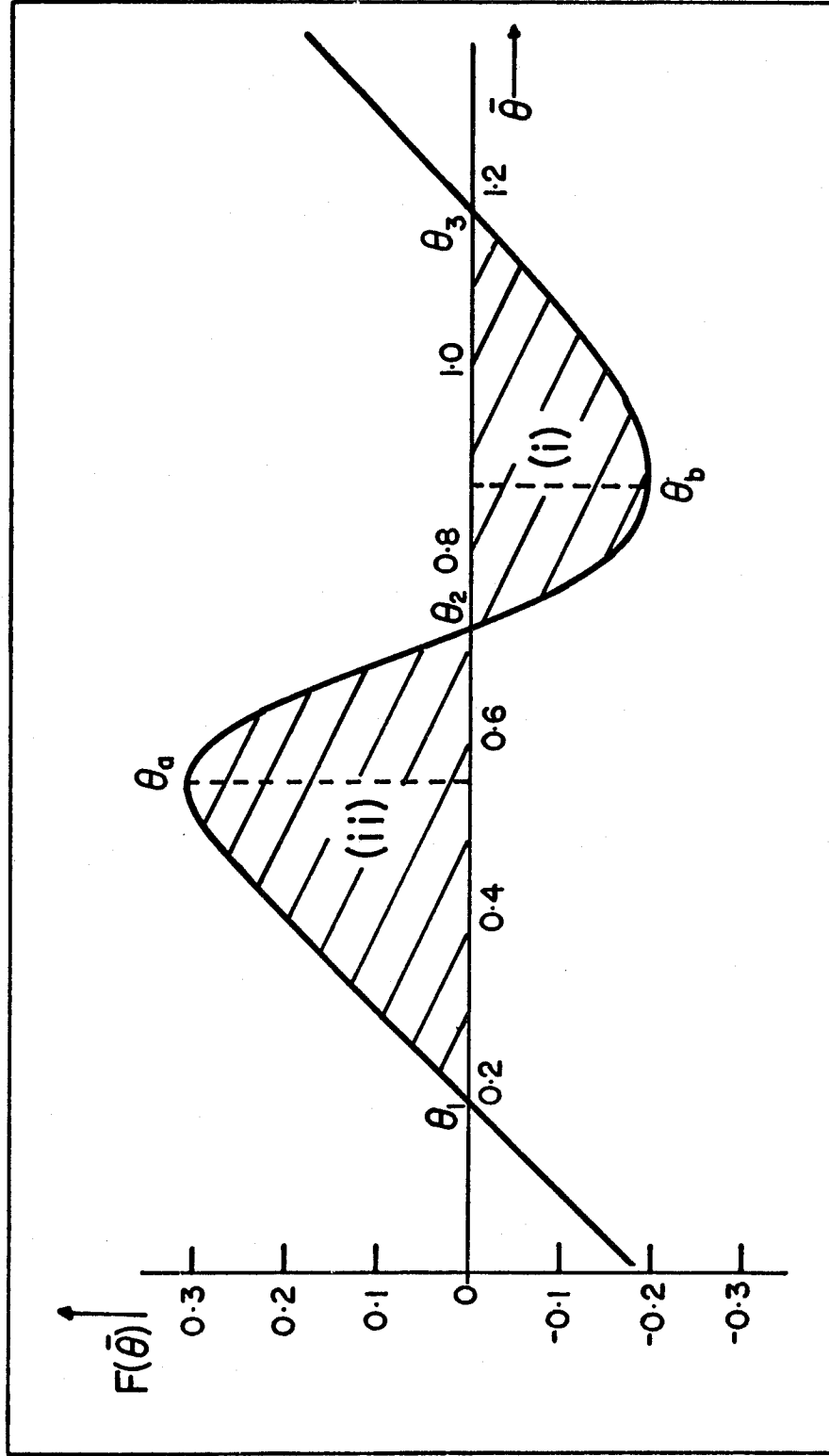


FIGURE 2: Form of the function $F(\bar{\theta})$ for $\theta_b = 0.19$, $A = 2.86 \times 10^4$ and $\epsilon = 7.2$

the area ii under the curve between θ_1 and θ_2 for the first set of values, while the area i is smaller than the area ii for the second set.

The model, represented by Equations (2.9) and (2.10), lends itself to a graphical analysis in which the dependent variables are plotted against one another on a phase-plane. The variables can be represented parametrically as trajectories satisfying the differential equation

$$\frac{d\bar{\theta}}{d\phi} = \frac{\phi}{F(\bar{\theta})} \quad (2.11)$$

A unique direction for a trajectory is defined by Equation (2.11) except where ϕ and $F(\bar{\theta})$ are both zero. Thus no trajectories can cross except at the singular points where both the numerator and denominator of the right-hand side of Equation (2.11) are zero.

The trajectories are mapped in Figures 3 and 4 for the two sets of parameter values being considered. The separatrices are indicated by heavier lines. $\phi > 0$ implies that $d\bar{\theta}/ds > 0$, so distance s increases on moving up the trajectories when $\phi > 0$; similarly, when $\phi < 0$, s increases on moving down the trajectories. Hence the arrowheads in Figures 3 and 4 indicate the direction of increase of s .

Consider an increment in s in moving from a point A to a point B along a trajectory. From Equation (2.9)

$$ds = d\bar{\theta} / \phi(\bar{\theta})$$

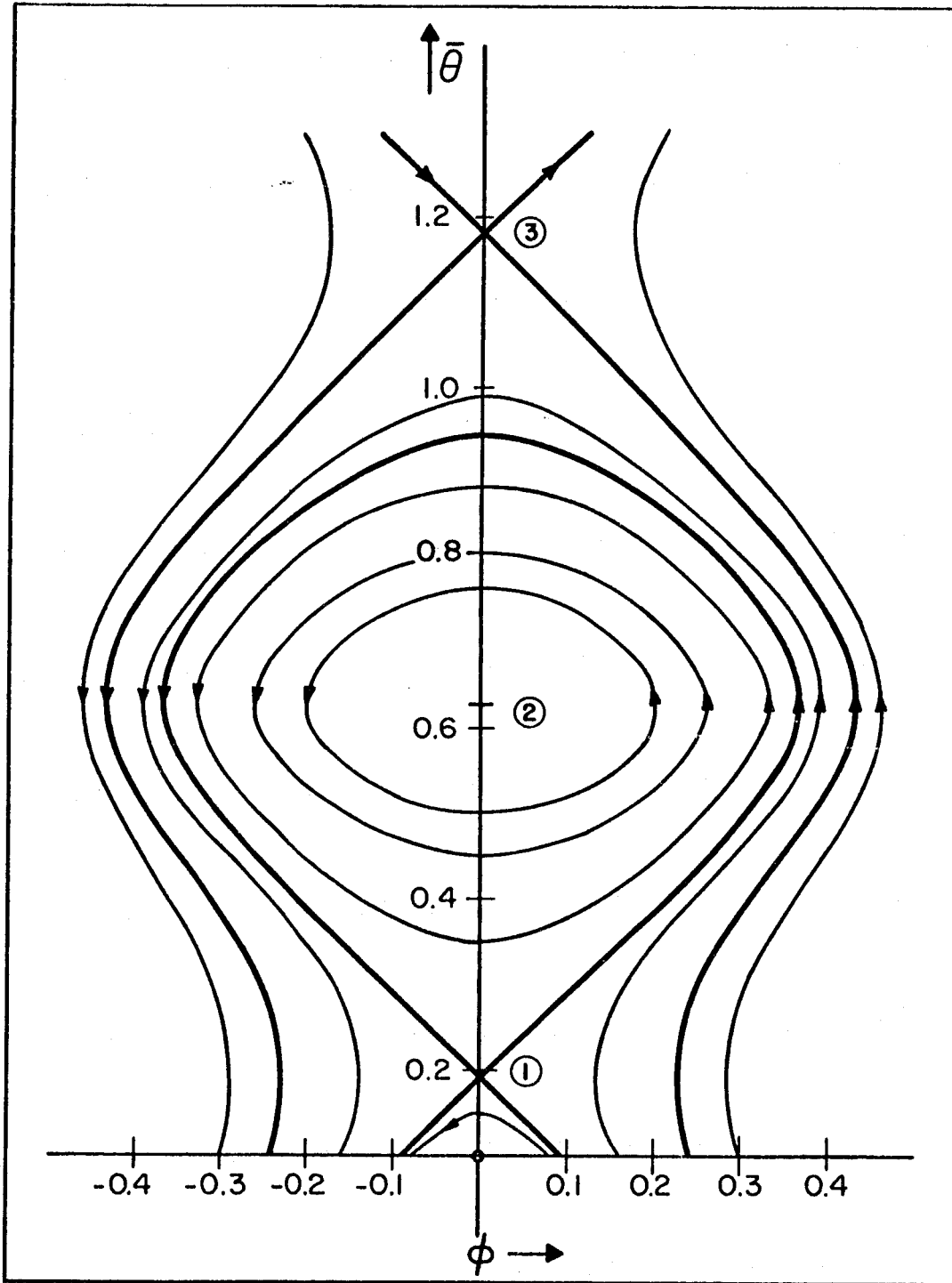


FIGURE 3: Phase trajectories in the $(\bar{\theta}, \phi)$ -plane representing solutions of the wire problem for $\theta_b = 0.19$, $A = 2.86 \times 10^4$ and $\epsilon = 6.6$

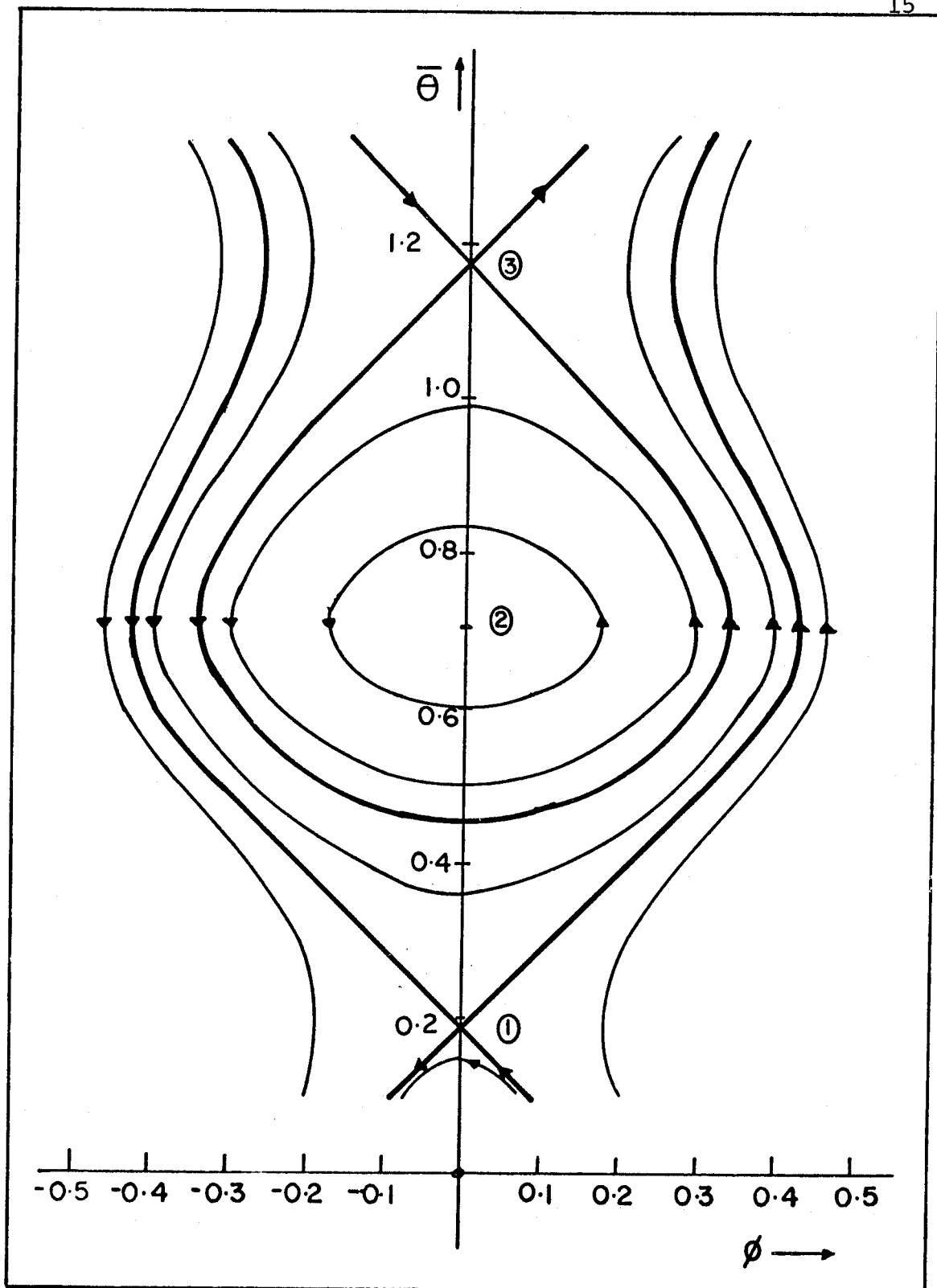


FIGURE 4: Phase trajectories in the $(\bar{\theta}, \phi)$ -plane representing solutions of the wire problem for $\theta_b = 0.19$, $A_c = 2.86 \times 10^4$ and $\epsilon = 7.2$

$$\text{and therefore } \Delta s = s_B - s_A = \int_{\theta_A}^{\theta_B} \frac{d\bar{\theta}}{\phi(\bar{\theta})} \quad (2.12)$$

Thus there are large increments of s corresponding to small increments in $\bar{\theta}$ when $\phi(\bar{\theta})$ is small and vice versa. The above can also be expressed as an integral with respect to ϕ

$$s_B - s_A = \int_{\phi_A}^{\phi_B} \frac{1}{\phi} \frac{d\bar{\theta}}{d\phi} d\phi \quad (2.13)$$

but since

$$\frac{d\bar{\theta}}{d\phi} = \frac{\phi}{F(\bar{\theta})}$$

then

$$s_B - s_A = \int_{\phi_A}^{\phi_B} \frac{d\phi}{F[\bar{\theta}(\phi)]} \quad (2.14)$$

In particular the increment in s in moving along a trajectory from the axis $\phi = 0$ is given by

$$\Delta s = \int_0^{\phi} \frac{d\phi}{F(\bar{\theta})} \quad (2.15)$$

This is finite, provided $F(\bar{\theta})$ is not equal to zero anywhere in this interval. It has been shown that unbounded increments of s corresponding to small increments in $\bar{\theta}$ occur when $\phi(\bar{\theta})$ is small. From the form of the functions $F(\bar{\theta})$

and $\phi(\bar{\theta})$ we see that only finite increments in s are obtained for small increments in $\bar{\theta}$ when ϕ is not small. So unbounded increments Δs from a bounded segment of a trajectory are obtained only for segments adjacent to $\phi = 0$, $\bar{\theta} = \theta_1$ and to $\phi = 0$, $\bar{\theta} = \theta_3$. (There being no trajectory approaching the $\phi = 0$ axis at $\bar{\theta} = \theta_2$.) In the neighborhood of θ_3 , for example,

$$F(\bar{\theta}) \simeq c_1(\bar{\theta} - \theta_3) \quad (2.16)$$

where c_1 is a constant, and therefore, from Equation (2.15)

$$\Delta s = \int_0^\phi \frac{d\phi}{c_1(\bar{\theta} - \theta_3)} \quad (2.17)$$

From Equation (2.11)

$$\frac{1}{2} d(\phi^2) = F(\bar{\theta}) d\bar{\theta} \quad (2.18)$$

This equation can be integrated from $(\theta_3, 0)$ to $(\bar{\theta}, \phi)$ to obtain

$$\frac{1}{2} \phi^2 = \int_{\theta_3}^{\bar{\theta}} c_1(\theta - \theta_3) d\theta \quad (2.19)$$

$$\text{Therefore } \phi = \sqrt{c_1} (\bar{\theta} - \theta_3) \quad (2.20)$$

$$\text{and } d\phi = \sqrt{c_1} d\bar{\theta} \quad (2.21)$$

Substituting Equations (2.20) and (2.21) in (2.17)

$$\Delta s \approx \int_{\theta_3}^{\bar{\theta}} \frac{\sqrt{c_1} d\bar{\theta}}{c_1(\bar{\theta} - \theta_3)} = \frac{1}{\sqrt{c_1}} \left(\log(\bar{\theta} - \theta_3) \right) \Big|_{\theta_3}^{\bar{\theta}} \quad (2.22)$$

which diverges at $\bar{\theta} = \theta_3$. Thus we do get an infinite contribution for Δs from finite segments of trajectories adjacent to $\phi = 0$, $\bar{\theta} = \theta_1$ and $\phi = 0$, $\bar{\theta} = \theta_3$.

The steady state equation

$$\frac{d^2 \bar{\theta}}{ds^2} = F(\bar{\theta}) \quad s \in \Omega \quad (2.23)$$

is subject to the following boundary conditions

$$\left(\frac{d\bar{\theta}}{ds} \right)_{s=s_0} = B \left(\bar{\theta}(s_0) - \theta_b \right) \quad (2.24)$$

$$\left(\frac{d\bar{\theta}}{ds} \right)_{s=s_1} = -B \left(\bar{\theta}(s_1) - \theta_b \right) \quad (2.25)$$

To obtain the temperature distribution in the wire, these boundary conditions can be superposed on the phase-plane diagram. When $B = 0$, the boundary conditions (2.24) and (2.25) become

$$\frac{d\bar{\theta}}{ds} = 0 \quad s = s_0, s_1 \quad (2.26)$$

This is equivalent to zero longitudinal heat flux at the ends. The boundary condition (2.26) is represented on the phase-plane diagram by the vertical line $\phi = 0$. Amongst the possible solutions in this case are the temperatures

θ_1 , θ_2 , and θ_3 corresponding to the roots of $F(\bar{\theta}) = 0$. These represent three uniform steady states of the wire. $\bar{\theta} = \theta_1$ being the unignited state and $\bar{\theta} = \theta_3$ the ignited one. In addition to these uniform solutions, some very interesting non-uniform solutions exist in the form of standing waves. All the closed loop trajectories encircling the intermediate uniform solution $\bar{\theta} = \theta_2$ are possible solutions. These trajectories represent standing wave solutions which vary periodically along the wire, and, unlike the uniform solutions are not invariant against all lateral translations. For a wire of finite length, L , only a finite number of solutions exist. This can be shown by the following argument. Consider solutions corresponding to very small loops about $\phi = 0$, $\bar{\theta} = \theta_2$. For such solutions $\bar{\theta}$ remains in the neighborhood of θ_2 everywhere on the wire. $F(\bar{\theta})$ can then be approximated by the first two terms of a Taylor series about $\bar{\theta} = \theta_2$. Thus, from Equation (2.23)

$$\frac{d^2 \bar{\theta}}{ds^2} = F(\theta_2) + (\bar{\theta} - \theta_2) \left(\frac{dF}{d\bar{\theta}} \right)_{\theta_2} \quad (2.27)$$

i.e.,

$$\frac{d^2 \bar{\theta}}{ds^2} = -H^2 (\bar{\theta} - \theta_2) \quad (2.28)$$

where $H^2 = - \left(\frac{dF}{d\bar{\theta}} \right)_{\theta_2}$ and, since $\bar{\theta} = \theta_2$ is a singular point, $F(\theta_2) = 0$. Solutions of Equation (2.28)

satisfying the boundary conditions $d\bar{\theta}/ds = 0$ at the ends of the wire (i.e., at $s = 0, L$) are

$$\bar{\theta} - \theta_2 = B \cos(Hs) \quad (2.29)$$

where $HL = \pi, 2\pi, 3\pi, \dots$. Thus a continuum of wave lengths between infinity and $2\pi/H$ exists for the standing waves in a wire of finite length. Since the wave lengths have a finite minimum value, with given L , there will be a finite number of solutions, of wave lengths $\infty, 2L, L, 2L/3, L/2, \dots$. Similar standing wave solutions, but infinite in number, exist for an infinite wire.

Some of the solutions represented by the closed loop trajectories are also asymmetric with respect to reflection in the center point of a wire of finite length. This can be seen quite easily by considering a closed loop. A typical closed loop is sketched in Figure 5. In order to satisfy boundary condition (2.26), $s = s_0$ must correspond to one of the points P, Q and so must $s = s_1$. Suppose the condition at $s = s_0$ is represented by the point P , and the condition at $s = s_1$ by Q , then a temperature distribution is obtained that is asymmetric with respect to reflection about the center plane.

Consideration will now be directed to the form the solutions take when B is non-zero. An infinite value of B corresponds formally to the ends of the wire held isothermally at $\bar{\theta} = \theta_b$. The boundary conditions are then

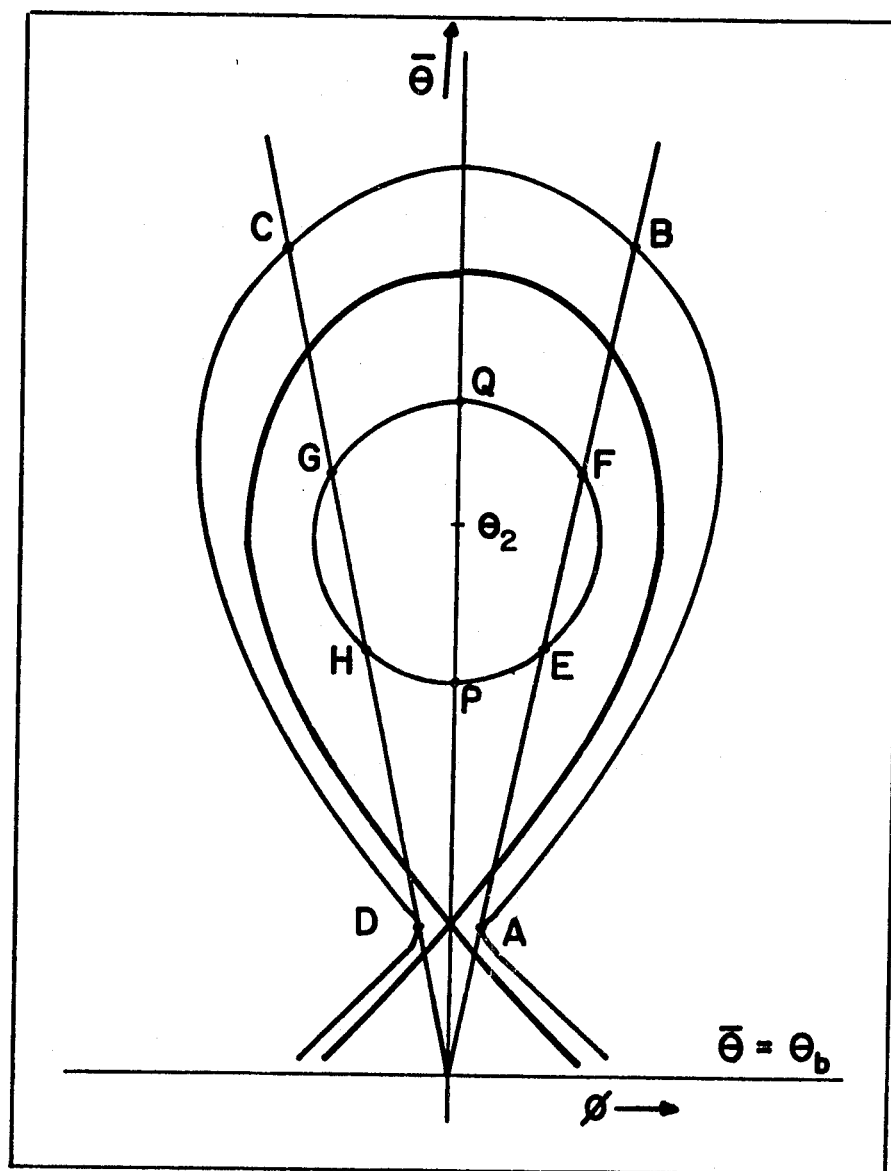


FIGURE 5: Sketch of the Phase Plane Diagram
With the Lines Representing the
Boundary Conditions Superposed

represented by the horizontal line $\bar{\theta} = \theta_b$ and the profiles for this case can be obtained by considering trajectories which intersect this horizontal line twice. Computationally the temperature distributions are obtained by integrating Equation (2.23) as a pair of first order equations, from an initial point with $\bar{\theta} = \theta_b$. The initial value of ϕ is free to be chosen. The forward integration is continued until a point is reached where the value of $\bar{\theta}$ is again θ_b . The corresponding value of s then gives the length of the wire. The integration method used was the Runge-Kutta-Merson method (see Lance²⁹) using variable step lengths. The order of convergence for this method is $O(h^5)$ and requires five evaluations of the function, with the arguments in each evaluation depending on the preceding evaluation. For a wire of fixed length, one or three solutions may exist. The three typical temperature distributions are shown in Figure 6 for $\epsilon = 6.6$. Although each profile shown corresponds to a wire of different length, it is expected that similar temperature distributions would be obtained for a wire of given length. The profile labelled 1 is the wire at the low temperature. The profiles 2 and 3 are the intermediate and high temperature profiles, respectively. The steady states shown are all symmetric about $s = 0$ and, for this case of the wire with ends held isothermally, all the profiles will be symmetric. If the length of the wire is shortened, profiles 2 and 3 will

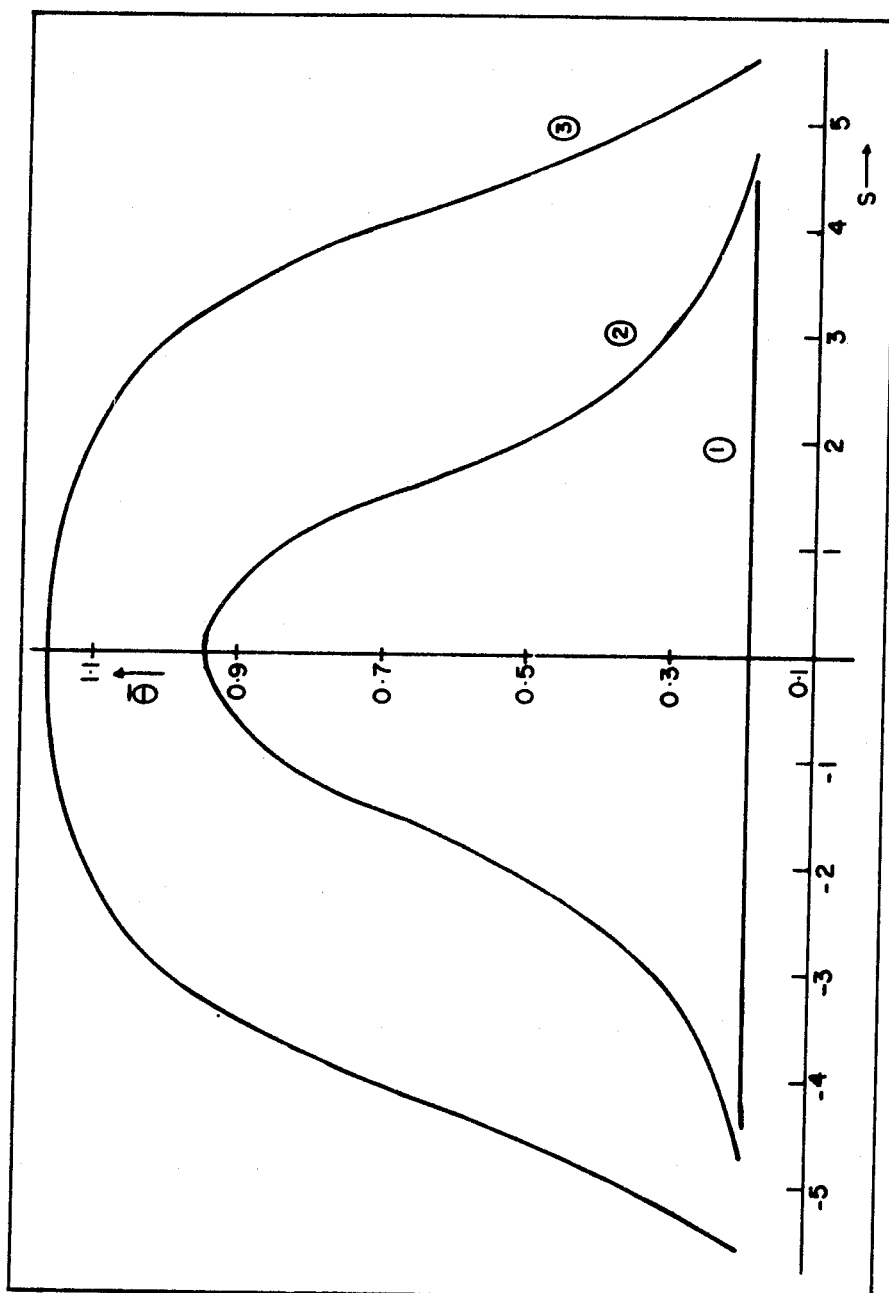


FIGURE 6: Temperature Profiles in Catalyst Wire with Ends Held Isothermally at $\theta = \theta_b$ for $\theta_b = 0.19$, $A = 2.86 \times 10^4$ and $\epsilon = 6.6$

come together as the phase trajectory corresponding to the profile 2 enlarges and that corresponding to profile 3 shrinks. Eventually the profiles will coincide. For wires shorter than this, the only surviving steady state would be the low temperature profile.

Small values of B correspond to almost adiabatic end conditions. Figure 5 shows a sketch of the trajectory map with lines representing the boundary conditions superposed. In the sketch only the inner separatrix is shown. The straight line with positive slope corresponds to the boundary condition at $s = s_0$, and that with a negative slope to the boundary condition at $s = s_1$. New forms of temperature distributions arise when the boundary condition lines intersect a trajectory more than once. The temperature profiles are obtained by integrating Equation (2.23) with initial conditions represented by either points A or B on Figure 5. The integration is continued until the point C is reached. Since this point lies on the line representing the boundary condition at $s = s_1$, the profile obtained satisfies the Equations (2.23) to (2.25). If the integration is further continued, another point will be reached where the boundary condition at $s = s_1$ is again satisfied. This will be at the point D, and the solution thus obtained also satisfies the system of Equations (2.23) to (2.25). Typical profiles are shown in Figure 7 (for $\epsilon = 6.6$). The steady states shown in Figure 8 (for $\epsilon = 6.6$) and Figure 9 (for $\epsilon = 7.2$)

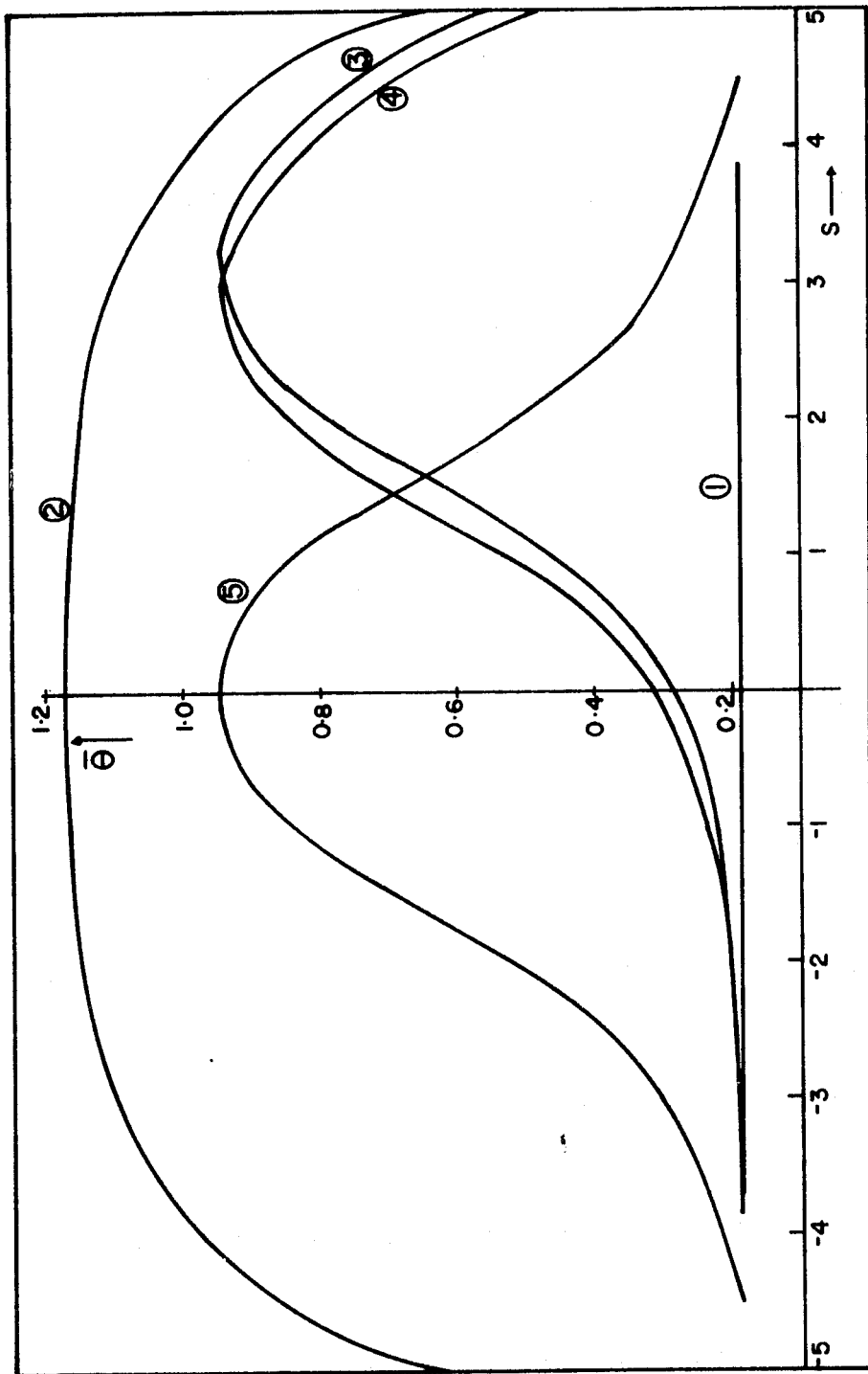
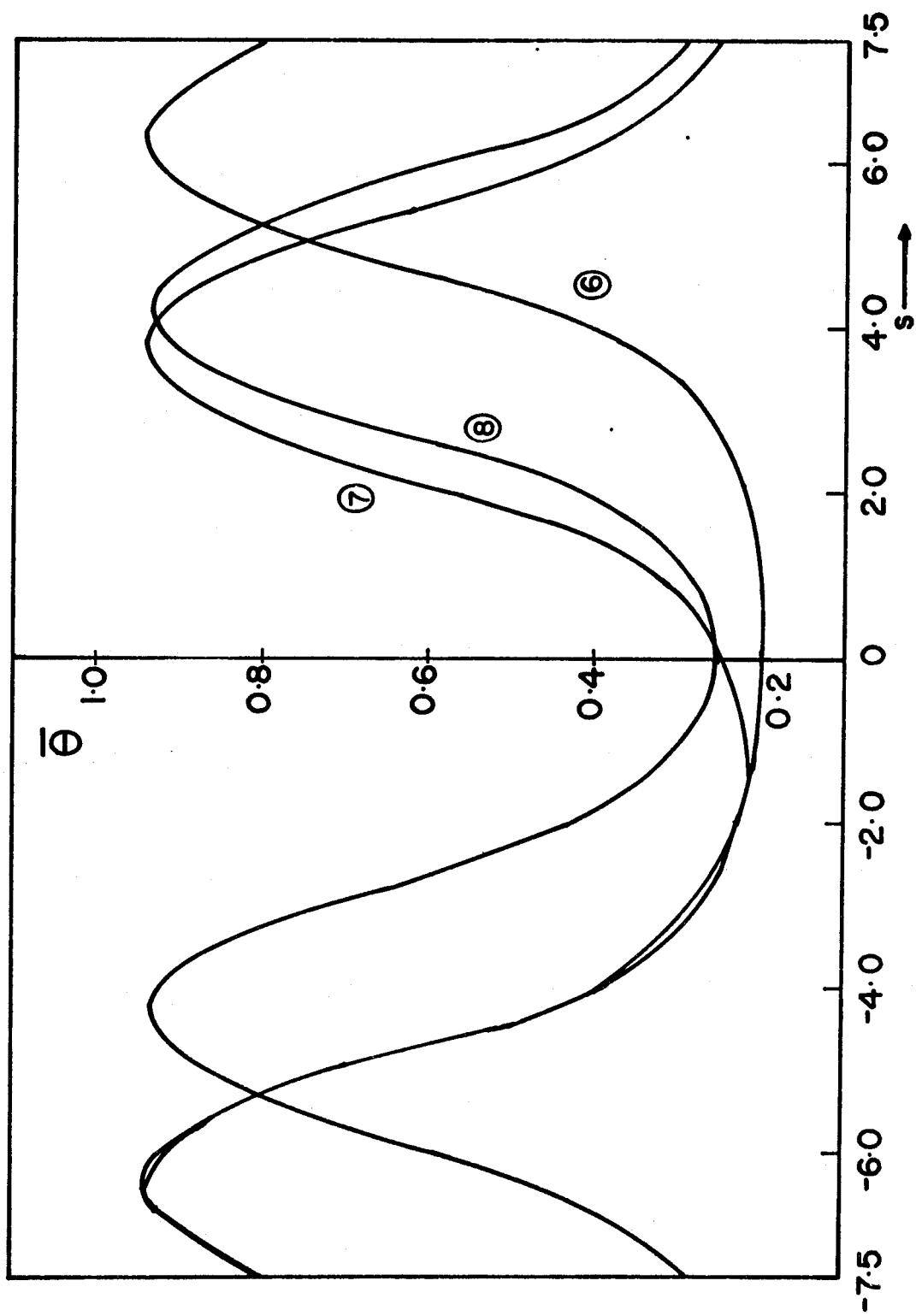


FIGURE 7: Temperature Profiles in Catalyst Wire for $\theta_b = 0.19$, $A = 2.86 \times 10^4$ and $\epsilon = 6.6$ and $B = 2.40$

FIGURE 8: Temperature Profiles in Catalyst Wire
for $\theta_b = 0.19$, $A = 2.86 \times 10^4$,
 $\epsilon = 6.6$, and $B = 1.80$



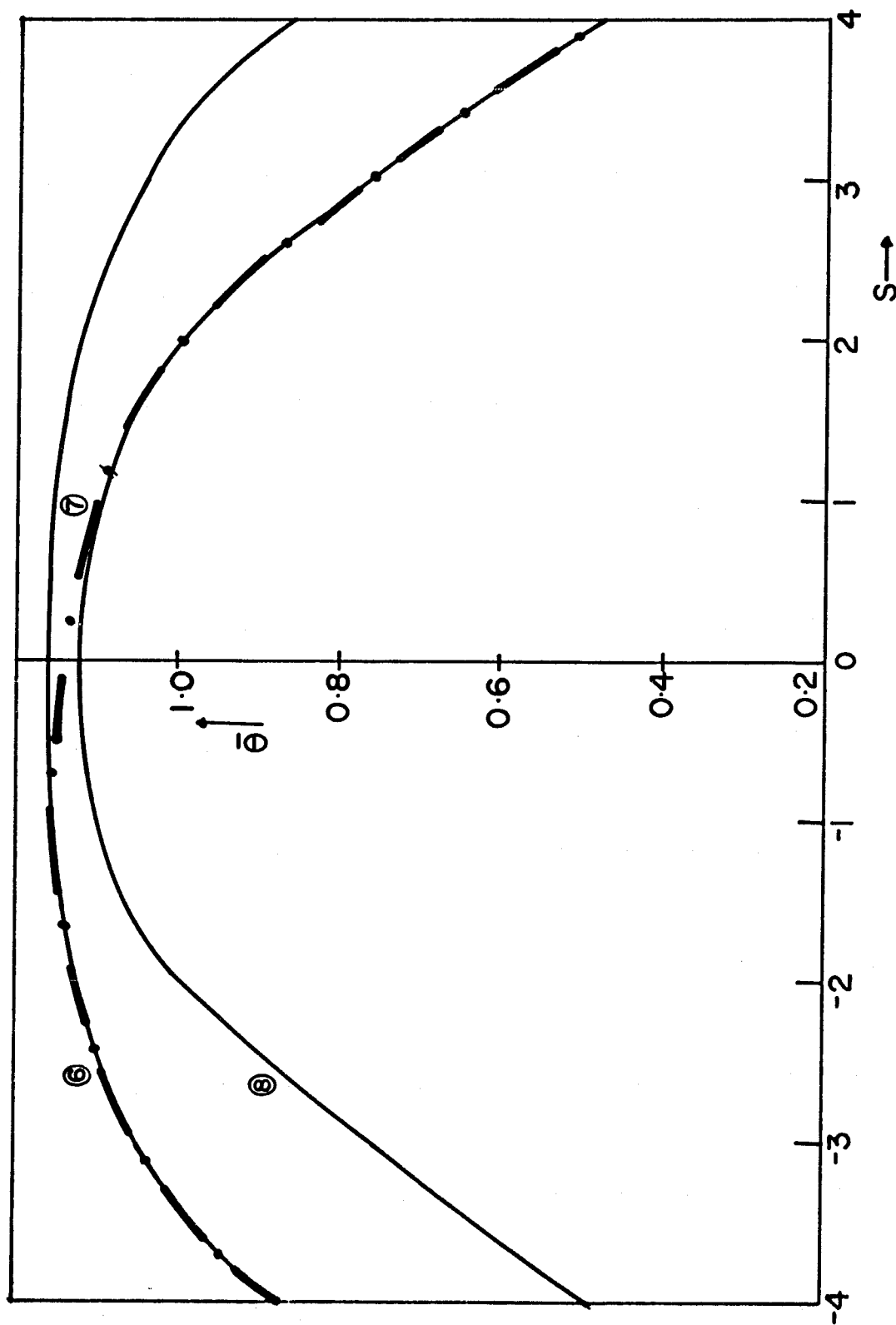


FIGURE 9: Temperature Profiles in Catalyst Wire for $\theta_b = 0.19$, $A = 2.86 \times 10^4$, $\epsilon = 7.2$, and $B = 2.50$

are obtained in an analogous manner but are represented by the closed loop trajectories. In order to satisfy the boundary conditions, $s = s_0$ must correspond to either points E or F in Figure 5 and $s = s_1$ to either points G or H in the same Figure. More and more peaks appear in the solution as longer wires and smaller closed loops are considered.

C. Stability of Steady States

A pertinent question in considering these steady states is whether any of them are stable and hence whether they can be realized in practice. A steady state is said to be stable if, when the particle is perturbed from the steady state, it tends to return to the same state. This is referred to as asymptotic stability. In this work, the transient equations are linearized about the steady state and the effect of small perturbations is considered. In order to determine the effect of large perturbations, complete transient calculations must be made.

Consider small perturbations, $\sigma(s, \tau)$, of the steady state, $\bar{\theta}(s)$. Thus

$$\theta(s, \tau) = \bar{\theta}(s) + \sigma(s, \tau). \quad (2.30)$$

Approximating $F(\theta)$ by the first two terms of a Taylor series

$$F(\theta) = F(\bar{\theta}) + \left(\frac{dF}{d\theta} \right)_{\theta = \bar{\theta}} \sigma(s, \tau) \quad (2.31)$$

Then $\sigma(s, \tau)$ must satisfy the linearized perturbation equation

$$\frac{\partial \sigma}{\partial \tau} = \frac{\partial^2 \sigma}{\partial s^2} - F'(\bar{\theta}) \sigma \quad (2.32)$$

with

$$\frac{\partial \sigma}{\partial s} = B \sigma \quad s = s_0 \quad (2.33)$$

$$\frac{\partial \sigma}{\partial s} = -B \sigma \quad s = s_1 \quad (2.34)$$

where the prime denotes differentiation with respect to θ .

We seek a separable solution of the form

$$\sigma(s, \tau) = \omega(\tau) \psi(s) \quad (2.35)$$

Hence

$$\frac{1}{\omega} \frac{d\omega}{d\tau} = \frac{1}{\psi} \frac{d^2 \psi}{ds^2} - F'(\bar{\theta}) \quad (2.36)$$

Since the left-hand side of Equation (2.36) is a function of τ only, and the right-hand side is a function of s only, each side must be equal to a constant $-\bar{\lambda}$, say. Thus

$$\omega(\tau) = \omega(0) e^{-\bar{\lambda} \tau} \quad (2.37)$$

and

$$\frac{d^2 \psi}{ds^2} - (F'(\bar{\theta}) - \bar{\lambda}) \psi = 0 \quad (2.38)$$

with

$$\left(\frac{d\psi}{ds} \right)_{s=s_0} = B \psi(s_0) \quad (2.39)$$

$$\left(\frac{d\psi}{ds} \right)_{s=s_1} = -B \psi(s_1) \quad (2.40)$$

To establish stability it is necessary to determine the signs of the eigenvalues $\bar{\lambda}$. From (2.37), it is sufficient for instability to show that the problem defined by Equations (2.38), (2.39), and (2.40) has at least one negative eigenvalue. Amundson,¹ using elementary results of Sturm theory, developed a theorem giving a test which can be performed from steady state information alone and involves only the solution of a linear differential equation. Introducing a function $v(s)$ which is the solution of the differential equation

$$\frac{d^2 v}{ds^2} - F'(\bar{\theta})v = 0 \quad (2.41)$$

with boundary conditions

$$v(0) = 1 \text{ and } \left(\frac{dv}{ds} \right)_{s=0} = B \quad (2.42)$$

Amundson shows that the system of Equations (2.38) through (2.40) has no negative eigenvalues if and only if both the following conditions

$$v(s) > 0 \quad \text{for } s \in (0, s_1] \quad (2.43)$$

and

$$\frac{1}{v(s_1)} \left(\frac{dv}{ds} \right)_{s=s_1} \geq -B \quad (2.44)$$

hold.

When the ends of the wire are held adiabatically, three uniform solutions and solutions that vary periodically along the wire exist.

For the uniformly ignited state $\bar{\theta} = \theta_3$, and it is independent of s . Then

$$F'(\theta_3) = G^2 > 0 \quad (2.45)$$

The linearized perturbation equation becomes

$$\frac{\partial \sigma}{\partial \tau} = \frac{\partial^2 \sigma}{\partial s^2} - G^2 \sigma \quad (2.46)$$

Trying the solution

$$\sigma(s, \tau) = \omega_1(\tau) e^{iks} \quad (2.47)$$

we have

$$\omega_1(\tau) = \omega_1(0) e^{-(k^2 + G^2)\tau} \quad (2.48)$$

which is always stable. By a similar argument the uniformly unignited state $\bar{\theta} = \theta_1$ can be shown to be stable.

For the intermediate steady state $\bar{\theta} = \theta_2$, and

$$F'(\theta_2) = -H^2 < 0 \quad (2.49)$$

and therefore

$$\omega_1(\tau) = \omega_1(0)e^{-(k^2 - H^2)\tau} \quad (2.50)$$

which is stable for $k^2 > H^2$ but unstable for $k^2 < H^2$. The uniform solution $\bar{\theta} = \theta_2$ is therefore unstable.

The stability of the standing wave solutions was investigated by using Amundson's criterion. It is expected that if any of the standing wave solutions are to be stable, then the ones most likely to be so would be those represented by the largest closed loop trajectories. The following argument, based on the application of calculus of variations to eigenvalue problems (see Courant and Hilbert⁹), shows that solutions represented by small closed loops are unstable. The eigenvalue problem for this case is defined by Equations (2.38) through (2.40) with $B = 0$.

Thus,

$$\frac{d^2\psi}{ds^2} - (F'(\bar{\theta}) - \bar{\lambda})\psi = 0 \quad (2.51)$$

with

$$\left(\frac{d\psi}{ds} \right)_{s=0} = 0 \quad (2.52)$$

$$\left(\frac{d\psi}{ds} \right)_{s=L} = 0 \quad (2.53)$$

where L is the length of the wire.

We are interested in the smallest eigenvalue $\bar{\lambda}_{\min}$.
According to Courant and Hilbert⁹

$$\bar{\lambda}_{\min} \leq \int_0^L \left[(\nu')^2 + F'(\bar{\theta}) \nu^2 \right] ds \quad (2.54)$$

such that

$$\int_0^L \nu^2 ds = 1 \quad (2.55)$$

Thus if we can find any function ν , properly normalized, that makes the right-hand side of the Inequality (2.54) negative, the solution $\bar{\theta}(s)$ is unstable. So a necessary condition for stability is

$$\int_0^L \left[(\nu')^2 + F'(\bar{\theta}) \nu^2 \right] ds \geq 0 \quad (2.56)$$

for all $\nu(s)$ satisfying Equation (2.55). This restriction may be dropped, since multiplying ν by a scaling constant does not alter the sign of the left-hand side of Inequality (2.56). Therefore a necessary condition for stability is

$$\int_0^L \left[(\nu')^2 + F'(\bar{\theta}) \nu^2 \right] ds \geq 0 \quad (2.57)$$

for all functions $\nu(s)$ which are continuous in $[0, L]$ and

have piecewise continuous derivatives in $(0,L)$. Weaker necessary conditions can be obtained by choosing particular forms of $\nu(s)$. The simplest one is to take $\nu(s) \equiv 1$ for $s \in [0,L]$. This gives

$$\int_0^L F'(\bar{\theta}) ds > 0 \quad (2.58)$$

as the necessary condition for stability. The condition shows that standing waves which cover ranges of $\bar{\theta}$ in which $F'(\bar{\theta}) < 0$ everywhere are unstable. Thus all oscillatory solutions circling $(\theta_2, 0)$ in the $(\bar{\theta}, \phi)$ -plane, with $\theta_{\max} \leq \theta_b$ and $\theta_{\min} \geq \theta_a$ are certainly unstable, where θ_a and θ_b are shown in Figures 1 and 2.

Amundson's test was performed on the biggest closed loop for both sets of parameters. For the set $A = 2.86 \times 10^4$, $\theta_b = 0.19$ and $\epsilon = 6.6$, the first condition was violated and $\nu(s)$ became negative at $\bar{\theta} = 0.94$. For the second set of parameters ($A = 2.86 \times 10^4$, $\theta_b = 0.19$ and $\epsilon = 7.2$), the first condition was again violated and $\nu(s)$ became negative at $\bar{\theta} = 1.01$. This result has been confirmed by Erwin and Luss¹⁴ using topological methods. Recently, Jackson,²⁵ using Amundson's criterion, established the instability of all standing wave steady states, by general reasoning, for the case of adiabatic end conditions, or an infinite wire.

Amundson's simple criterion was also applied to the profiles shown in Figures 6 to 9. The results are summarized

in Table 1.

We have thus shown that, for the particular cases computed, the standing wave solutions in a catalyst wire are unstable. Instability of all of the standing wave steady states has recently been established^{14,25} for adiabatic end conditions or for wires of infinite length. Instability of particular examples of steady states that are asymmetric with respect to reflection across the center plane has also been demonstrated in this work, and it is expected that all the solutions exhibiting reflective asymmetry are unstable.

TABLE 1

RESULTS OF AMUNDSON'S STABILITY CRITERION

<u>Figure Number</u>	<u>Profile Number</u>	<u>Stable or Unstable</u>	<u>Comments</u>
6	1	Stable	
6	2	Unstable	$v < 0$ at $\bar{\theta} = 0.94$
6	3	Stable	
7	1	Stable	
7	2	Stable	
7	3	Unstable	$v < 0$ at $\bar{\theta} = 0.94$
7	4	Unstable	$v < 0$ at $\bar{\theta} = 0.94$
7	5	Unstable	$v < 0$ at $\bar{\theta} = 0.94$
8	6	Unstable	$v < 0$ at $\bar{\theta} = 0.3$
8	7	Unstable	$v < 0$ at $\bar{\theta} = 0.3$
8	8	Unstable	$v < 0$ at $\bar{\theta} = 0.94$
9	6	Stable	
9	7	Unstable	$v > 0$ for $s \in (s_0, s_1)$, but Equation (1.41) is violated.
9	8	Unstable	$v < 0$ at $\bar{\theta} = 0.94$

III. SOLUTIONS NOT INVARIANT UNDER REFLECTION

A. Mathematical Description of the Problem

We consider a catalytic slab, infinite in two directions and of finite thickness in the third, with diffusive resistances to heat and mass flux in its interior and Newtonian resistances to heat and mass transfer at its faces. It is surrounded by gas at uniform temperature T_b with a uniform concentration c_b of reactant. For simplicity, we consider a single, irreversible, first order, exothermic reaction with Arrhenius temperature dependence and assume that the thermal and mass diffusivities are constant. The conservation equations needed to describe reaction and diffusion in the slab are

$$\frac{\partial c}{\partial t} = D \frac{\partial^2 c}{\partial x^2} - ck_0 e^{-E/RT} \quad x \in (x_0, x_1), \quad t > 0 \quad (3.1)$$

$$\rho c_p \frac{\partial T}{\partial t} = K \frac{\partial^2 T}{\partial x^2} + Qck_0 e^{-E/RT} \quad x \in (x_0, x_1), \quad t > 0 \quad (3.2)$$

where x is a coordinate measured normal to the slab faces and x_0 and x_1 are the coordinates of the slab faces, the suffix 0 referring to the left-hand face and 1 to the right-hand face. D and K are the effective diffusion coefficient and thermal conductivity, respectively; and Q is the heat of reaction, considered positive for an exothermic reaction. Equations (3.1) and (3.2) are subject to the following

boundary conditions

$$D \left(\frac{\partial c}{\partial x} \right)_{x_0} = \ell (c(x_0) - c_b) \quad (3.3)$$

$$D \left(\frac{\partial c}{\partial x} \right)_{x_1} = -\ell (c(x_1) - c_b) \quad (3.4)$$

and

$$K \left(\frac{\partial T}{\partial x} \right)_{x_0} = m (T(x_0) - T_b) \quad (3.5)$$

$$K \left(\frac{\partial T}{\partial x} \right)_{x_1} = -m (T(x_1) - T_b) \quad (3.6)$$

where ℓ and m are the mass and heat transfer coefficients, respectively, at the boundaries.

It is convenient to make the equations dimensionless by introducing the following variables

$$z = c/c_b, \quad y = T/T_b, \quad \gamma = E/RT_b, \quad \xi = \left(\frac{k_0 e^{-\gamma}}{D} \right)^{\frac{1}{2}} x,$$

$$\beta = \frac{QDC_b}{KT_b}, \quad \tau = k_0 e^{-\gamma} t, \quad Le = \frac{\rho c_p D}{K}$$

The above system then becomes

$$\frac{\partial z}{\partial \tau} = \frac{\partial^2 z}{\partial \xi^2} - z e^{\gamma(y-1)/y} \quad \xi \in (\xi_0, \xi_1), \tau > 0 \quad (3.7)$$

$$Le \frac{\partial y}{\partial \tau} = \frac{\partial^2 y}{\partial \xi^2} + \beta z e^{\gamma(y-1)/y} \quad \xi \in (\xi_0, \xi_1), \tau > 0 \quad (3.8)$$

with boundary conditions

$$\left(\frac{\partial z}{\partial \xi} \right)_{\xi_0} = p(z(\xi_0) - 1) \quad (3.9)$$

$$\left(\frac{\partial z}{\partial \xi} \right)_{\xi_1} = -p(z(\xi_1) - 1) \quad (3.10)$$

and

$$\left(\frac{\partial y}{\partial \xi} \right)_{\xi_0} = q(y(\xi_0) - 1) \quad (3.11)$$

$$\left(\frac{\partial y}{\partial \xi} \right)_{\xi_1} = -q(y(\xi_1) - 1) \quad (3.12)$$

where

$$p = \frac{\ell}{\sqrt{Dk_0 e^{-\gamma}}}, \quad q = \frac{L}{K} \frac{m}{\sqrt{Dk_0 e^{-\gamma}}} \quad (3.13)$$

B. Steady State Analysis

The steady states $\bar{z}(s)$ and $\bar{y}(s)$ are obtained by setting the left-hand sides of Equation (3.7) and Equation (3.8) equal to zero.

The conservation equations then become

$$\bar{z}'' = \bar{z} \exp \left(\frac{\gamma(\bar{y}-1)}{\bar{y}} \right) \quad \xi \in (\xi_0, \xi_1) \quad (3.14)$$

$$\bar{y}'' = -\beta \bar{z} \exp \left(\frac{\gamma(\bar{y}-1)}{\bar{y}} \right) \quad \xi \in (\xi_0, \xi_1) \quad (3.15)$$

with boundary conditions

$$(\bar{z}')_{\xi_0} = p(\bar{z}(\xi_0) - 1) \quad (3.16)$$

$$(\bar{z}')_{\xi_1} = -p(\bar{z}(\xi_1) - 1) \quad (3.17)$$

and

$$(\bar{y}')_{\xi_0} = q(\bar{y}(\xi_0) - 1) \quad (3.18)$$

$$(\bar{y}')_{\xi_1} = -q(\bar{y}(\xi_1) - 1) \quad (3.19)$$

where the primes denote differentiation with respect to ξ .

In the usual manner we may define the effectiveness factor η as the ratio of the total rate of reaction in the slab to the total reaction rate which would be obtained if the reactant concentration and temperature retained the values c_p and T_p , respectively, throughout the slab. Then, in terms of the dimensionless variables introduced here

$$\eta = \frac{1}{2} \frac{l}{a k_o e^{-\gamma}} \left(2 - \bar{z}(\xi_0) - \bar{z}(\xi_1) \right)$$

where a is the half-thickness of the slab. Furthermore, the Thiele modulus λ is defined by

$$\lambda = \frac{1}{2} \left(\frac{k_o e^{-\gamma}}{D} \right)^{\frac{1}{2}} (x_1 - x_0)$$

or, in terms of the dimensionless distance ξ

$$\lambda = \frac{1}{2} (\xi_1 - \xi_0) \quad (3.20)$$

showing that the Thiele modulus is simply the dimensionless half-thickness of the slab. Using (3.20) the expression for the effectiveness factor may be reduced to

$$\eta = \frac{1}{2} \frac{p}{\lambda} \left(2 - \bar{z}(\xi_0) - \bar{z}(\xi_1) \right) \quad (3.21)$$

This may also be written

$$\eta = \frac{1}{2} (\eta_0 + \eta_1) \quad (3.22)$$

where

$$\eta_0 = \frac{p}{\lambda} \left(1 - \bar{z}(\xi_0) \right) \quad \text{and} \quad \eta_1 = \frac{p}{\lambda} \left(1 - \bar{z}(\xi_1) \right) \quad (3.23)$$

will be called the one-sided effectiveness factors corresponding to the left and right-hand faces of the slab, respectively.

C. Solution Procedure

Linear combination of Equations (3.14) and (3.15) gives:

$$\beta \bar{z}'' + \bar{y}'' = 0 \quad (3.24)$$

whence, after integrating twice

$$\beta \bar{z} + \bar{y} = \alpha_1 + \alpha_2 \xi \quad (3.25)$$

where α_1 and α_2 are integration constants. Equation (3.25) may be used to eliminate either \bar{y} or \bar{z} from (3.14) to (3.19); thus, eliminating \bar{y} , these equations reduce to

$$\bar{z}'' = \bar{z} \exp \left\{ \frac{\gamma(\alpha_1 + \alpha_2 \xi - \beta \bar{z} - 1)}{\alpha_1 + \alpha_2 \xi - \beta \bar{z}} \right\} \quad (3.26)$$

with the boundary conditions

$$(\bar{z}')_{\xi_0} = p(\bar{z}(\xi_0) - 1) \quad (3.27)$$

$$N \equiv \beta(p-q)\bar{z}(\xi_0) + q(\alpha_1 + \alpha_2 \xi_0 - 1) - \alpha_2 - \beta p = 0 \quad (3.28)$$

$$(\bar{z}')_{\xi_1} = -p(\bar{z}(\xi_1) - 1) \quad (3.29)$$

and

$$M \equiv \beta(p-q)\bar{z}(\xi_1) + q(\alpha_1 + \alpha_2 \xi_1 - 1) + \alpha_2 - \beta p = 0 \quad (3.30)$$

When $\alpha_2 = 0$ solutions of (3.26) are symmetric about a minimum where $\bar{z}' = 0$, while values of $\alpha_2 \neq 0$ lead to solutions which are asymmetric about a minimum. If these asymmetric solutions can be made to satisfy the boundary conditions (3.27) to (3.30), they generate asymmetric steady states. Indeed, it is easily checked that, if $\bar{z}(\xi)$ satisfies Equations (3.26) to (3.30) and $\bar{y}(\xi)$ is generated from $\bar{z}(\xi)$

using Equation (3.25), then the pair $\bar{y}(\xi), \bar{z}(\xi)$ satisfies the original Equations (3.14) to (3.19).

Equation (3.26) is a second order differential equation containing two undetermined parameters (α_1 and α_2), and four boundary conditions are to be satisfied. Many possible approaches to the solution of such a problem suggest themselves and no claim is made that the one to be adopted here is the most efficient numerical procedure. It was selected for two reasons; firstly, when $\alpha_2 = 0$, it reduces to a well known method of generating the symmetric steady states, so the relation of the unsymmetric to the symmetric solutions is particularly clear, and secondly, it demonstrates in a very direct way that solutions of Equation (3.26) with $\alpha_2 \neq 0$ can be made to satisfy the boundary conditions, and hence that asymmetric steady states exist.

For fixed values of the physical parameters p, q, β , and γ (which are all independent of the slab thickness), the solution is initiated by choosing a value for α_2 , which remains fixed throughout the calculation. The origin for ξ is chosen as the minimum of the function $\bar{z}(\xi)$, so that $\bar{z} = \bar{z}(0)$, $\bar{z}' = 0$ at $\xi = 0$. Guessing values for $\bar{z}(0)$ and α_1 , Equation (3.26) can then be integrated forward from $\xi = 0$ and, since \bar{z}' increases monotonically from zero, a value of ξ is eventually reached where (3.29) is satisfied. However, condition (3.30) is not, in general, satisfied at this point, and it is necessary to adjust the guesses of

$\bar{z}(0)$ and/or α_1 until both conditions (3.29) and (3.30) are satisfied at some positive value ξ_1 of ξ . In this way a set of pairs of values of $\bar{z}(0)$ and α_1 can be found for which conditions (3.29) and (3.30) are simultaneously satisfied and, if we regard each pair as defining a point in the $(\bar{z}(0), \alpha_1)$ -plane, the set defines a curve in this plane, which we will refer to as the M=0 curve.

Similarly, integrating backward from $\xi = 0$, one may seek points in the $(\bar{z}(0), \alpha_1)$ - plane such that conditions (3.27) and (3.28) are simultaneously satisfied for some negative value ξ_0 of ξ . Once again, the set of all such points defines a curve, which we will refer to as the N=0 curve.

Then any intersection of the M=0 curve with the N=0 curve defines a pair of values $\bar{z}(0), \alpha_1$ which generate a solution of (3.26) satisfying all the boundary conditions, and hence an asymmetric steady state. From the values of ξ_0 and ξ_1 the Thiele modulus follows using Equation (3.20), and the values of $\bar{z}(\xi_0)$ and $\bar{z}(\xi_1)$ then permit the one-sided effectiveness factors to be calculated from Equations (3.23), and hence the overall effectiveness factor from Equation (3.22). Thus, corresponding to each intersection of the M=0 curve with the N=0 curve, for given α_2 , there corresponds a point in the (η, λ) - plane or, if η_0 and η_1 are plotted separately, two points with a common abscissa. The M=0 curve may intersect the N=0 curve in several points, in which case we obtain an equal number of points in the

(η, λ) - plane (or twice this number if η_0 and η_1 are plotted separately) from the solutions generated with a single value of α_2 . However, to complete the representation of all steady states in the (η, λ) - plane, the whole computation must be repeated for a sequence of values of α_2 , which we may restrict to non-negative values without loss of generality, since replacing α_2 by $-\alpha_2$ merely replaces the temperature and composition profiles by their mirror images in the center plane of the slab, and does not generate an essentially new solution.

Though each non-zero value of α_2 generates, at most, a small number of points in the (η, λ) - plane representing asymmetric steady states, the complete set of symmetric steady states is obtained from the single value $\alpha_2 = 0$. To see why this is so, note that the symmetry of the solutions in this case implies that whenever conditions (3.29) and (3.30) are satisfied for some positive ξ_1 , conditions (3.27) and (3.28) are also satisfied for $\xi = \xi_0 = -\xi_1$. Thus the $M=0$ curve and the $N=0$ curve coincide when $\alpha_2 = 0$, so every point on the curve $M=0$ (or $N=0$) is an intersection point of the two curves, and hence gives values of $\bar{z}(0)$ and α_1 which generate a symmetric solution satisfying the boundary conditions at both faces. In this case our method has degenerated into a familiar procedure for generating the set of symmetric steady states and the corresponding curves in the (η, λ) - plane.

It is seen that the construction by this method of the new branches of the (η, λ) plot, corresponding to asymmetric states, is a much more formidable computational undertaking than the construction of the symmetric branches, and it may occur to the reader that the burden of iterative calculation could be greatly reduced by starting the integration of Equation (3.26) from the left-hand face of the slab rather than the minimum of $\bar{z}(\xi)$. For a given value of α_2 it would be necessary only to guess a value for $\bar{z}(\xi_0)$. Boundary conditions (3.27) and (3.28) would then determine $\bar{z}'(\xi_0)$ and α_1 , and Equation (3.26) could be integrated forward to a value of ξ where condition (3.29) was satisfied. By iterative adjustment of the guessed value of $\bar{z}(\xi_0)$ one could ensure that condition (3.30) was satisfied simultaneously, yielding a solution satisfying all the boundary conditions. Unfortunately this attractive procedure fails because of the extreme sensitivity of the solution of (3.26) to the value of $\bar{z}(\xi_0)$, as a result of which it is impossible to obtain solutions for Thiele moduli large enough to permit asymmetric states.

D. Numerical Results and Discussion

All the computations were performed with values of the physical parameters fixed at $\beta = 0.0667$, $\gamma = 29.5$, $p = 40.0$, and $q = 4.0$. The necessary condition for the existence of asymmetric states derived by Jackson and Horn²⁶ is satisfied by these values of p and q . In their survey

on realistic parameter ranges, Mercer and Aris³⁸ cite work in which a value of β as high as 0.95 has been reported, although McGreavy and Creswell³⁷ believe the realistic upper bound for β to be 0.07. The Mercer-Aris survey puts the range of values of γ to be between 0 and 60.

Considering first $\alpha_2 = 0$, Figure 10 shows the curve $M=0$ (or $N=0$) in the $(\bar{z}(0), \alpha_1)$ - plane. Note that in this and subsequent diagrams of this type, the scale on the $\bar{z}(0)$ - axis is logarithmic and reversed in direction, so that $\bar{z}(0)$ decreases on passing to the right along the axis. The corresponding (η, λ) - plot is shown in Figure 11, which demonstrates the existence of three states for all sufficiently large values of λ . In this respect it differs from earlier studies of the symmetric states,¹⁸ which find an interval of multiplicity bounded both above and below. This difference arises from the fact that our calculations are performed at constant values of p and q , which means that the heat and mass transfer coefficients at the surfaces do not change with the slab thickness, while the earlier computations were performed at constant Sherwood and Nusselt numbers, in which case the transfer coefficients are inversely proportional to the thickness. Thus the apparent difference merely reflects a different mode of presenting the results.

For different values of the physical parameters, the peak on the lower curve in Figure 11 could develop to the

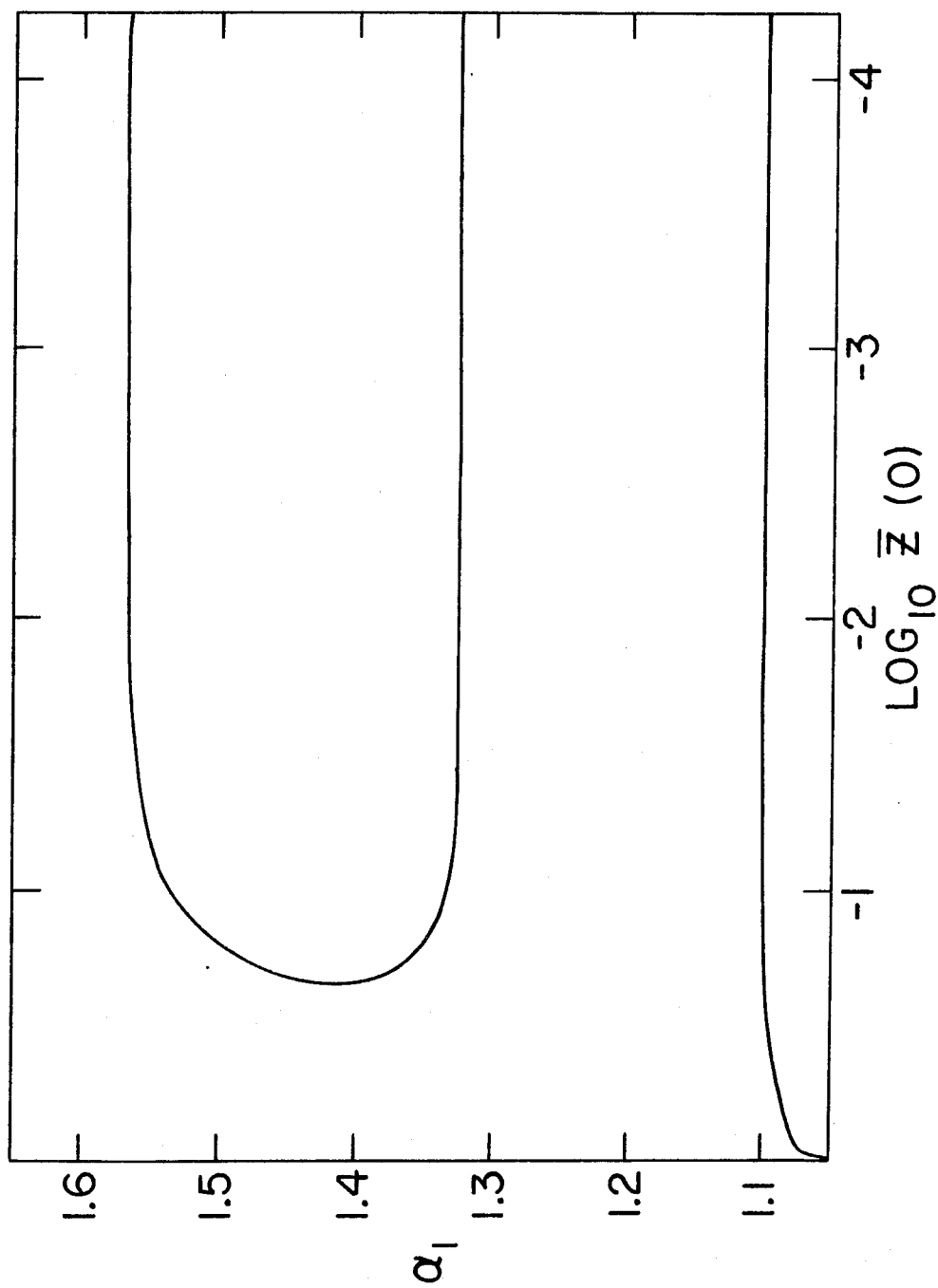


FIGURE 10: Curves $M=0$ and $N=0$; $\alpha_2 = 0$

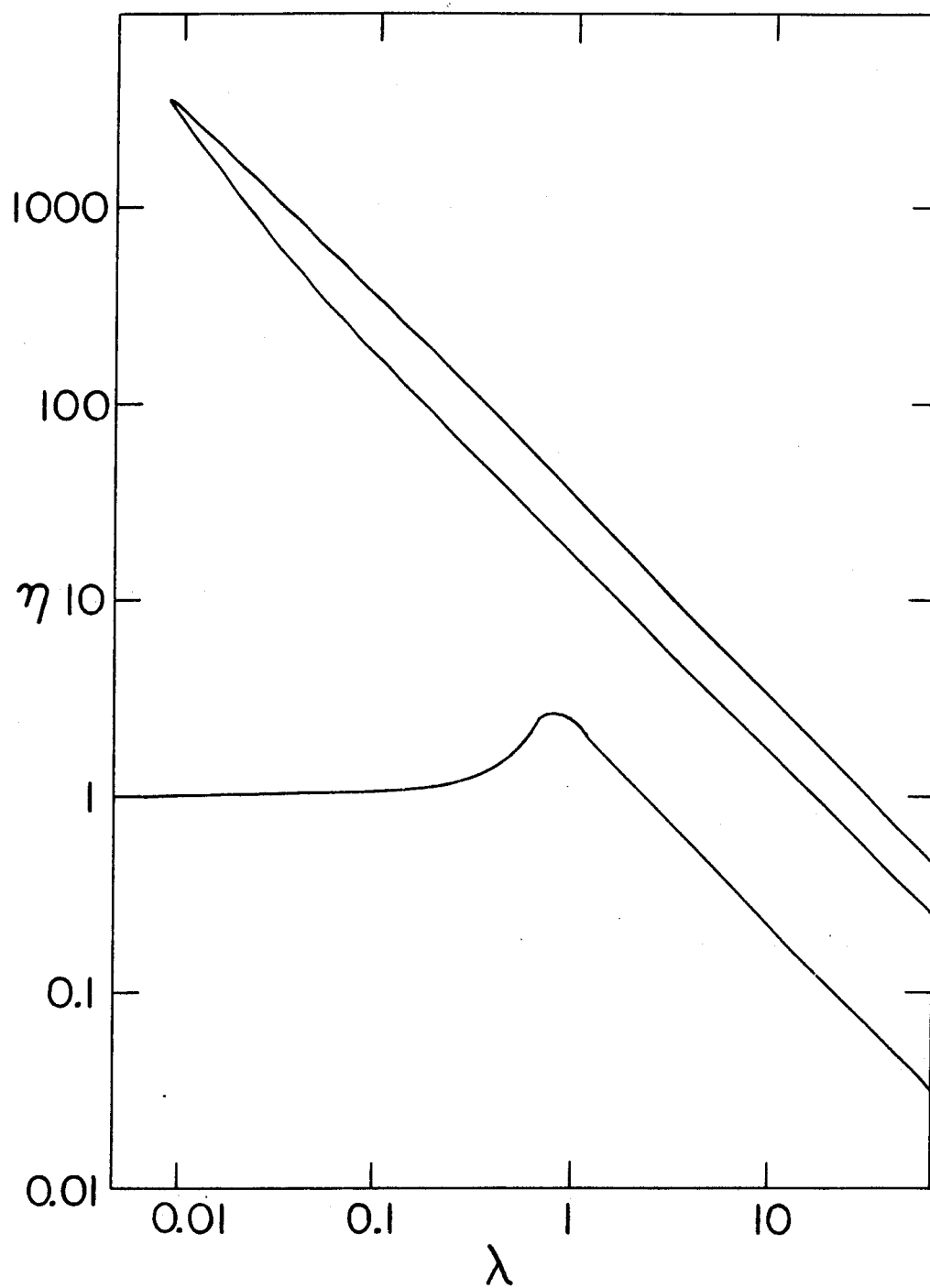


FIGURE 11: Thiele Modulus-Effectiveness Factor for Symmetric Solutions

point that the curve reflexes, thus having an interval in which there are five symmetric steady states, as reported by Hatfield and Aris.¹⁸

Figure 12 shows the $M=0$ and $N=0$ curves for $\alpha_2 = 0.02$, and it is seen that there are just four intersection points (numbered 1 to 4), each corresponding to an asymmetric state. Note that there is a substantial change of scale on the $\bar{z}(0)$ axis at $\bar{z}(0) = 10^{-1}$ in order to accommodate on a single diagram both the intersection points and the behavior of the curves for large values of $\bar{z}(0)$. The great disparity in scale between the different regions of interest is a major problem in unravelling and depicting the behavior of the system as α_2 increases. To clarify this, Figure 13 shows sketches of the $M=0$ and $N=0$ curves for successively increasing values of α_2 , distorted to avoid the scale problem, but otherwise true representations of the interrelation of the curves.

Figure 13a corresponds to Figure 10, with $\alpha_2 = 0$, and Figure 13b to Figure 12. As α_2 increases, the shapes of both curves change, as can be seen from Figure 14, which shows the computed curves for $\alpha_2 = 0.09$. However, no major qualitative change occurs until the central salient of the $N=0$ curve retracts far enough to eliminate the intersection points 2 and 4 as shown in Figure 13c. A further increase in α_2 causes the salient to retract so far that intersections 1 and 3 are also eliminated, as shown in Figure 13d.

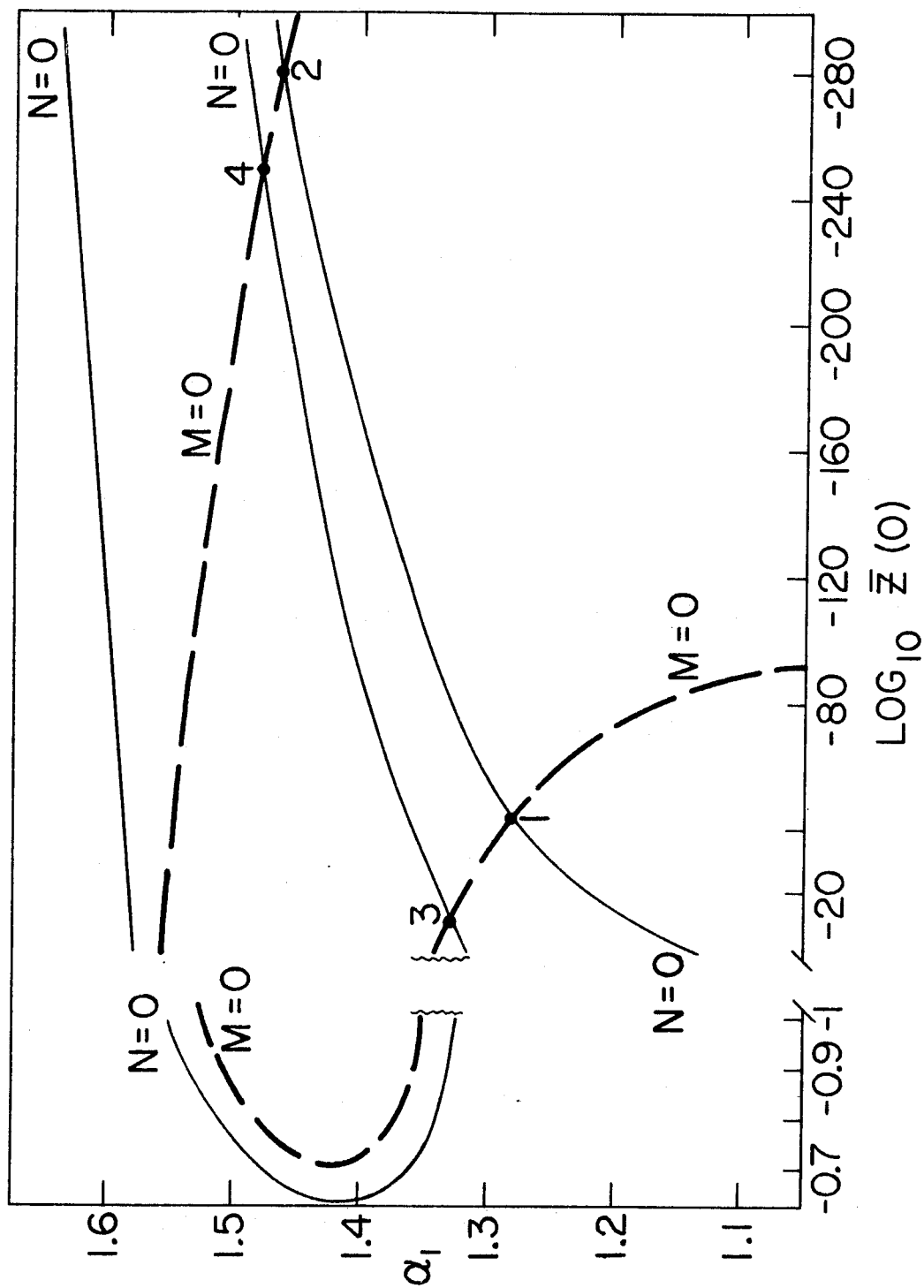
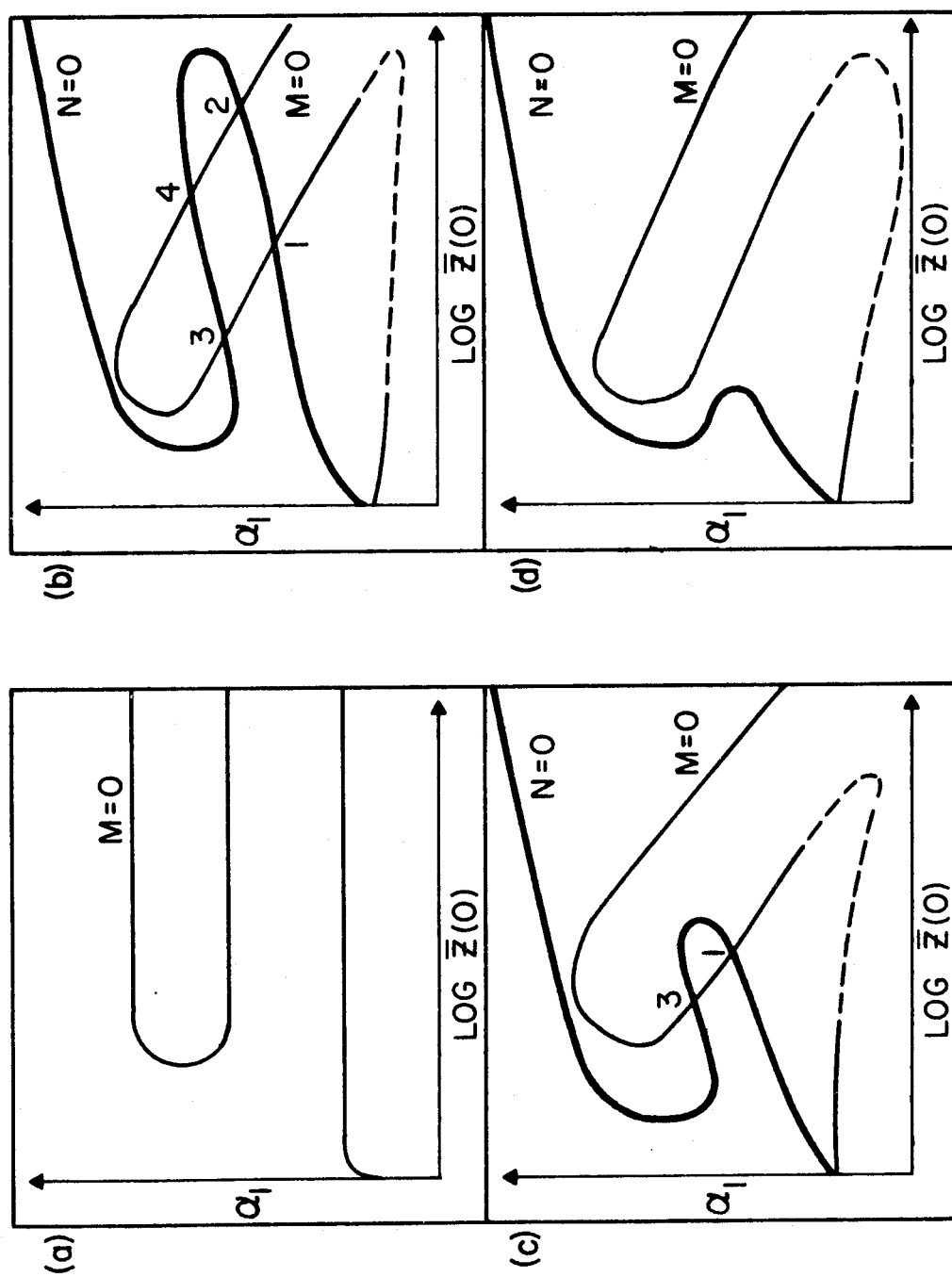


FIGURE 12: Curves $M=0$ and $N=0$; $\alpha_2 = 0.02$

FIGURE 13: Sketches of Curves $M=0$ and $N=0$

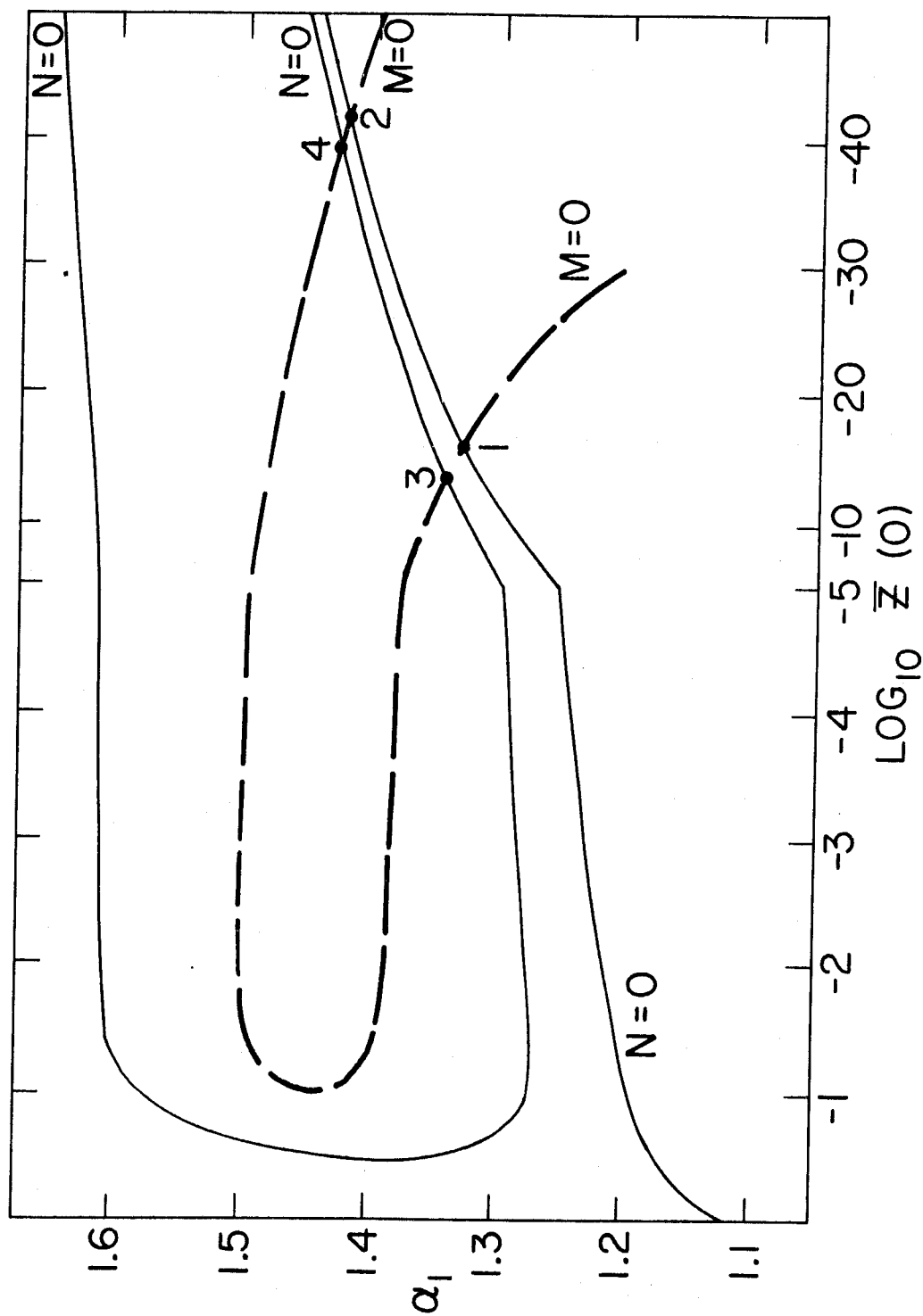


FIGURE 14: Curves $M=0$ and $N=0$; $\alpha_2 = 0.09$

Thus, there is a maximum value of α_2 beyond which no asymmetric states may exist. Figure 15 shows the computed curves for $\alpha_2 = 0.11$, when the situation corresponds to the sketch of Figure 13d.

Note that the portion of the $M=0$ curve indicated by a broken line in Figures 13b, 13c, and 13d is speculative. Computations were not carried out in this region, since it encompasses no intersections of the curves, and the corresponding parts of the $M=0$ curve are therefore absent from Figures 12, 14, and 15.

Figure 16 shows the one-sided effectiveness factors for the asymmetric states, and they are seen to fall into three branches, one indicated by a continuous curve, one by a broken curve, and one by a chain-dotted curve. As $\lambda \rightarrow \infty$ the continuous curves approach the effectiveness factors of the upper and middle symmetric states, as can be seen by comparing Figure 16 with Figure 11. It is therefore appropriate to refer to the branch represented by the continuous curve as the hm (high-medium) branch of asymmetric states. Similarly, the branch represented by the broken curve will be referred to as the hl (high-low) branch, and the branch represented by the chain-dotted curve as the ml (medium-low) branch. Referring to the numbering of the intersection points of $M=0$ and $N=0$ curves in Figure 13, points 1 and 3 always generate solutions belonging to the ml branch, point 2 gives solutions on the hl branch and point 4 gives solutions

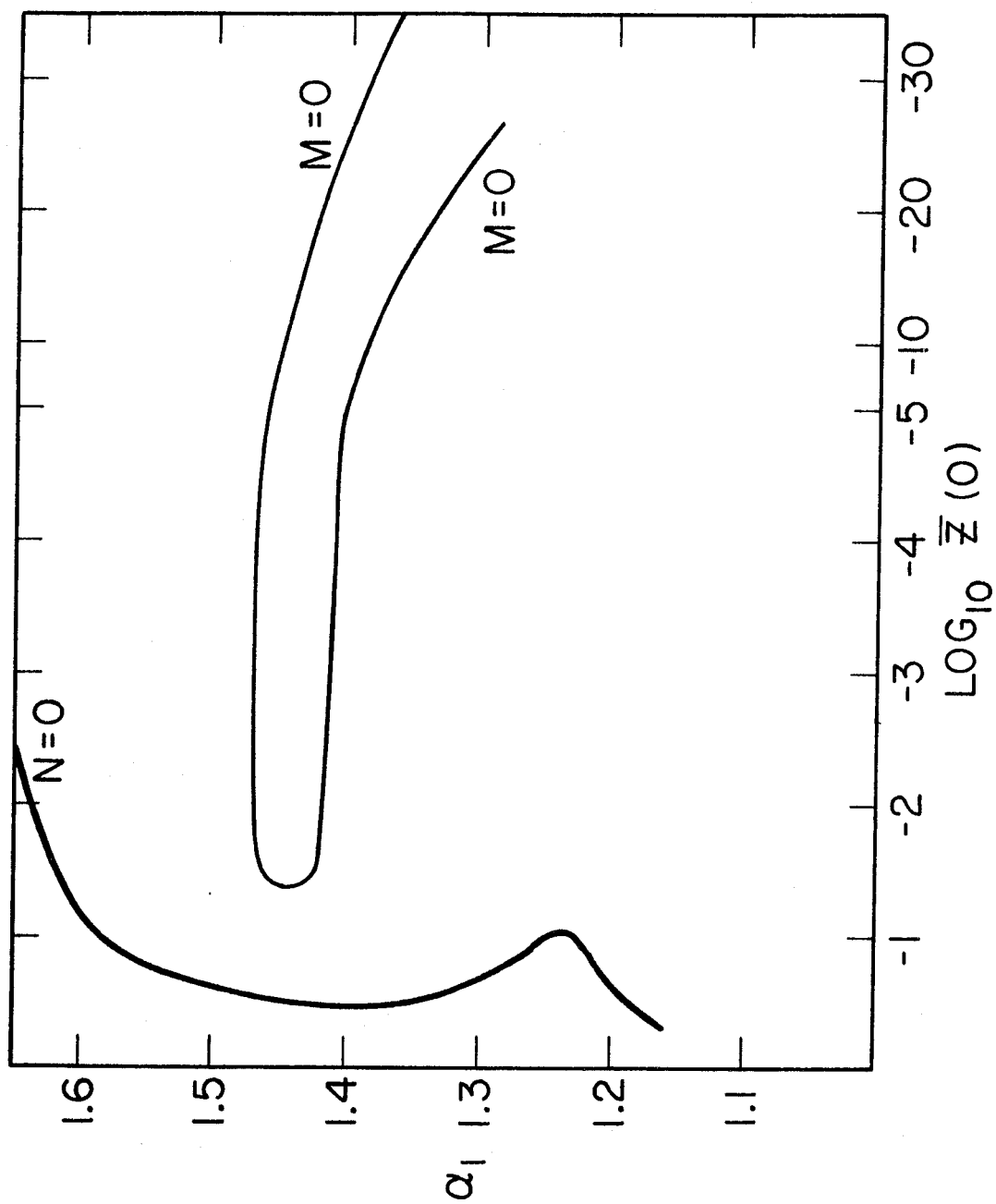


FIGURE 15: Curves $M=0$ and $N=0$; $\alpha_2 = 0.11$

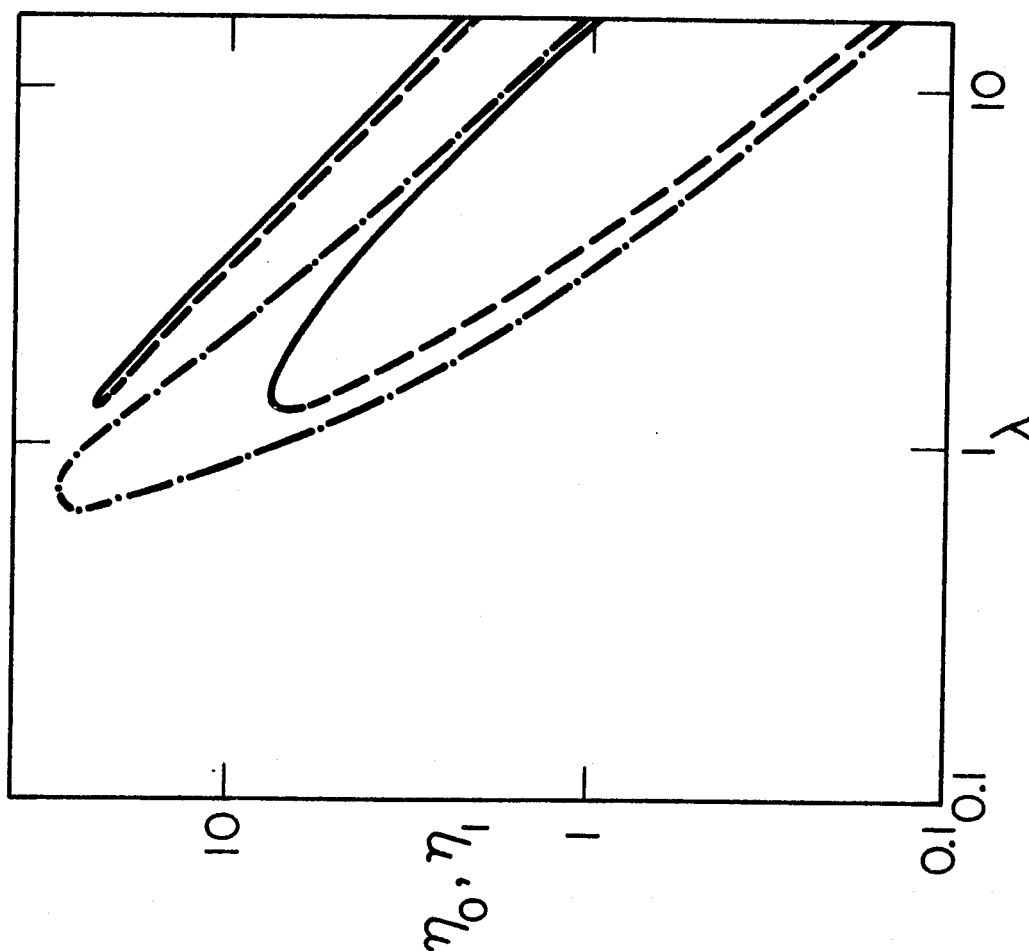


FIGURE 16: One-Sided Effectiveness Factors---Thiele Modulus Curves for Asymmetric Solutions

on the hm branch.

The ml branch is seen to extend to lower values of the Thiele modulus than the hm and hl branches, and it terminates by joining itself to form a loop. At the closure of the loop the one-sided effectiveness factors are identical, so the solution is symmetric; indeed, comparison of Figures 11 and 16 shows that this point belongs to the middle branch of symmetric states. In contrast, the hm and hl branches terminate by joining each other, so the corresponding solutions do not become symmetric where these branches terminate.

Combining the one-sided effectiveness factors to give the overall effectiveness factor and plotting the overall effectiveness factors for both symmetric and asymmetric states on a single diagram, we obtain Figure 17, the complete (η, λ) - diagram for the particular values of β, γ, p , and q chosen. Recalling that each asymmetric solution corresponds to two steady states, mirror images of each other in the center plane, it is seen that the λ - axis divides into four intervals with differing multiplicities of states. When $\lambda < \lambda_1$, there is a unique symmetric state. When $\lambda_1 < \lambda < \lambda_2$, there are three states, all symmetric. When $\lambda_2 < \lambda < \lambda_3$, there are five states, three symmetric and two asymmetric, the asymmetric states being mirror images. Finally, when $\lambda_3 < \lambda$, there are nine states, three of which are symmetric while the remaining six can be grouped into three pairs of mirror images.

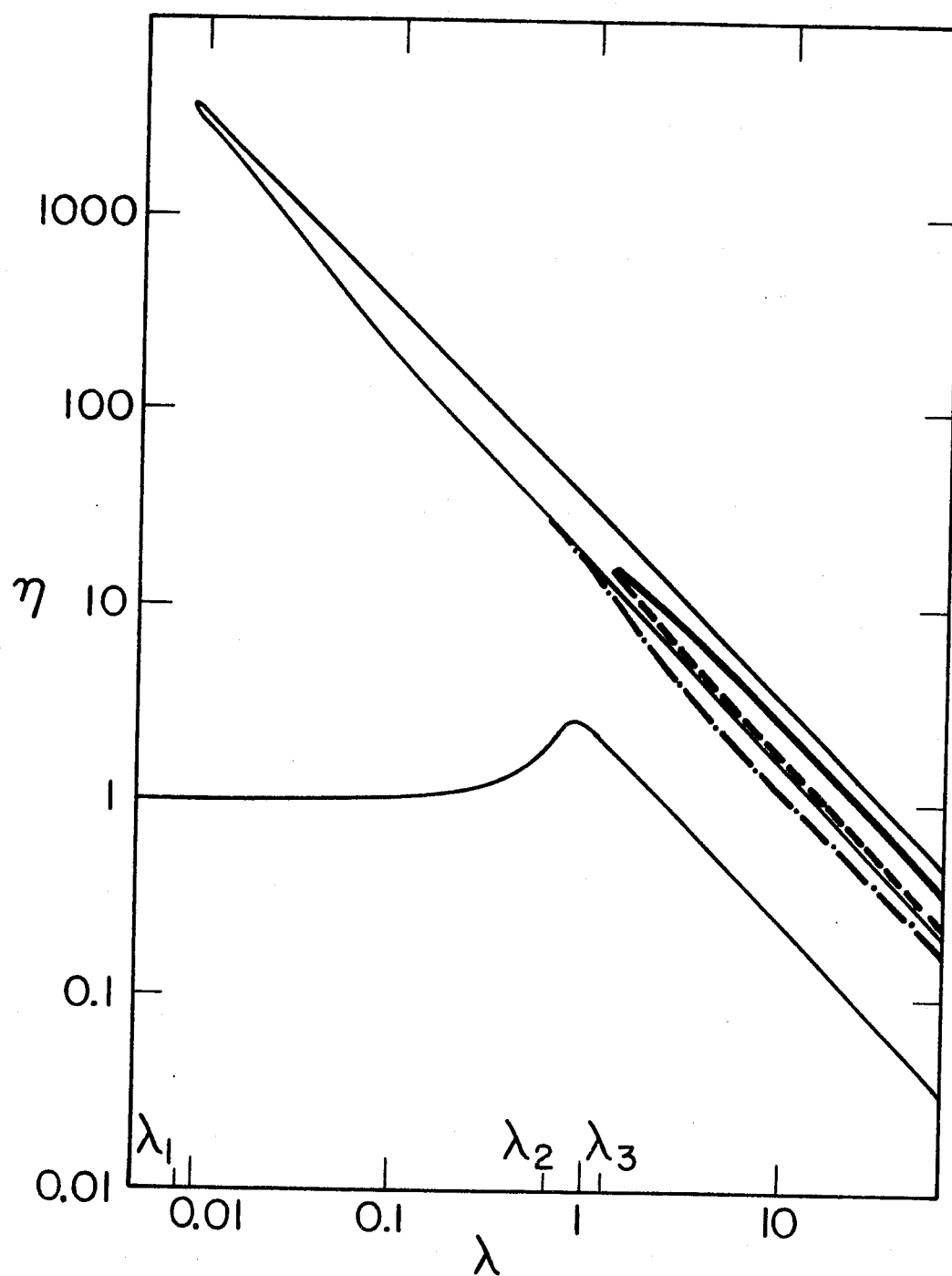


FIGURE 17: Complete Thiele-Modulus-Effectiveness Factor Diagram

A comparison of our results with those of Pis'men and Kharkats⁴¹ reveals that the branching of asymmetric states is the same in both cases. Furthermore, Pis'men and Kharkats found that two of their asymmetric branches contained unstable states while the third was stable. Their stable branch corresponds to the h1 branch in the present work, and it is intuitively reasonable that states of this branch should be stable, at least for sufficiently large λ . A formal analysis of stability for the solutions presented here is carried out in the next chapter.

Figure 18 shows $\bar{z}(\xi)$ and $\bar{y}(\xi)$ for one particular asymmetric state, namely that corresponding to the intersection point labelled 1 in Figure 14. This belongs to the m1 branch of solutions. Indeed, referring to Figure 13 intersection points labelled 1 and 3 in all cases generate solutions belonging to the m1 branch. The intersection point labelled 2 gives solutions of the h1 branch, and the corresponding $\bar{z}(\xi)$ and $\bar{y}(\xi)$ are mapped in Figure 19. The steady states profiles, $\bar{z}(\xi)$ and $\bar{y}(\xi)$, shown in Figure 20, correspond to the point labelled 4, which gives solutions of the hm branch.

Finally, in Table 2 values of α_1 and $\log_{10} \bar{z}(0)$ of the intersection points and their corresponding effectiveness factors and Thiele moduli are tabulated for a range of α_2 .

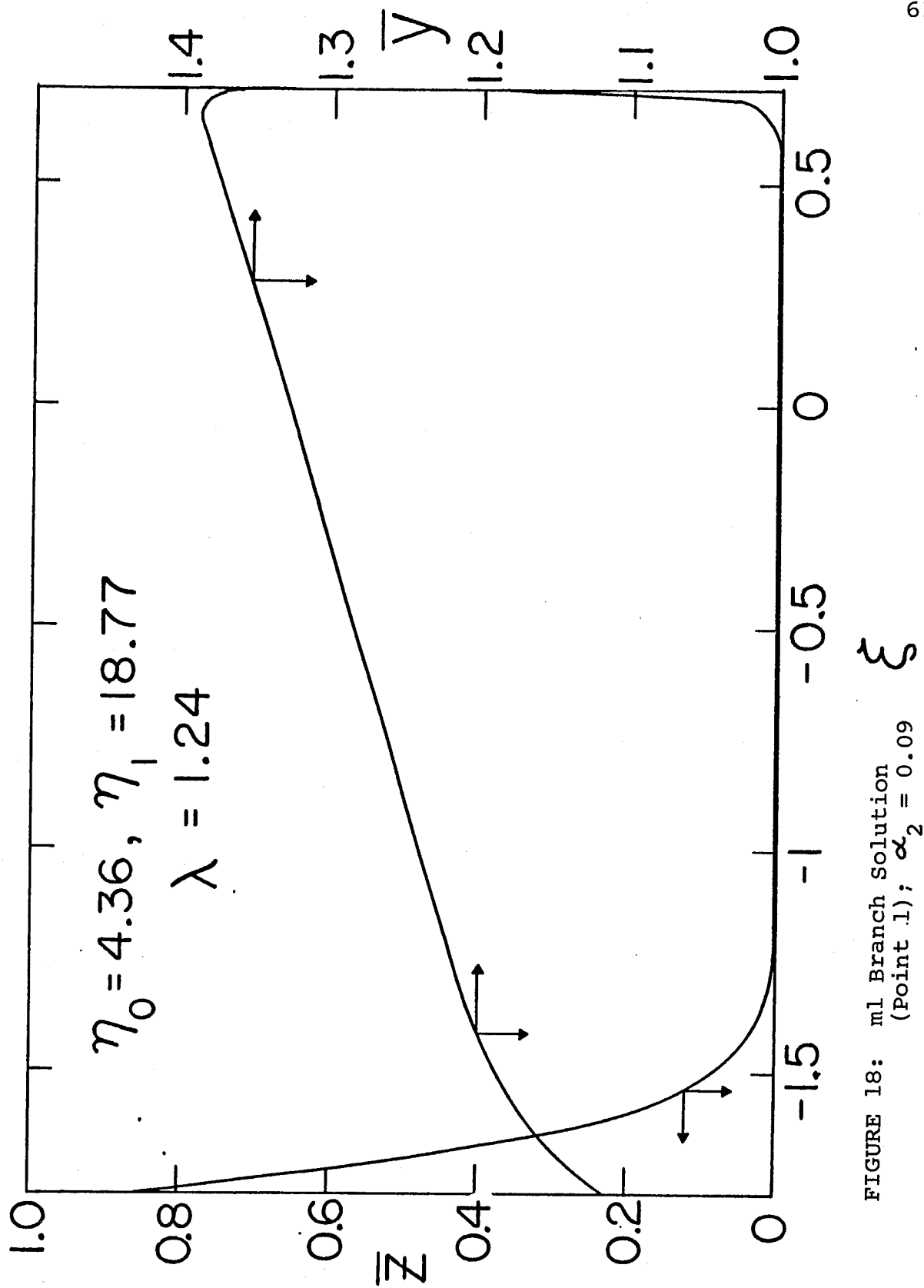


FIGURE 18: m1 Branch Solution
 (Point 1); $\alpha_2 = 0.09$

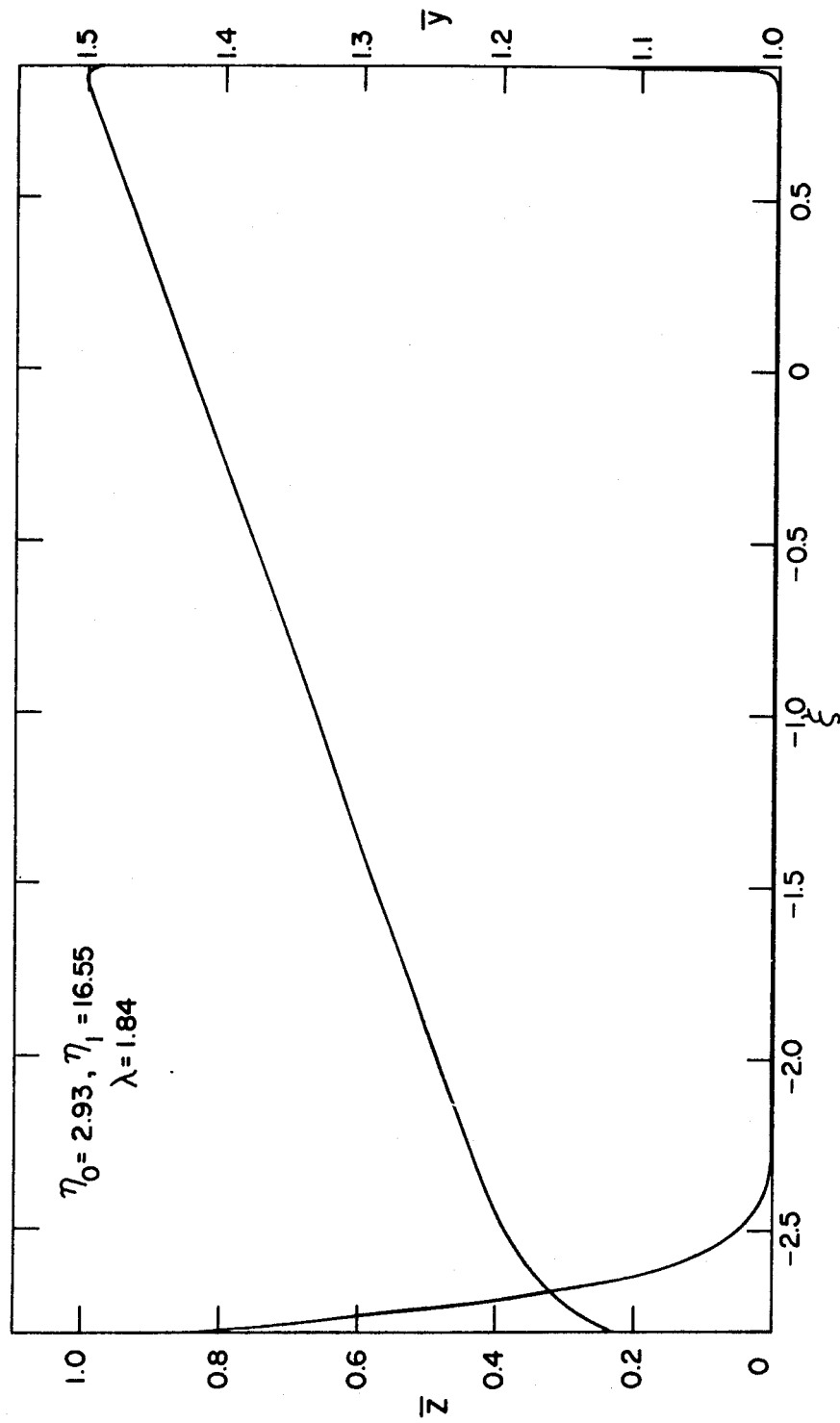


FIGURE 19: h1 Branch Solution (Point 2); $\alpha_2 = 0.09$

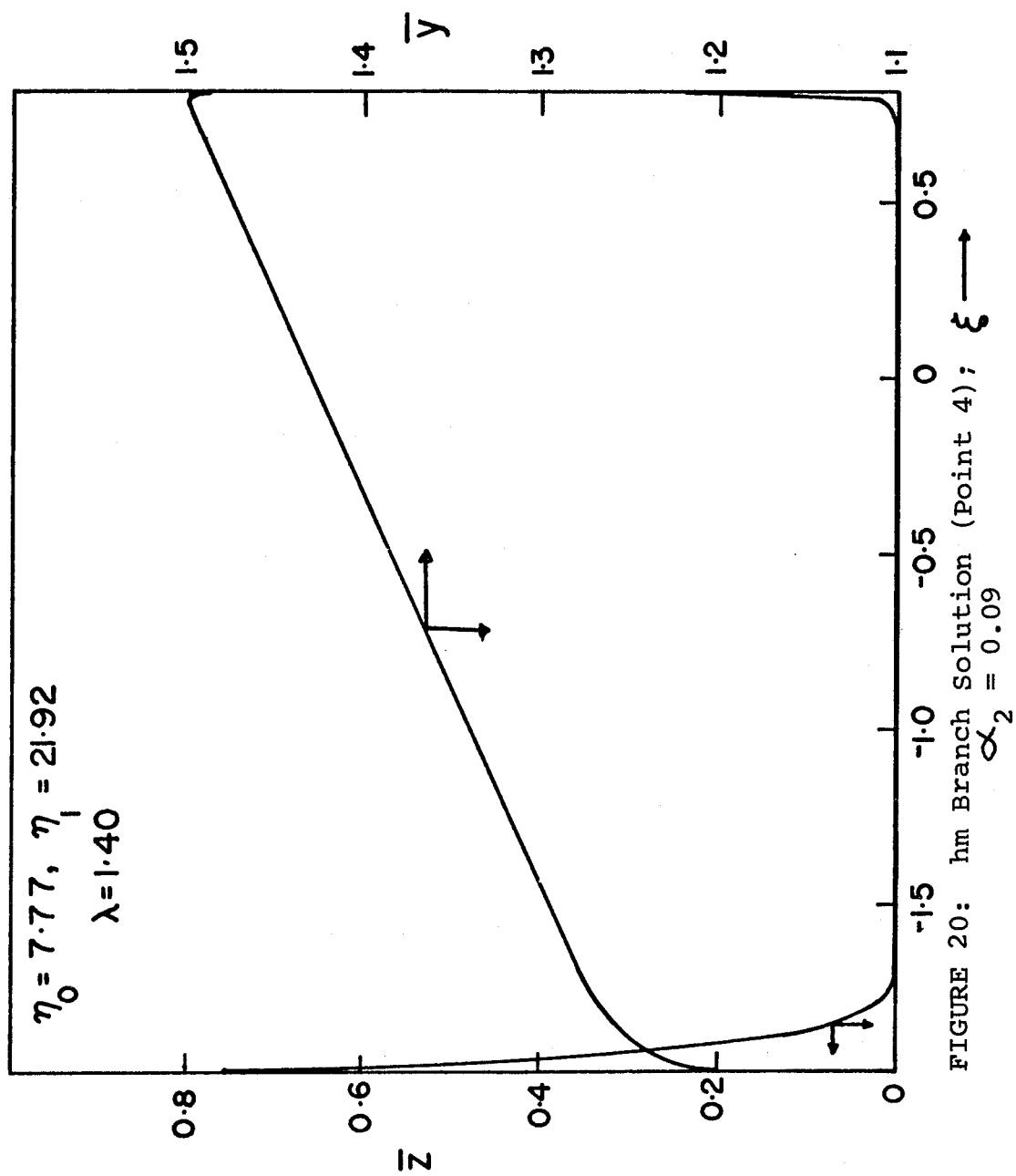


TABLE 2

INTERSECTION POINTS FOR $p = 40$, $q = 4$, $\beta = 0.0667$
AND $\gamma = 29.5$

α_2	points	α_1	$\log_{10} \bar{z}(0)$	η_0	η_1	λ
0.02	1	1.2772	-43.69	0.472	3.255	5.679
0.02	2	1.4659	-283.32	0.242	2.968	11.067
0.02	3	1.3254	-10.35	24.614	28.308	0.649
0.02	4	1.4787	-245.13	2.623	5.397	6.099
0.04	1	1.2902	-24.72	1.139	6.939	2.945
0.04	2	1.4555	-129.16	0.622	6.208	5.214
0.04	3	1.3286	-11.22	21.400	28.667	0.689
0.04	4	1.4676	-115.63	4.817	10.583	3.059
0.06	1	1.3042	-18.82	2.068	11.120	1.894
0.06	2	1.4440	-77.47	1.210	9.823	3.237
0.06	3	1.3326	-11.60	18.766	29.567	0.712
0.06	4	1.4545	-70.24	6.504	15.469	2.055
0.08	1	1.3204	-16.35	3.401	15.950	1.412
0.08	2	1.4307	-50.96	2.172	14.038	2.212
0.08	3	1.3389	-12.46	15.616	29.804	0.755
0.08	4	1.4390	-47.08	7.575	19.949	1.557
0.09	1	1.3299	-15.79	4.361	18.766	1.244
0.09	2	1.4230	-41.76	2.932	16.548	1.848
0.09	3	1.3434	-13.16	13.692	29.471	0.792
0.09	4	1.4297	-39.09	7.774	21.916	1.395

TABLE 2 (Continued)

α_2	points	α_1	$\log_{10} \bar{z}(0)$	η_0	η_1	λ
0.10	1	1.3417	-15.62	5.775	22.076	1.101
0.10	2	1.4139	-33.84	4.169	19.684	1.523
0.10	3	1.3490	-14.22	11.222	28.452	0.854
0.10	4	1.4182	-32.46	7.477	28.405	1.281
0.1056	1	1.3511	-15.45	7.988	25.687	0.970
0.1056	2	1.4088	-29.40	5.988	22.776	1.296
0.1056	3	1.3518	-15.40	8.348	26.106	0.955
0.1056	4	1.4092	-29.28	6.314	23.144	1.276

IV. STABILITY ANALYSIS FOR STEADY STATES ASYMMETRIC WITH RESPECT TO REFLECTION ACROSS CENTER PLANE

A. Introduction

In the previous chapter a numerical study of the complete set of steady states with surface resistances was undertaken. Symmetry about the center plane was not assumed and the existence of asymmetric steady states in the porous slab was demonstrated.

An obvious question that arises is one of stability, as the physical significance of the steady states depends on this. The most common method of stability analysis for the distributed system is to confine attention to small perturbations about the steady state. From the resulting system of linear partial differential equations, an eigenvalue ordinary differential equation problem can be obtained by separation of variables. Instability can then be established by considering the signs of the real parts of the eigenvalues of the non-self adjoint eigenvalue problem so generated. A systematic means for the analysis of the eigenvalue equations, such as Sturm theory or topological methods, is lacking for non-self adjoint problems, and the eigenvalues are usually estimated by the Galerkin method. The question of completeness of the set of eigenfunctions for this problem is still a matter of investigation. Thus there is no guarantee that the critical eigenvalue is a member of the set being approximated. In contrast, the self adjoint eigenvalue problem has

real eigenvalues and the Galerkin procedure reduces to the Rayleigh-Ritz method. For this self adjoint problem, the eigenvalues are approximated successively starting with the largest one (see Sagan⁴⁴).

Another approach that has been used is to integrate the linearized perturbation equations numerically, forward in time. It is hoped that these equations model the system accurately for small initial perturbations of the steady state. Though the failure to find a perturbation that grows is no guarantee of stability, since it is not possible to consider all conceivable initial perturbations, the existence of a perturbation that grows is a good indication of instability.

In this work, stability of the steady state will be analysed by applying some sufficient conditions given by Nishimura and Matsubara,³⁹ and by numerically integrating the linearized perturbation equations.

B. Method of Nishimura and Matsubara

We linearize the unsteady state Equations (3.7) to (3.12) about the steady state using the first two terms of the Taylor series. Let $u_1(\xi, \tau)$ and $u_2(\xi, \tau)$ represent the concentration and temperature perturbations from the steady states. Thus,

$$z(\xi, \tau) = \bar{z}(\xi) + u_1(\xi, \tau) \quad (4.1)$$

$$y(\xi, \tau) = \bar{y}(\xi) + u_2(\xi, \tau) \quad (4.2)$$

where $\bar{z}(\xi)$ and $\bar{y}(\xi)$ are the steady state dimensionless concentration and temperature, respectively. Let

$$f(z, y) = z \exp \left\{ \frac{\gamma(y-1)}{y} \right\} \quad (4.3)$$

Linearizing about the steady state

$$f(z, y) = \bar{f} + \left(\frac{\partial f}{\partial z} \right)_e u_1 + \left(\frac{\partial f}{\partial y} \right)_e u_2 \quad (4.4)$$

where

$$\bar{f} = f(\bar{z}, \bar{y}) \quad (4.5)$$

$$\left(\frac{\partial f}{\partial z} \right)_e = \frac{\partial f}{\partial z}(\bar{z}, \bar{y}) \quad (4.6)$$

$$\left(\frac{\partial f}{\partial y} \right)_e = \frac{\partial f}{\partial y}(\bar{z}, \bar{y}) \quad (4.7)$$

From the unsteady state Equations (3.7) to (3.12), u_1 and u_2 satisfy the following equations

$$\frac{\partial u_1}{\partial \tau} = \frac{\partial^2 u_1}{\partial \xi^2} - \left(\frac{\partial f}{\partial z} \right)_e u_1 - \left(\frac{\partial f}{\partial y} \right)_e u_2 \quad (4.8)$$

$$\text{Le} \frac{\partial u_2}{\partial \tau} = \frac{\partial^2 u_2}{\partial \xi^2} + \beta \left(\frac{\partial f}{\partial z} \right)_e u_1 + \beta \left(\frac{\partial f}{\partial y} \right)_e u_2 \quad (4.9)$$

$$\tau > 0, \xi \in (\xi_0, \xi_1)$$

with

$$\left(\frac{\partial u_1}{\partial \xi} \right)_{\xi_0} = p u_1(\xi_0) \quad (4.10)$$

$$\left(\frac{\partial u_2}{\partial \xi} \right)_{\xi_0} = q u_2(\xi_0) \quad (4.11)$$

$$\left(\frac{\partial u_1}{\partial \xi} \right)_{\xi_1} = -p u_1(\xi_1) \quad (4.12)$$

$$\left(\frac{\partial u_2}{\partial \xi} \right)_{\xi_1} = -q u_2(\xi_1) \quad (4.13)$$

In a compact matrix notation this becomes

$$L \underline{U} = \frac{\partial \underline{U}}{\partial \tau} - \frac{\partial}{\partial \xi} \left(P \frac{\partial \underline{U}}{\partial \xi} \right) - Q \underline{U} = 0 \quad (4.14)$$

$$\tau > 0 \quad \xi \in (\xi_0, \xi_1)$$

with

$$P \frac{\partial \underline{U}}{\partial \xi} - S_1 \underline{U} = 0 \quad \xi = \xi_0 \quad (4.15)$$

$$P \frac{\partial \underline{U}}{\partial \xi} - S_2 \underline{U} = 0 \quad \xi = \xi_1 \quad (4.16)$$

where

$$P = \begin{bmatrix} 1 & 0 \\ 0 & 1/Le \end{bmatrix} \quad (4.17)$$

$$Q = \begin{bmatrix} \left(\frac{\partial f}{\partial z}\right)_e & \left(\frac{\partial f}{\partial y}\right)_e \\ -\frac{\beta}{Le} \left(\frac{\partial f}{\partial z}\right)_e & -\frac{\beta}{Le} \left(\frac{\partial f}{\partial y}\right)_e \end{bmatrix} \quad (4.18)$$

$$S_1 = \begin{bmatrix} p & 0 \\ 0 & q/Le \end{bmatrix} \quad (4.19)$$

$$S_2 = \begin{bmatrix} -p & 0 \\ 0 & -q/Le \end{bmatrix} \quad (4.20)$$

and

$$\underline{U} = \begin{bmatrix} u_1 \\ u_2 \end{bmatrix} \quad (4.21)$$

These matrices can easily be identified with those used by Nishimura and Matsubara.³⁹ It is convenient to introduce a symmetric matrix

$$\hat{Q} = \frac{1}{2} (Q^T + Q) \quad (4.22)$$

where Q^T is the transpose of matrix Q . The matrices P , S_1 , and S_2 are already symmetric. A sufficient condition for the stability of the steady state has been given by Nishimura and Matsubara.³⁹ Introducing an auxiliary matrix $V(\xi)$ defined by the differential equation

$$\frac{d}{d\xi} \left(P \frac{dV}{d\xi} \right) - \hat{Q}V = 0 \quad (4.23)$$

together with

$$V = I \quad \text{at } \xi = \xi_0 \quad (4.24)$$

and

$$P \frac{dV}{d\xi} - S_1 V = 0 \quad \text{at } \xi = \xi_0 \quad (4.25)$$

where I is the identity matrix, they show that a sufficient condition for the steady state to be asymptotically stable is that both the following conditions hold simultaneously:

$$(i) \quad V(\xi) \text{ is nonsingular on } [\xi_0, \xi_1], \text{ and} \quad (4.26)$$

$$(ii) \quad \text{the matrix } \left[P \frac{dV}{d\xi} V^{-1} - S_2 \right] \text{ is positive definite at} \\ \xi = \xi_1 \quad (4.27)$$

For the problem under investigation the size of the matrix V is 2×2 . Equation (4.23) represents four second order

ordinary differential equations with initial conditions given by Equations (4.24) and (4.25). Computationally, the system was solved as a set of eight first order equations by the Runge-Kutta-Merson method. The automatic step change mechanism was not used because it was found to be too conservative. The test was applied to high, medium, and low symmetric steady states, and to high-low, medium-low, and high-medium asymmetric steady states. The asymmetric steady states used were those represented by the intersection points 2, 3, and 4 on Figure 14 and which are mapped in Figures 18, 19, and 20.

In all cases considered, the first condition, namely that the matrix $V(\xi)$ be non-singular was violated. However, since the criterion developed by Nishimura and Matsubara is merely sufficient for stability, no positive conclusion can be drawn from these results.

Thus the use of Nishimura and Matsubara's sufficient conditions for stability leaves the question of stability of the steady states open.

C. Continuous Time Galerkin Approximation to Linearized Perturbation Equations

Stability can be investigated by the direct numerical integration, forward in time, of the linearized perturbation Equations (4.8) to (4.13). The discovery of any small perturbation of the steady state which grows is an indication that the steady state is unstable. Since it is impossible

to consider all conceivable perturbations, the failure to find a perturbation that grows does not guarantee stability.

The method used to integrate Equations (4.8) to (4.13) (or the system of Equations (4.14) to (4.16)) numerically was the Galerkin method (see Collatz⁷ and Kantorovich and Krylov²⁷). Hermite cubic polynomials were used as basis functions. A brief description of these follows. Let

$\Delta: x_0 = x_1 < x_2 < \dots < x_{r+1} = L$ denote any partition of $[x_0, L]$ with grid points x_i . The Hermite cubic polynomials are a collection of real piecewise polynomial functions $w(x)$ defined on $[x_0, L]$ such that $w(x) \in C^1([x_0, L])$ and the polynomial is of degree three on each subinterval $[x_i, x_{i+1}]$.

The defining equations are

$$w_{2i-1}(x) = \begin{cases} 1 - 3 \left(\frac{x-x_i}{x_i-x_{i-1}} \right)^2 + 2 \left(\frac{x-x_i}{x_i-x_{i-1}} \right)^3 & x_{i-1} \leq x \leq x_i \\ 1 - 3 \left(\frac{x-x_i}{x_{i+1}-x_i} \right)^2 + 2 \left(\frac{x-x_i}{x_{i+1}-x_i} \right)^3 & x_i \leq x \leq x_{i+1} \\ 0 & x \in \left\{ [x_0, L] - [x_{i-1}, x_{i+1}] \right\} \end{cases} \quad (4.28)$$

$$w_{2i}(x) = \begin{cases} (x-x_{i-1}) \left(1 + \frac{x-x_i}{x_i-x_{i-1}} \right)^2 & x_{i-1} \leq x \leq x_i \\ (x-x_i) \left(1 - \frac{x-x_i}{x_{i+1}-x_i} \right)^2 & x_i \leq x \leq x_{i+1} \\ 0 & x \in \left\{ [x_0, L] - [x_{i-1}, x_{i+1}] \right\} \end{cases} \quad (4.29)$$

$i = 1, 2, \dots, N$

These functions are graphed in Figure 21. At any node point x_i the value of the function w_{2i-1} is 1 and the slope of the function w_{2i} is 1. We can thus assign values to the coefficients of $w_{2i-1}(x_i)$ and $w_{2i}(x_i)$ at each node x_i , so that the piece-wise cubic polynomials agree with the value of the function being approximated at each node point, and also with the slope of the function at each node.

We define the Galerkin approximation $\underline{G}(\xi, \tau)$ to the solution of (4.14) to (4.16) by requiring that \underline{G} lie in a finite dimensional space of functions and be such that $\underline{L}\underline{U}$ (as defined by Equation (4.14)) is orthogonal to this space for each τ . This type of Galerkin approximation can be determined by a system of ordinary differential equations. Using Hermite cubic polynomials as basis functions, Douglas and Dupont¹² have shown that the order of convergence is $O(h^3 + \Delta t^2)$, where h is the mesh size and Δt the time step. Recently, Wheeler⁴⁷ has shown that the method is, in fact, fourth order with respect to h . This is a considerable improvement over the finite-difference methods. The use of the Hermite functions also ensures that the solution is a smooth function which is piecewise polynomial, and this means the smooth graphical representation of the results can be obtained.

The practical implementation of the Galerkin method for the problem under consideration is based on Douglas and Dupont¹² and Douglas.¹¹ The basis functions w_1, w_2, \dots, w_{2r}

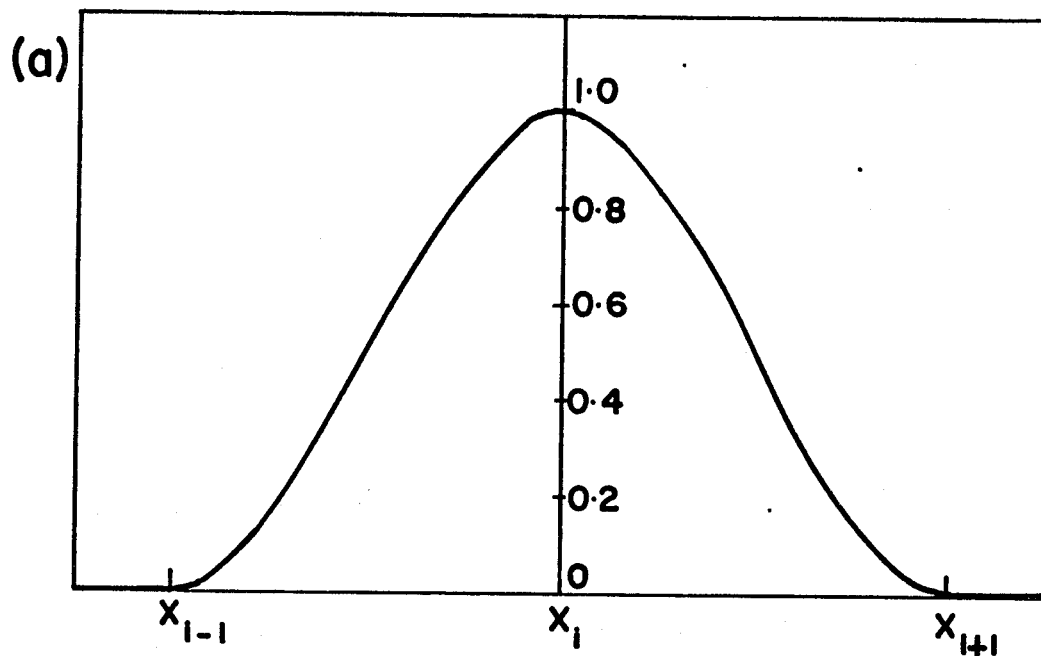


FIGURE 21a: Hermite Cubic Polynomial-Value Function,
 $w_{2i-1}(x)$

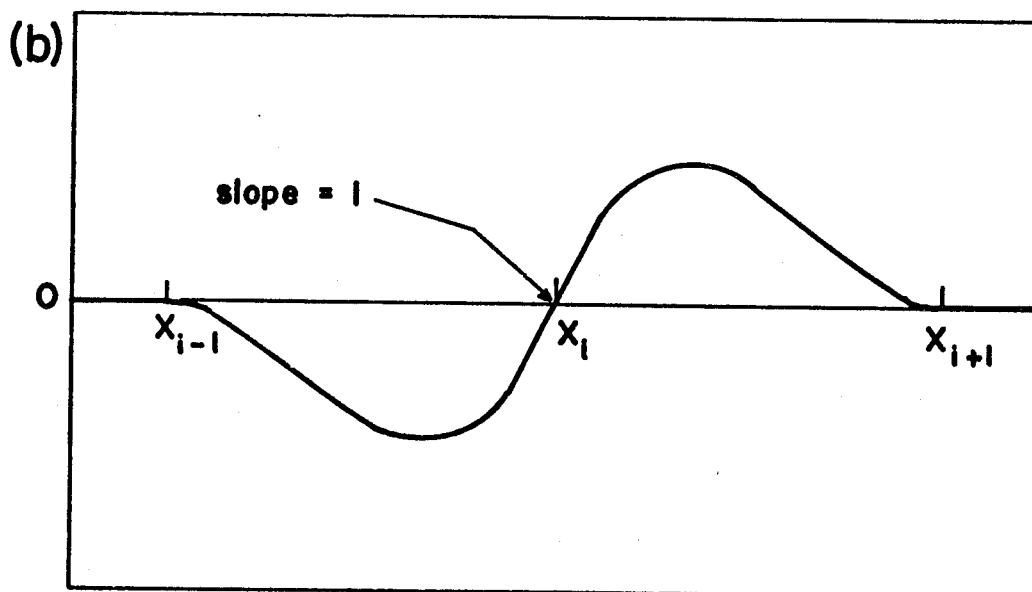


FIGURE 21b: Hermite Cubic Polynomial-Slope Function,
 $w_{2i}(x)$

are linearly independent. Denote by \mathcal{W} the subspace spanned by w_1, w_2, \dots, w_{2r} , where r is the number of grid points. That is,

$$\mathcal{W} = \text{sp} \{ w_1, w_2, \dots, w_{2r} \} \quad (4.30)$$

The variables u_1 and u_2 of Equations (4.8) to (4.13) are approximated by the functions $U(\xi, \tau)$ and $W(\xi, \tau)$, respectively, where

$$U(\xi, \tau) = \sum_{i=1}^{2r} \alpha^i(\tau) w_i(\xi) \quad (4.31)$$

and

$$W(\xi, \tau) = \sum_{i=1}^{2r} \beta^i(\tau) w_i(\xi) \quad (4.32)$$

$\left(\frac{\partial u_1}{\partial \xi} \right)_{\xi_0}$, $\left(\frac{\partial u_2}{\partial \xi} \right)_{\xi_0}$, $\left(\frac{\partial u_1}{\partial \xi} \right)_{\xi_1}$, and $\left(\frac{\partial u_2}{\partial \xi} \right)_{\xi_1}$ are specified by

Equations (4.10) to (4.13), hence the coefficients of $w_2(\xi)$ and $w_{2r}(\xi)$ can be calculated. We are left with $(2r-2)$ unknowns $\beta^i(\tau)$ and $(2r-2)$ unknowns $\alpha^i(\tau)$. The Galerkin method gives relations that can be used to calculate these $\alpha^i(\tau)$ and $\beta^i(\tau)$.

Consider first the Equation (4.8)

$$\frac{\partial u_1}{\partial \tau} = \frac{\partial^2 u_1}{\partial \xi^2} - A(\xi) u_1 - B(\xi) u_2 \quad (4.33)$$

where

$$A(\xi) = \left(\frac{\partial f}{\partial z} \right)_e \text{ and } B(\xi) = \left(\frac{\partial f}{\partial y} \right)_e \quad (4.34)$$

Define an inner product by

$$\langle w, v \rangle = \int_{\xi_0}^{\xi_1} w(x) \overline{v(x)} dx \quad (4.35)$$

we have

$$\left\langle \frac{\partial u_1}{\partial \tau}, w_i \right\rangle = \left\langle \frac{\partial^2 u_1}{\partial \xi^2}, w_i \right\rangle - \langle Au_1, w_i \rangle - \langle Bu_2, w_i \rangle \quad (4.36)$$

$$i \neq 2, 2r$$

Using the approximation for u_1 and u_2

$$\left\langle \frac{\partial U}{\partial \tau}, w_i \right\rangle = \left\langle \frac{\partial^2 U}{\partial \xi^2}, w_i \right\rangle - \langle AU, w_i \rangle - \langle BU, w_i \rangle \quad (4.37)$$

$$i \neq 2, 2r$$

$$w \in \mathcal{W}$$

Integrating the first term of the right-hand side by parts

$$\left\langle \frac{\partial^2 U}{\partial \xi^2}, w_i \right\rangle = \left. \frac{\partial U}{\partial \xi} w_i \right|_{\xi_0}^{\xi_1} - \left\langle \frac{\partial U}{\partial \xi}, \frac{dw_i}{d\xi} \right\rangle \quad (4.38)$$

Now

$$\left. \frac{\partial U}{\partial \xi} w_i \right|_{\xi_0}^{\xi_1} = 0 \text{ for } i \neq 1, 2r-1 \quad (4.39)$$

Since $w_i = 0$ at $\xi = \xi_0$ and at $\xi = \xi_1$ for $i \neq 1, 2r-1$, and

$$\left. \frac{\partial U}{\partial \xi} w_1 \right|_{\xi_0}^{\xi_1} = -p \alpha^1(\tau) \quad (4.40)$$

$$\left. \frac{\partial U}{\partial \xi} w_{2r-1} \right|_{\xi_0}^{\xi_1} = -p \alpha^{2r-1}(\tau) \quad (4.41)$$

Using the expansions for U and W and Equation (4.37), the continuous time Galerkin approximation becomes

$$\begin{aligned} \sum_{j=1}^{2r} \langle w_j, w_i \rangle \frac{d\alpha^j}{d\tau} + \sum_{j=1}^{2r} \langle w'_j, w'_i \rangle \alpha^j + \sum_{j=1}^{2r} \langle Aw_j, w_i \rangle \alpha^j \\ + \sum_{j=1}^{2r} \langle Bw_j, w_i \rangle \beta^j = \left. \frac{\partial U}{\partial \xi} w_i \right|_{\xi_0}^{\xi_1} \end{aligned} \quad (4.42)$$

$i \neq 2, 2r$

where the primes denote differentiation with respect to ξ .

The boundary conditions (4.10) and (4.12) give

$$\alpha^2(\tau) = p \alpha^1(\tau) \quad (4.43)$$

$$\alpha^{2r}(\tau) = -p \alpha^{2r-1}(\tau) \quad (4.44)$$

By a similar analysis, Equation (4.9) becomes

$$\begin{aligned} \text{Le} \sum_{j=1}^{2r} \langle w_j, w_i \rangle \frac{d\beta^j}{d\tau} + \sum_{j=1}^{2r} \langle w'_j, w'_i \rangle \beta^j - \beta \sum_{j=1}^{2r} \langle Bw_j, w_i \rangle \beta^j \\ - \beta \sum_{j=1}^{2r} \langle Aw_j, w_i \rangle \alpha^j = \frac{\partial W}{\partial \xi} w_i \bigg|_{\xi_0}^{\xi_1} \quad i \neq 2, 2r \quad (4.45) \end{aligned}$$

where

$$\frac{\partial W}{\partial \xi} w_i \bigg|_{\xi_0}^{\xi_1} = 0 \quad i \neq 1, 2r-1 \quad (4.46)$$

$$\frac{\partial W}{\partial \xi} w_1 \bigg|_{\xi_0}^{\xi_1} = -q \beta^1(\tau) \quad (4.47)$$

$$\frac{\partial W}{\partial \xi} w_{2r-1} \bigg|_{\xi_0}^{\xi_1} = -q \beta^{2r-1}(\tau) \quad (4.48)$$

while the boundary conditions (4.11) and (4.13) give

$$\beta^2(\tau) = q \beta^1(\tau) \quad (4.49)$$

$$\beta^{2r}(\tau) = -q \beta^{2r-1}(\tau) \quad (4.50)$$

Defining

$$\zeta_{ij} = \langle w_i, w_j \rangle \quad (4.51)$$

$$\epsilon_{ij} = \langle w'_i, w'_j \rangle \quad (4.52)$$

$$a_{ij} = \langle Aw_j, w_i \rangle \quad (4.53)$$

$$b_{ij} = \langle Bw_j, w_i \rangle \quad (4.54)$$

the continuous time Galerkin approximation to Equations (4.8) to (4.13) is

$$\sum_{j=1}^{2r} \zeta_{ij} \frac{d\alpha^j}{d\tau} + \sum_{j=1}^{2r} (\epsilon_{ij} + a_{ij}) \alpha^j + \sum_{j=1}^{2r} b_{ij} \beta^j = \frac{\partial U}{\partial \xi} w_i \bigg|_{\xi_0}^{\xi_1} \quad i \neq 2, 2r \quad (4.55)$$

$$\begin{aligned} \text{Le} \sum_{j=1}^{2r} \zeta_{ij} \frac{d\beta^j}{d\tau} + \sum_{j=1}^{2r} (\epsilon_{ij} - \beta b_{ij}) \beta^j - \beta \sum_{j=1}^{2r} a_{ij} \alpha^j \\ = \frac{\partial W}{\partial \xi} w_i \bigg|_{\xi_0}^{\xi_1} \quad i \neq 2, 2r \quad (4.56) \end{aligned}$$

with

$$\alpha^2(\tau) = p \alpha^1(\tau) \quad (4.57)$$

$$\beta^2(\tau) = q \beta^1(\tau) \quad (4.58)$$

$$\alpha^{2r}(\tau) = -p \alpha^{2r-1}(\tau) \quad (4.59)$$

$$\beta^{2r}(\tau) = -q \beta^{2r-1}(\tau) \quad (4.60)$$

Equations (4.55) and (4.56) represent $(2r-2)$ equations each, and together with Equations (4.56) to (4.60), we have $4r$ equations in the $4r$ unknowns α^i and β^i .

Let $q_0(\xi)$ and $q_1(\xi)$ represent the initial perturbations u_1 and u_2 , respectively. That is,

$$u_1(\xi, 0) = q_0(\xi) \quad (4.61)$$

$$u_2(\xi, 0) = q_1(\xi) \quad (4.62)$$

Thus initial coefficients $\alpha^i(0)$ and $\beta^i(0)$ can be evaluated from the following equations

$$\sum_{j=1}^{2r} \zeta_{ij} \alpha^j(0) = \langle q_0(\xi), w_i \rangle \quad i \neq 2, 2r \quad (4.63)$$

$$\sum_{j=1}^{2r} \zeta_{ij} \beta^j(0) = \langle q_1(\xi), w_i \rangle \quad i \neq 2, 2r \quad (4.64)$$

with

$$\alpha^2(0) = p \alpha^1(0) \quad (4.65)$$

$$\beta^2(0) = q \beta^1(0) \quad (4.66)$$

$$\alpha^{2r}(0) = -p \alpha^{2r-1}(0) \quad (4.67)$$

$$\beta^{2r}(0) = -q \beta^{2r-1}(0) \quad (4.68)$$

D. Numerical Considerations and Results

There are several practical problems that arise in the solution of the continuous time Galerkin approximation equations. The first is the question of evaluation of the coefficients a_{ij} and b_{ij} . It is important to establish a procedure for treating these quadratures that is efficient, otherwise the calculations required to complete a time step become so extensive that it may not be feasible to use the Galerkin method with a Hermite basis. The coefficients $A(\xi)$ and $B(\xi)$ are approximated in the subspace \mathcal{M} and the integrations are then carried out explicitly by formula.

Consider the approximation of $A(\xi)$. (The approximation of $B(\xi)$ is carried out in an analogous manner.)

Let

$$\bar{A}(\xi) = \sum_{k=1}^r \left\{ A(\xi_k) w_{2k-1}(\xi) + A'(\xi_k) w_{2k}(\xi) \right\} \quad (4.69)$$

$$= \sum_{k=1}^{2r} \left\{ \chi_k w_k(\xi) \right\} \quad (4.70)$$

where

$$\begin{aligned} \chi_{2k-1} &= A(\xi_k) \text{ and } \chi_{2k} = A'(\xi_k) \\ &\text{for } k = 1, 2, \dots, r \end{aligned} \quad (4.71)$$

$a_{ij} = \langle A w_i, w_j \rangle$ is then approximated by

$$a_{ij} = \langle \bar{A} w_i, w_j \rangle \quad (4.72)$$

$$a_{ij} = \sum_{k=1}^{2r} \delta_{kij} x_k \quad (4.73)$$

$$\text{where } \delta_{kij} = \int_{\xi_0}^{\xi_1} w_k(x) w_i(x) w_j(x) dx \quad (4.74)$$

The values of δ_{kij} are calculated only once per problem. Most δ_{kij} are zero, and, in fact, for a given (i,j) there are at most six non-zero δ_{kij} for the Hermite cubic polynomials. Since the w_i 's are polynomials on each interval (ξ_{i-1}, ξ_{i+1}) , δ_{kij} can be evaluated by performing the integration by polynomial multiplication and polynomial integration routines, or, by hand. The values of the integrals δ_{kij} , ζ_{ij} , and ϵ_{ij} are tabulated in Appendix I.

Similarly, b_{ij} is approximated by

$$b_{ij} = \sum_{k=1}^{2r} \psi_k \delta_{kij} \quad (4.75)$$

where

$$\psi_{2k-1} = B(\xi_k) \text{ and } \psi_{2k} = B'(\xi_k) \quad k = 1, 2, \dots, r \quad (4.76)$$

The time-discretization of the system of ordinary differential Equations (4.55) and (4.56) can be accomplished by the Crank-Nicolson procedure. Let $\tau_m = m \Delta \tau$, $\alpha_m^i = \alpha^i(\tau_m)$ and $\beta_m^i = \beta^i(\tau_m)$ and by using the finite difference formulas:

$$\frac{d\alpha^j}{d\tau} \approx \frac{\alpha_{n+1}^j - \alpha_n^j}{\Delta\tau} \quad (4.77)$$

$$\frac{d\beta^j}{d\tau} \approx \frac{\beta_{n+1}^j - \beta_n^j}{\Delta\tau} \quad (4.78)$$

$$\alpha^j \approx \frac{\alpha_{n+1}^j + \alpha_n^j}{2} \quad (4.79)$$

$$\beta^j \approx \frac{\beta_{n+1}^j + \beta_n^j}{2} \quad (4.80)$$

the Equations (4.55) and (4.56) become

$$\sum_{j=1}^{2r} \left\{ \zeta_{ij} + \frac{\Delta\tau}{2} (\epsilon_{ij} + a_{ij}) \right\} \alpha_{n+1}^j + \left(\frac{\Delta\tau}{2} \right) \sum_{j=1}^{2r} b_{ij} \beta_{n+1}^j = \phi_n^i$$

$$i \neq 2, 2r \quad (4.81)$$

and

$$\sum_{j=1}^{2r} \left\{ \zeta_{ij} + \frac{\Delta\tau}{2} (\epsilon_{ij} - \beta b_{ij}) \right\} \beta_{n+1}^j - \left(\frac{\beta \Delta\tau}{2} \right) \sum_{j=1}^{2r} a_{ij} \alpha_{n+1}^j = \eta_n^i$$

$$i \neq 2, 2r \quad (4.82)$$

where

$$\begin{aligned} \phi_n^i = & \Delta\tau \frac{\partial U}{\partial \xi} w_i \bigg|_{\xi_0}^{\xi_1} + \sum_{j=1}^{2r} \left\{ \zeta_{ij} - \frac{\Delta\tau}{2} (\epsilon_{ij} + a_{ij}) \right\} \alpha_n^j \\ & - \left(\frac{\Delta\tau}{2} \right) \sum_{j=1}^{2r} b_{ij} \beta_n^j \end{aligned} \quad (4.83)$$

$$\eta_n^i = \Delta\tau \frac{\partial W}{\partial \xi} w_i \bigg|_{\xi_0}^{\xi_1} + \sum_{j=1}^{2r} \left\{ L e \zeta_{ij} - \frac{\Delta\tau}{2} (\epsilon_{ij} - \beta_{ij}^b) \right\} \beta_n^j + \left(\frac{\beta \Delta\tau}{2} \right) \sum_{j=1}^{2r} a_{ij} \alpha_n^j \quad (4.84)$$

The boundary conditions (4.57) to (4.60) become

$$\alpha_{n+1}^2 = p \alpha_{n+1}^1 \quad (4.85)$$

$$\beta_{n+1}^2 = q \beta_{n+1}^1 \quad (4.86)$$

$$\alpha_{n+1}^{2r} = -p \alpha_{n+1}^{2r-1} \quad (4.87)$$

$$\beta_{n+1}^{2r} = -q \beta_{n+1}^{2r-1} \quad (4.88)$$

Using the notation of Douglas and Dupont we call the system of Equations (4.81) to (4.88) the Crank-Nicolson-Galerkin approximation. Let

$$\underline{\alpha}^n = (\alpha_n^1, \beta_n^1, \alpha_n^2, \beta_n^2, \dots, \alpha_n^{2r}, \beta_n^{2r})^T \quad (4.89)$$

and

$$\underline{\phi}^n = (\phi_n^1, \eta_n^1, \phi_n^2, \eta_n^2, \dots, \phi_n^{2r}, \eta_n^{2r})^T \quad (4.90)$$

The system of Equations (4.81) to (4.88) can then be represented by

$$D \underline{\alpha}^{n+1} = \underline{\phi}^n \quad (4.91)$$

where D is a matrix with at most 12 non-zero elements per row. The initial conditions for the problem are obtained from Equations (4.63) to (4.68). Matrix D can be considered as either a 15 band matrix with 7 sub-diagonal elements and 7 super-diagonal elements or as a block tridiagonal matrix, the size of each block being 4×4 .

Gaussian elimination can be readily employed to solve the Equation (4.91). If D is treated as a band matrix, then a considerable saving in computer storage can be effected (i.e., $4r \times 15$ as opposed to $4r \times 4r$). The solution procedure is then to factorize D into upper and lower triangular matrices using partial pivoting as discussed by Martin and Wilkinson³⁵ and by Bowdler, Martin, Peters, and Wilkinson.⁶ Treating D as a block-tridiagonal matrix also economizes the storage requirements. The solution procedure in this case is analogous to the solution of a tridiagonal system, (the algorithm for which appears in Henrici¹⁹), except that division by a scalar quantity is replaced by multiplication by the inverse of the corresponding matrix.

The system represented by Equation (4.91) was solved by two methods: one treating D as a band matrix and the other treating D as a block-tridiagonal matrix. Computationally it was found that the solution obtained by considering D as a band matrix required slightly less time than that obtained by treating D as a block-tridiagonal matrix. Rachford⁴² has suggested that for systems with bigger blocks (16×16 or

or greater) the block-tridiagonal method would be faster.

All computations were performed with the Lewis number, Le , equal to 1. The numerical method described above was used in all computations. For all the transients, a grid of 13 points was used. A small grid spacing was employed at the ends of the slab where the concentration and temperature changes were rapid. In the interior of the slab, where the changes were slight, a larger grid spacing was used. Typically, four steps of size h were used at each end of the slabs and four steps of sizes varying from $6h$ to $20h$ in the middle of the slabs. The grid spacing used is tabulated in Appendix II.

The effect of a small perturbation of the high, medium, and low symmetric steady states was considered. In all these cases, the same initial disturbance of the steady state was employed. The concentration and temperature responses are shown in Figures 22 and 23 for the low symmetric steady state, in Figures 24 and 25 for the medium steady state, and in Figures 26 and 27 for the high steady state. Since symmetric perturbations of the steady states were considered, it is expected that the transients will be symmetric and this is indicated in Figures 22 and 23. In the following four figures, the transients for only half the slab are shown.

As expected, the perturbations of the medium steady state grow in time indicating that this steady state is

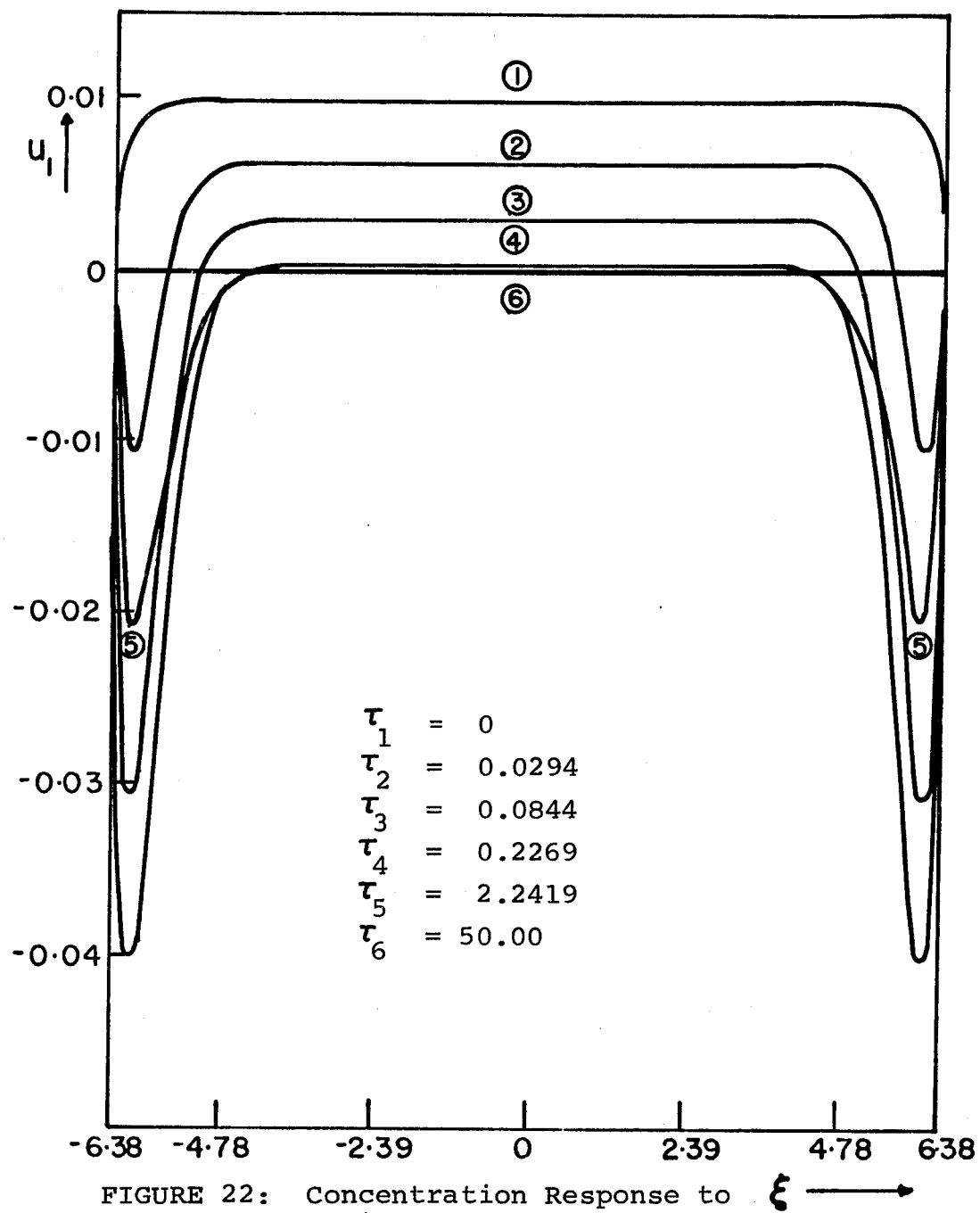


FIGURE 22: Concentration Response to a Disturbance of the Low Symmetric Steady State

$\tau_1 = 0$
 $\tau_2 = 0.1169$
 $\tau_3 = 5.2419$
 $\tau_4 = 20.9919$
 $\tau_5 = 45.00$
 $\tau_6 = 50.00$

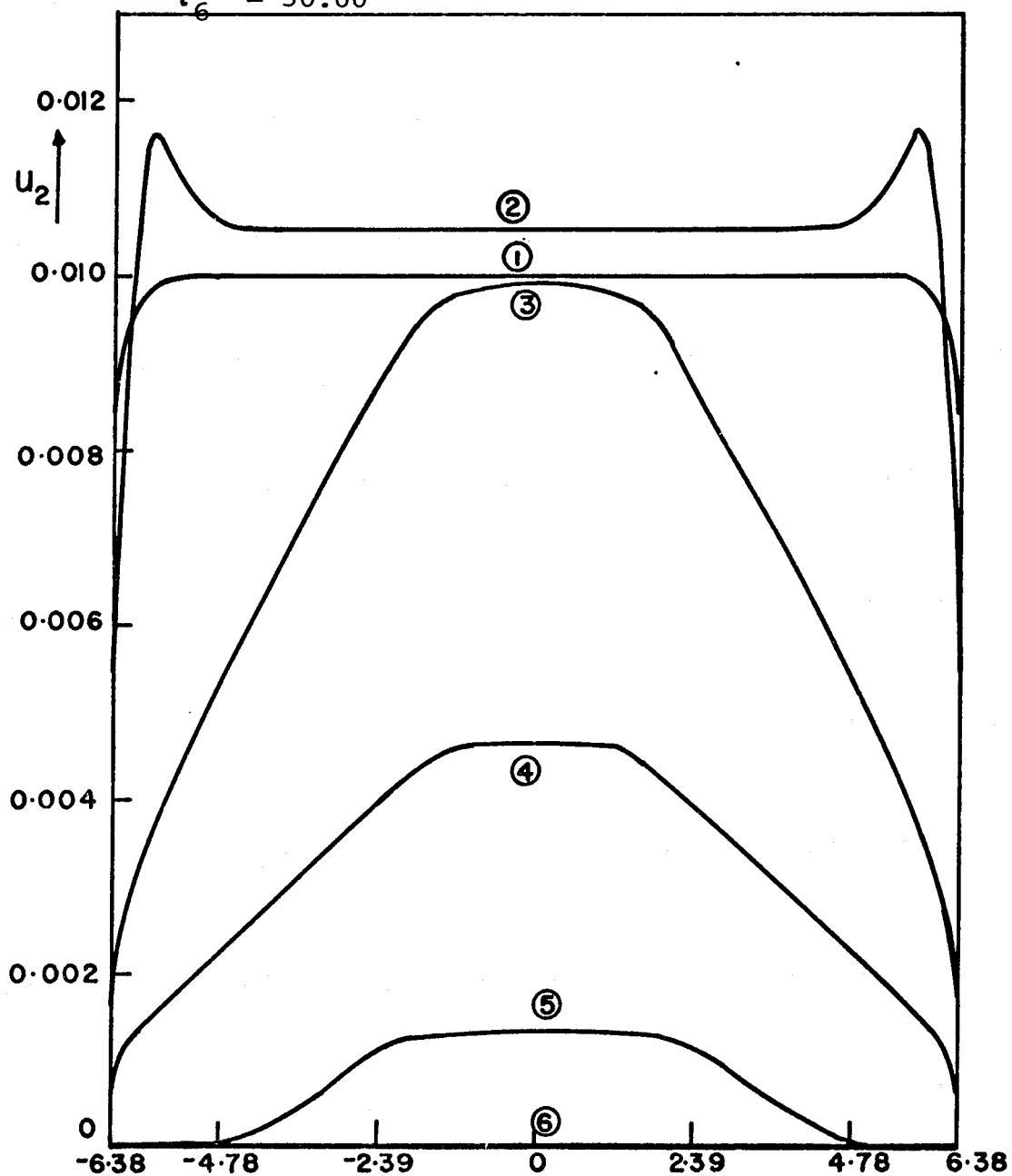


FIGURE 23: Temperature Response to a Disturbance of the Low Symmetric Steady State

$\xi \longrightarrow$

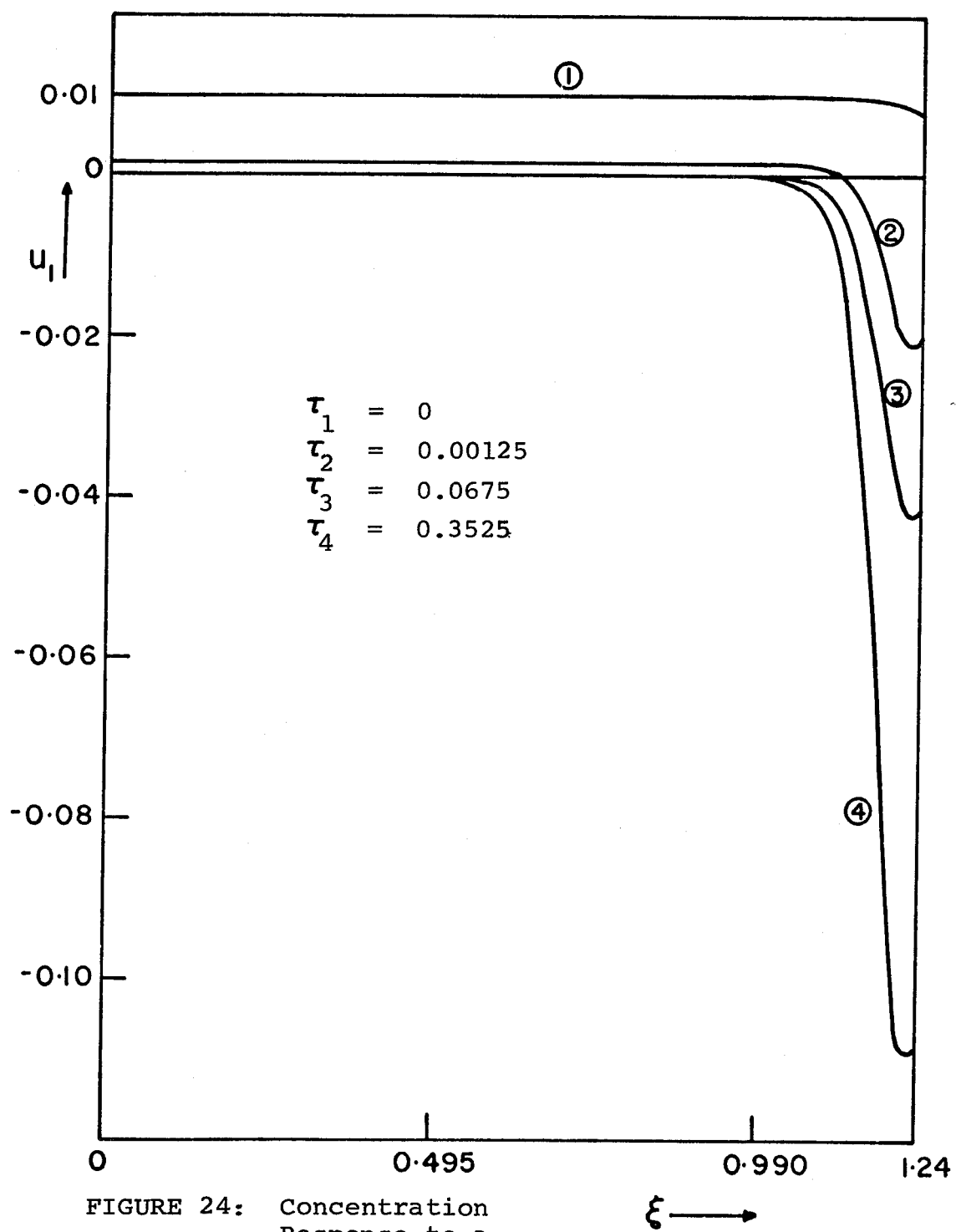


FIGURE 24: Concentration
Response to a
Disturbance of the Medium
Symmetric Steady State

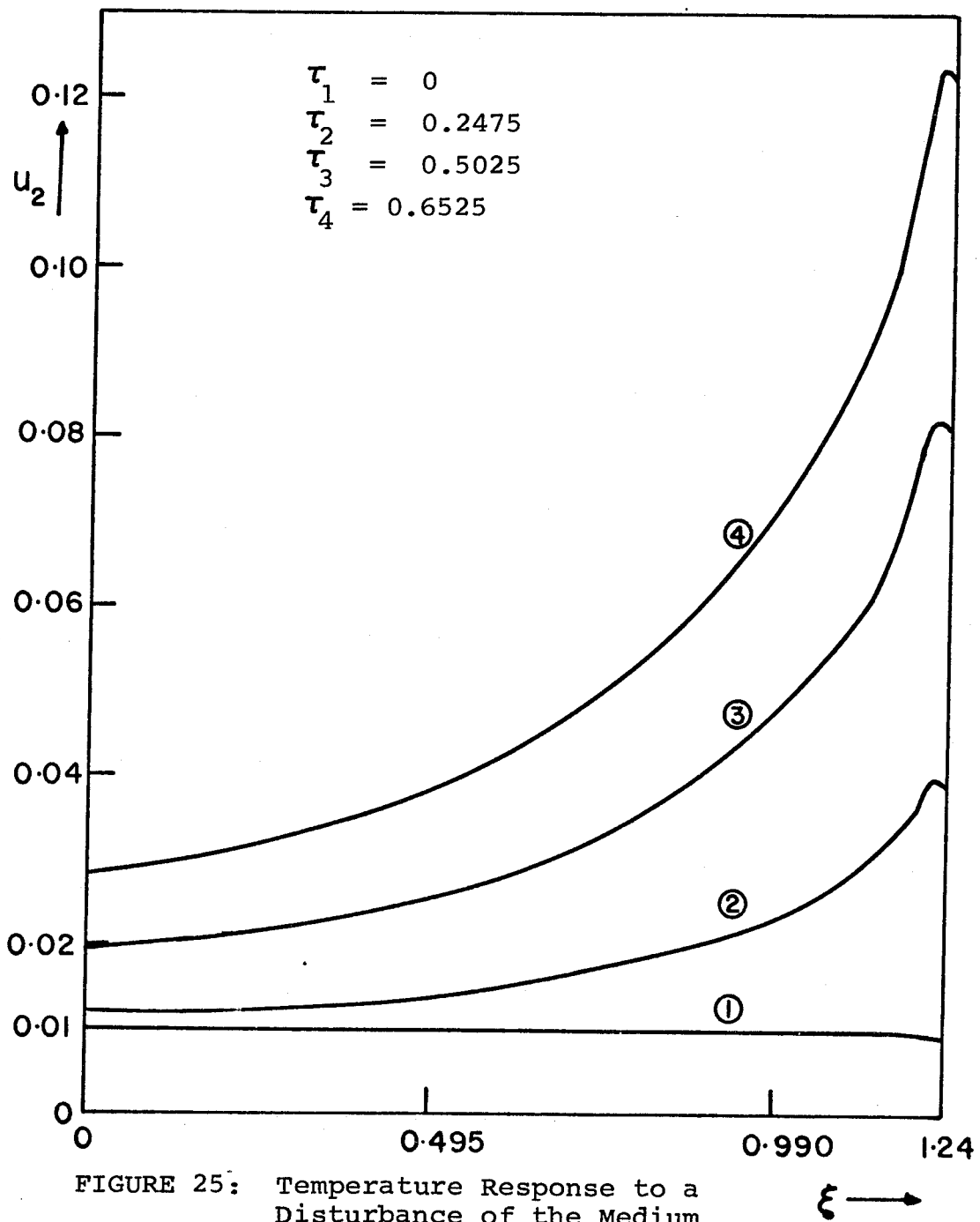


FIGURE 25: Temperature Response to a Disturbance of the Medium Symmetric Steady State

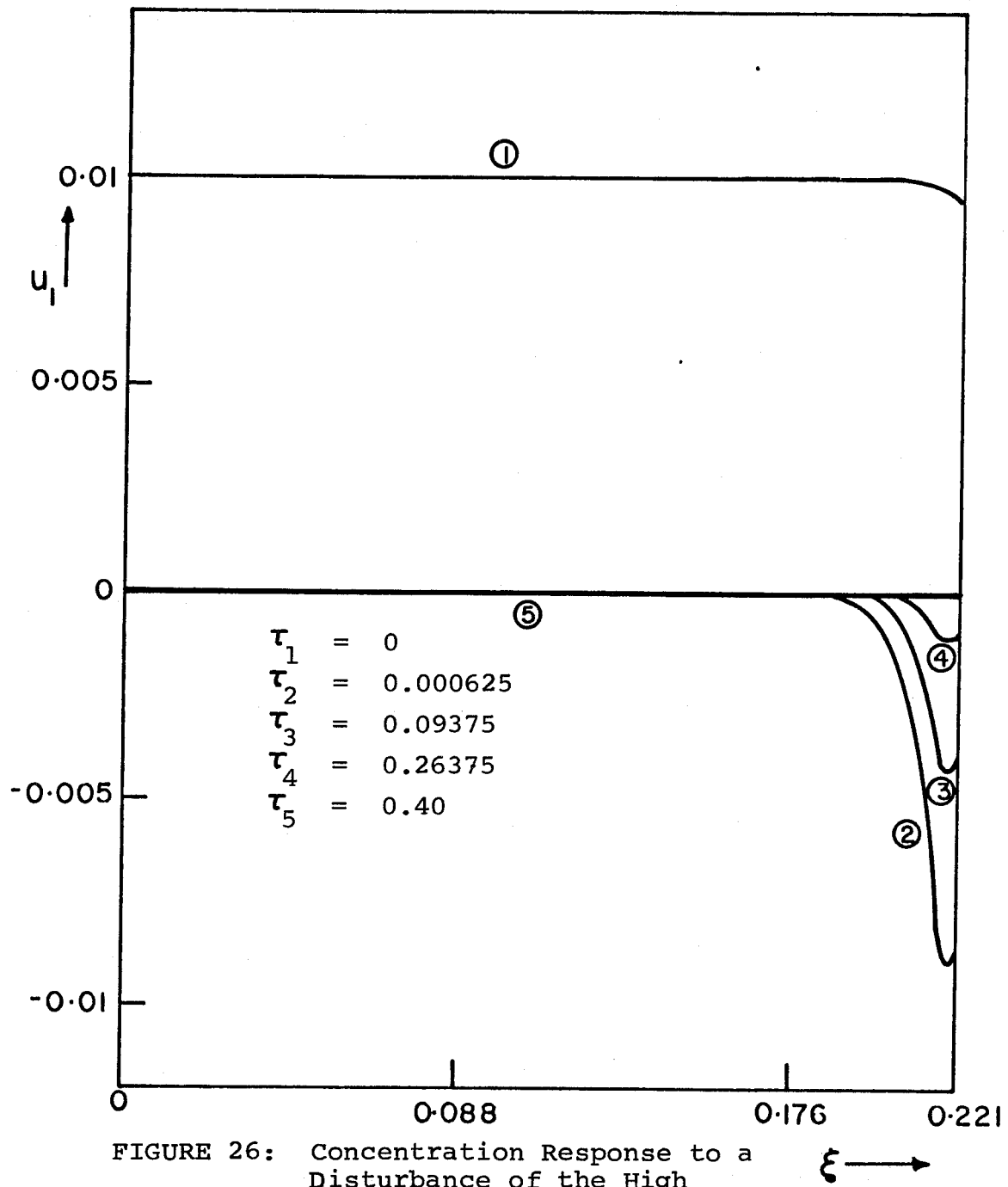


FIGURE 26: Concentration Response to a Disturbance of the High Symmetric Steady State

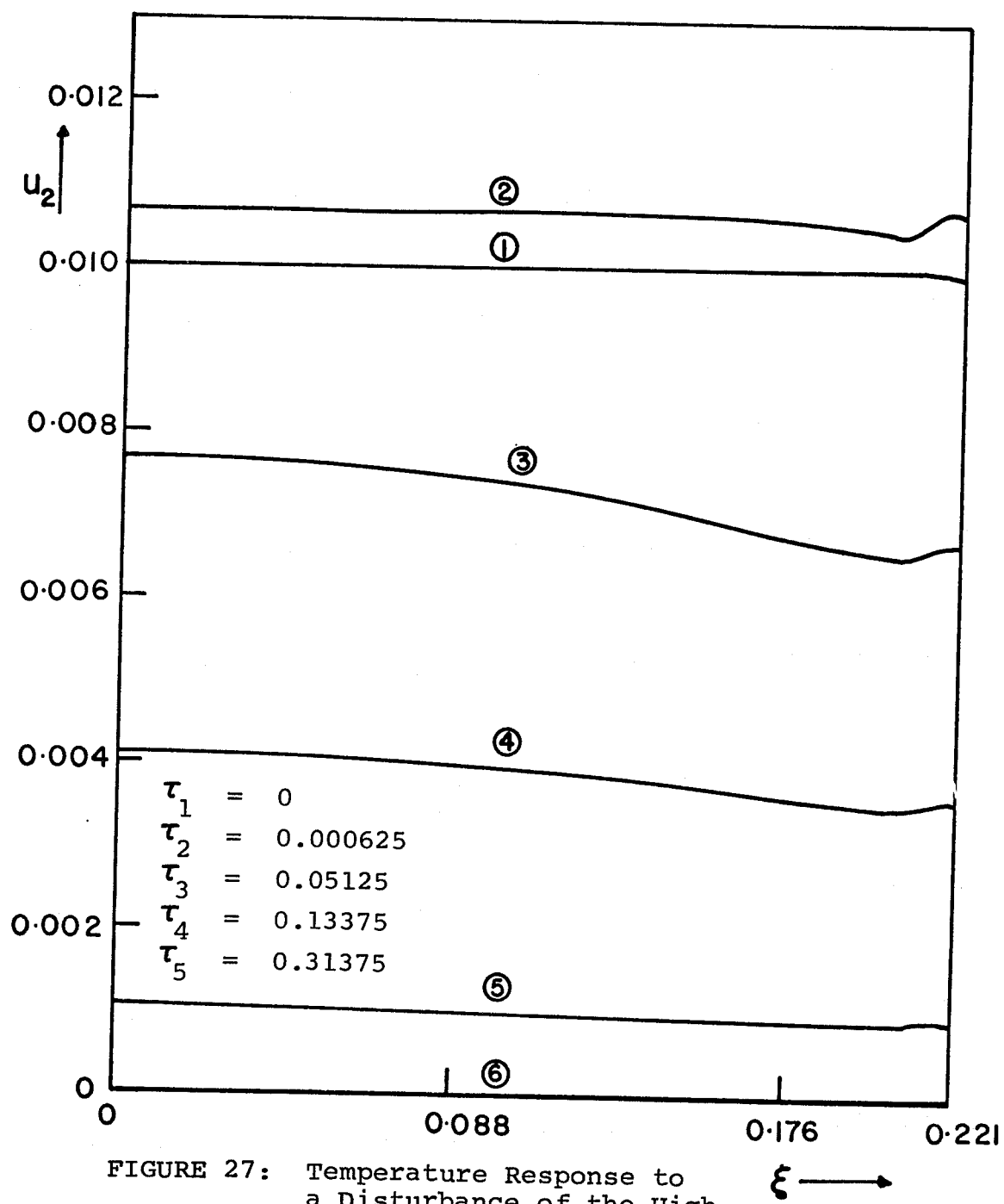


FIGURE 27: Temperature Response to a Disturbance of the High Symmetric Steady State

unstable. Both Figures 24 and 25 show maximum value of u_1 and u_2 of about 0.11, although computations have been carried out to values of u_1 and u_2 of about 1. The form of the growth was maintained in both cases.

After a slight overshoot, the disturbances of the high and low steady states decayed in time, indicating that these steady states are stable for the perturbations considered. Since the primary purpose of this work is to consider the asymmetric steady states, the effect of different disturbances was not considered. However, based on these results, and the results of previous work, it can be conjectured that the high and low symmetric steady states are stable.

The effect of a small disturbance on the asymmetric steady states was also investigated by solving the Crank-Nicolson-Galerkin approximation. The asymmetric steady states considered are those corresponding to the intersection points in Figure 14 for $\alpha_2 = 0.09$ and those in Figure 12 for $\alpha_2 = 0.02$. The former set represents slabs of small thicknesses while the latter represents slabs of large thicknesses.

Considering the smaller slabs first, Figures 28 and 29 show the concentration and temperature responses of the medium-low asymmetric steady state to a small positive disturbance. Instability is indicated by the growth of the perturbation in time. Instability of the high-medium steady state is also indicated by the growth of small positive

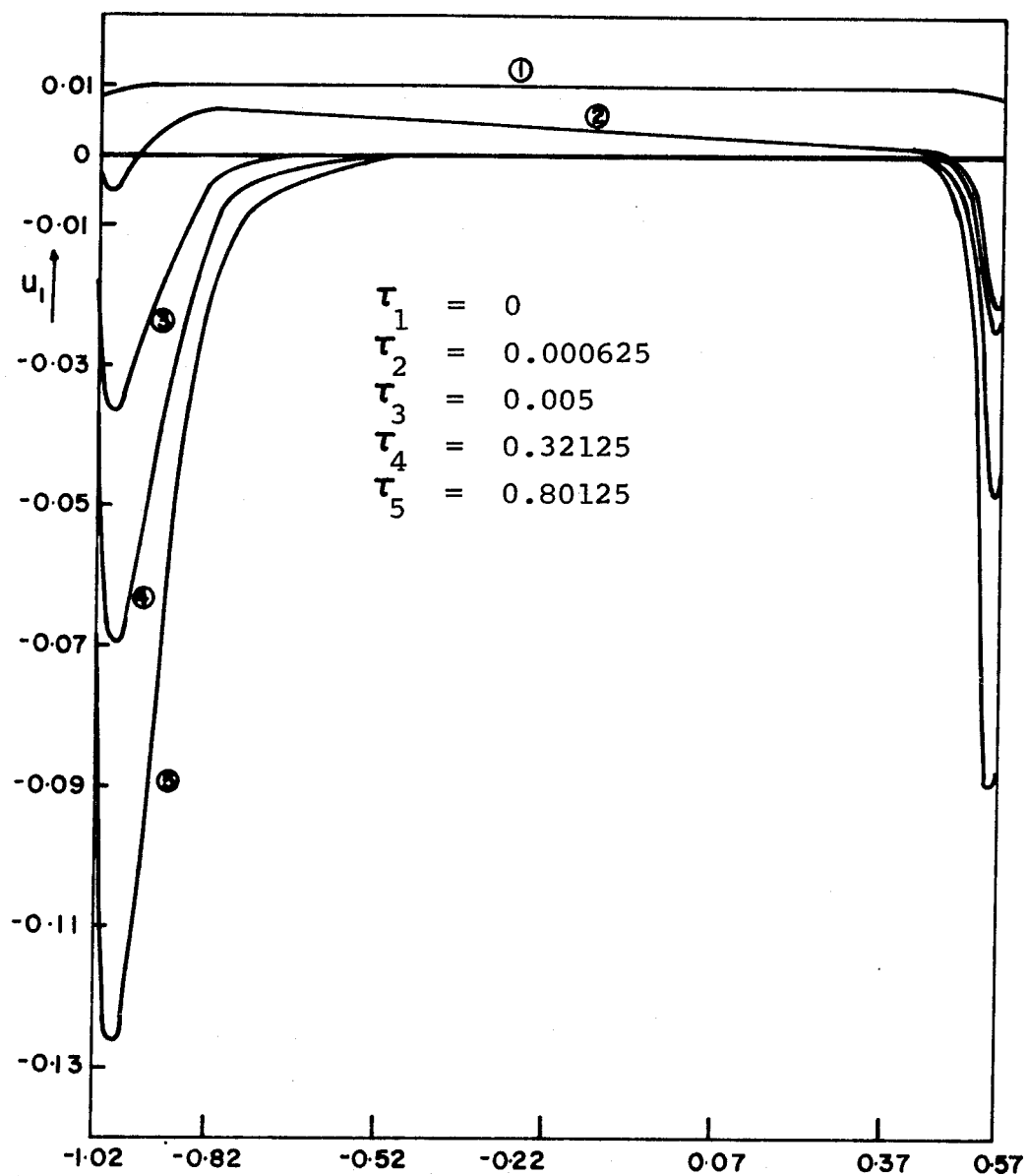


FIGURE 28: Concentration Response to a Disturbance of the m_1 Asymmetric Steady State (Point 3, $\alpha_2 = 0.09$)

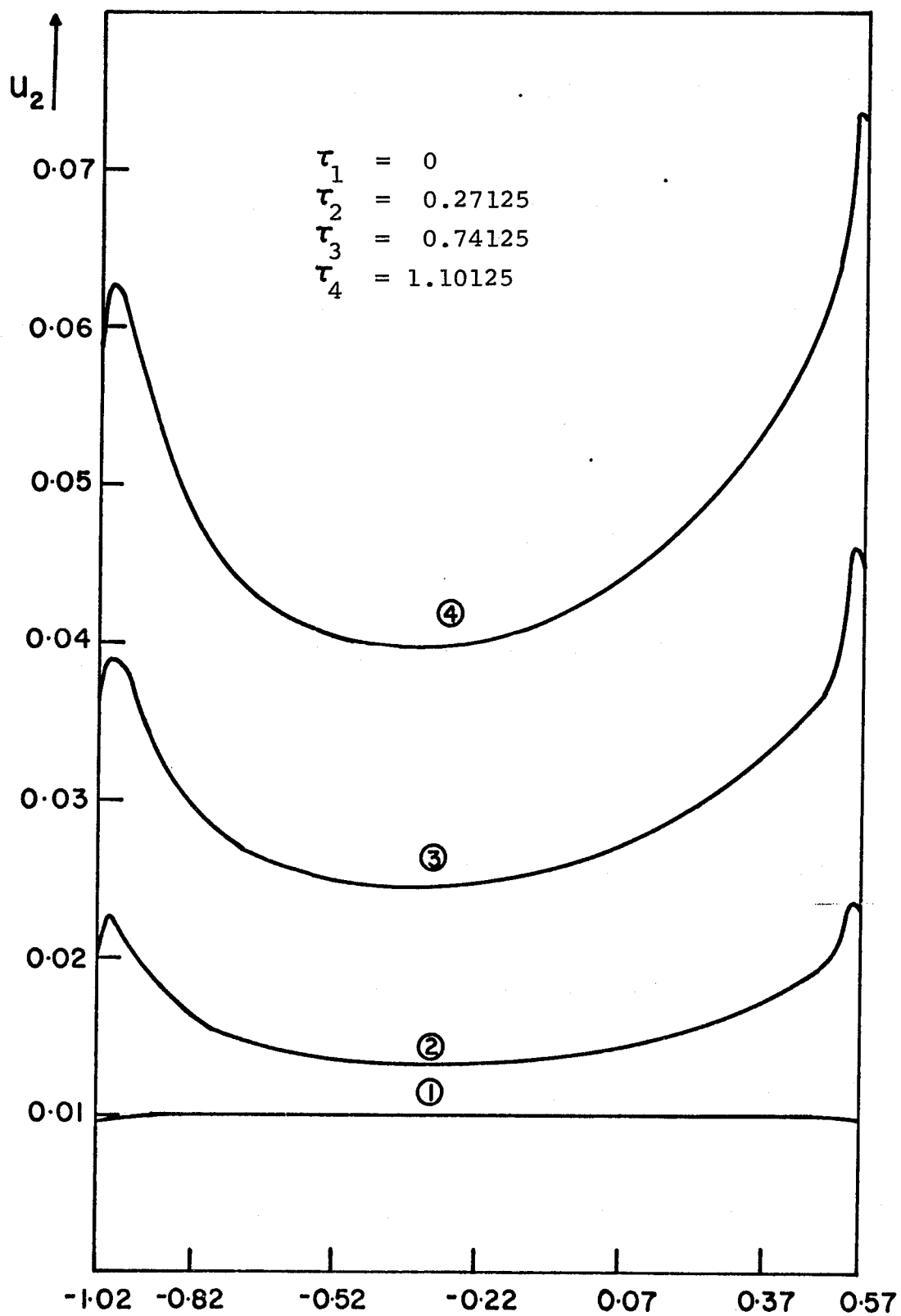


FIGURE 29: Temperature Response to a Disturbance of the m1 Asymmetric Steady State (Point 3, $\alpha_2 = 0.09$)

disturbances in time and these are graphed in Figures 30 and 31. In both cases computations were carried out beyond the dimensionless time shown and the form of the growth was maintained.

The effect of the small positive disturbances on the high-low steady state was also investigated. Figures 32 and 33 show these concentration and temperature responses. It is seen that the disturbances decay with time, after an overshoot, indicating the stability of the high-low steady state to the disturbance considered. Two other forms of initial disturbances were then considered: one a straight line satisfying $u_1(\xi, 0) = u_2(\xi, 0) = [0.02/(\xi_1 - \xi_0)](\xi - \xi_1) + 0.01$, and the other approximating an asymmetric step function. In both cases, the disturbances decayed in time, again after an overshoot. These responses are shown in Figures 34, 35, 36, and 37. As has been indicated earlier, it is impossible to establish stability with the method being used since it is impossible to consider all conceivable perturbations. However, from the computational results presented here, and by considering the results of Pis'men and Kharkats,⁴¹ it is reasonable to conclude that the high-low steady state is stable.

Perturbations of the three types of asymmetric steady states in larger slabs were also investigated. The responses are shown in Figures 38 to 43 where the horizontal scale has been split up in order to indicate the behavior of the

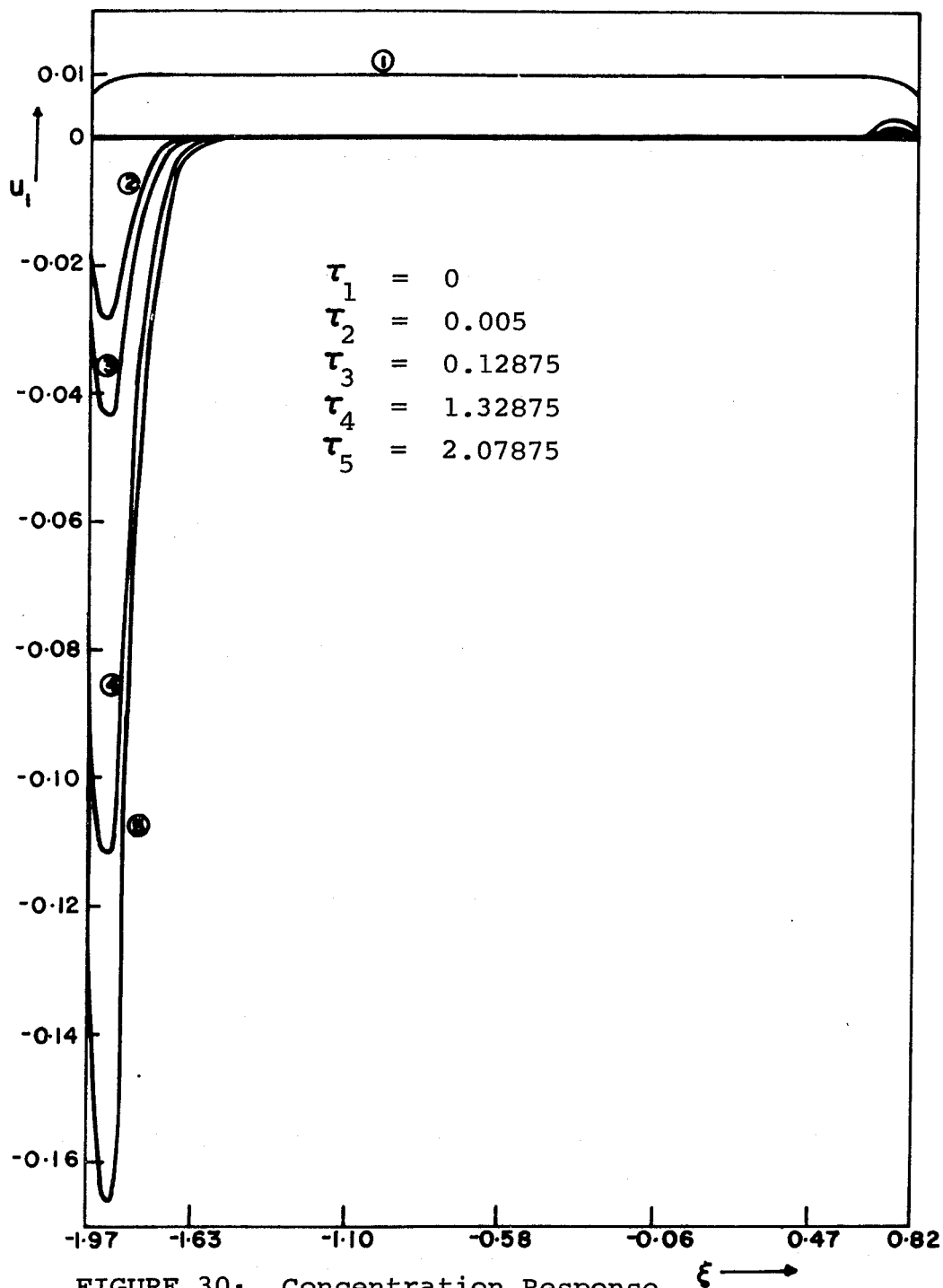


FIGURE 30: Concentration Response to a Disturbance of the hm Asymmetric Steady State (Point 4, $\alpha_2 = 0.09$)

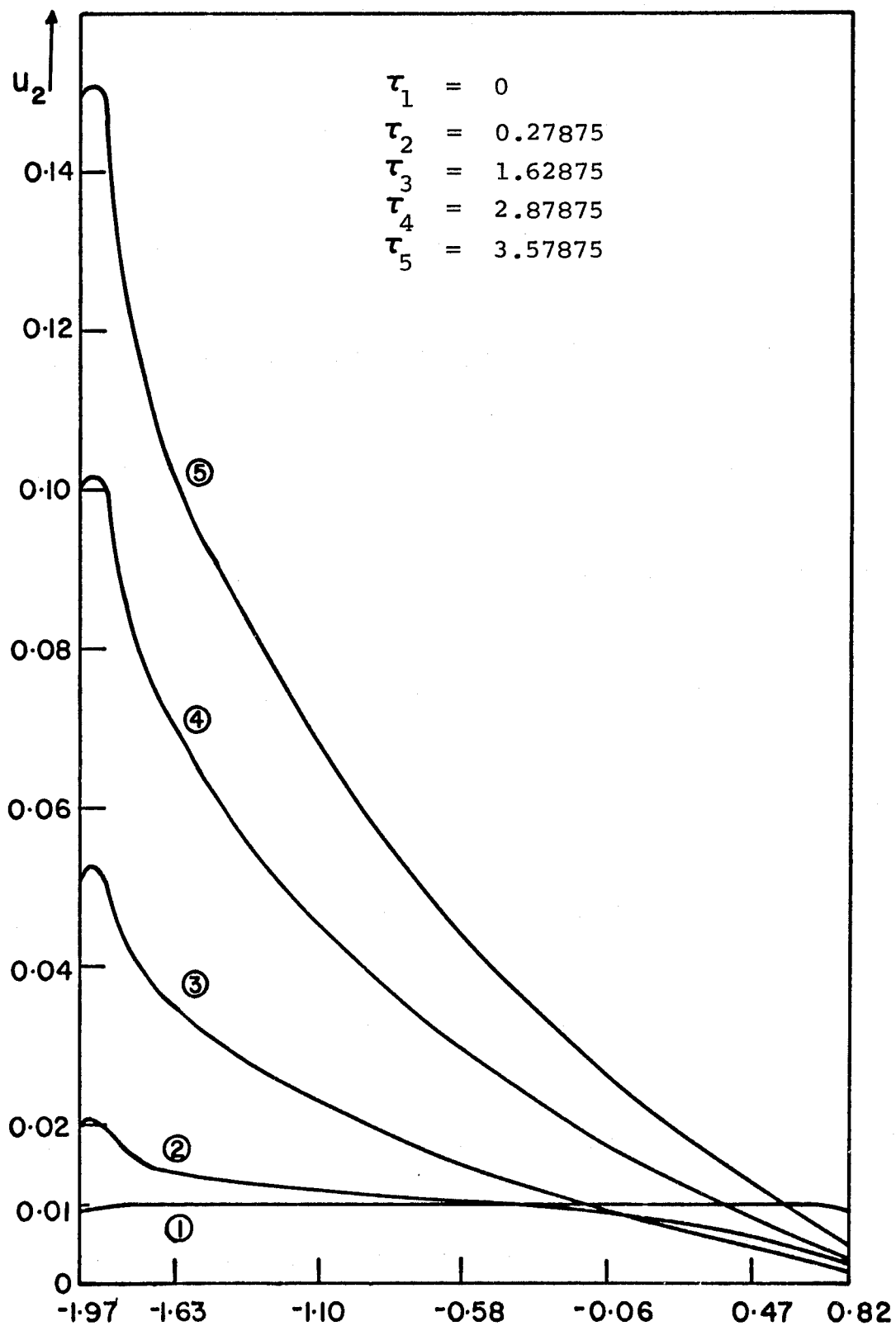


FIGURE 31: Temperature Response to a Disturbance of the hm Asymmetric Steady State (Point 4, $\alpha_2 = 0.09$)

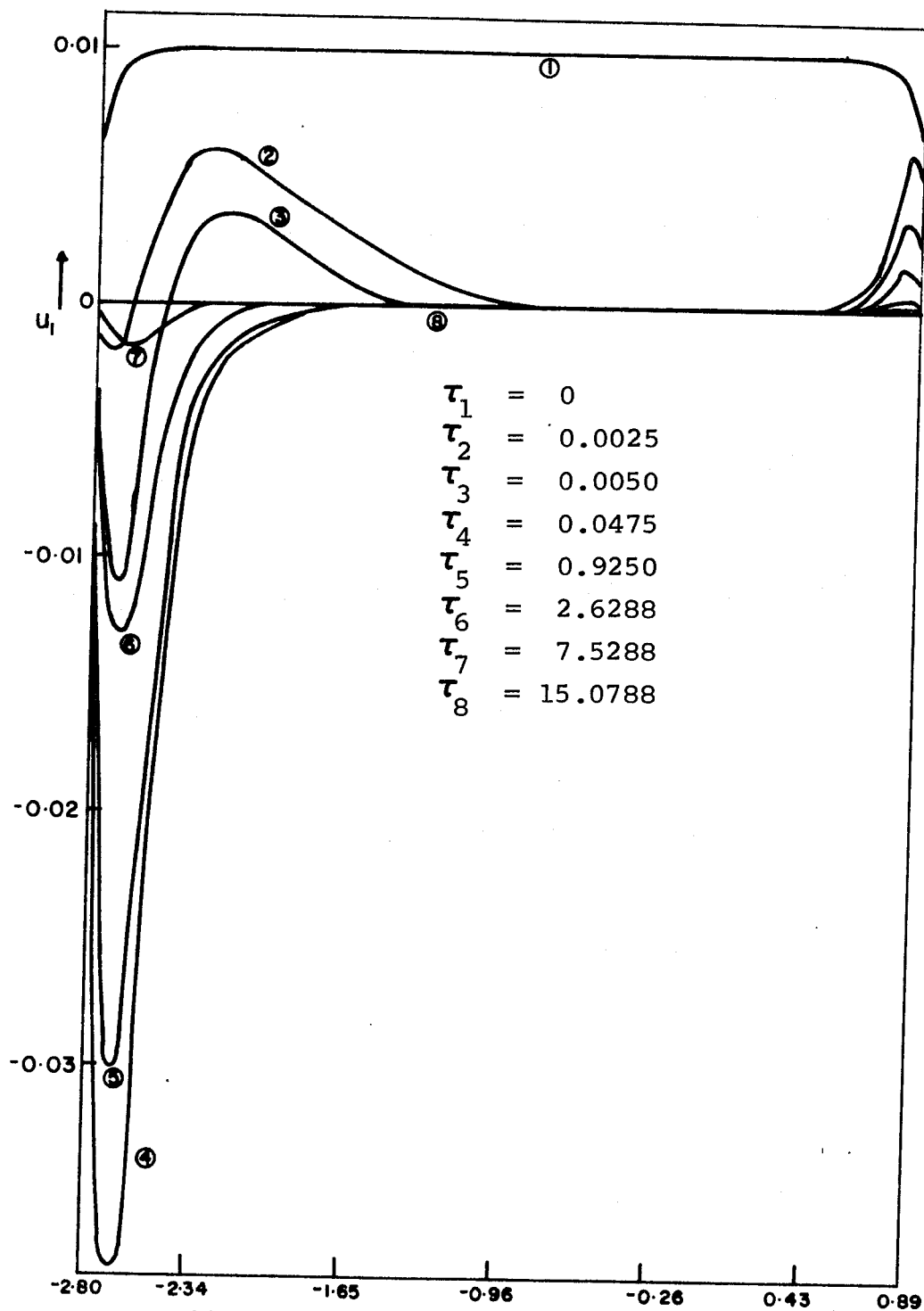


FIGURE 32: Concentration Response to a Disturbance of the h1 Asymmetric Steady State (Point 2, $\alpha_2 = 0.09$)

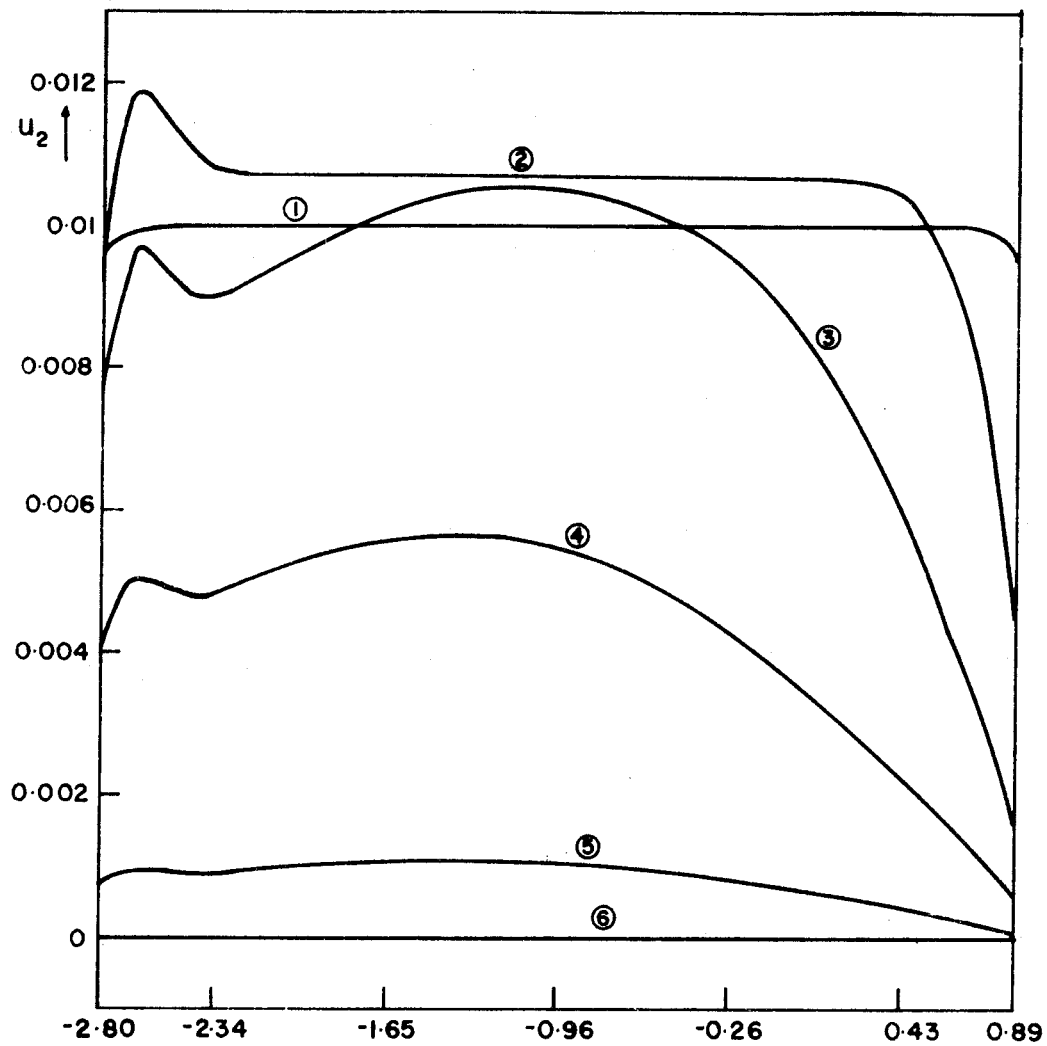


FIGURE 33: Temperature Response $\xi \rightarrow$
to a Disturbance of the h1 Asymmetric
Steady State (Point 2, $\alpha_2 = 0.09$)

$$\begin{aligned}\tau_1 &= 0 \\ \tau_2 &= 0.030 \\ \tau_3 &= 0.320 \\ \tau_4 &= 2.030 \\ \tau_5 &= 6.280 \\ \tau_6 &= 15.079\end{aligned}$$

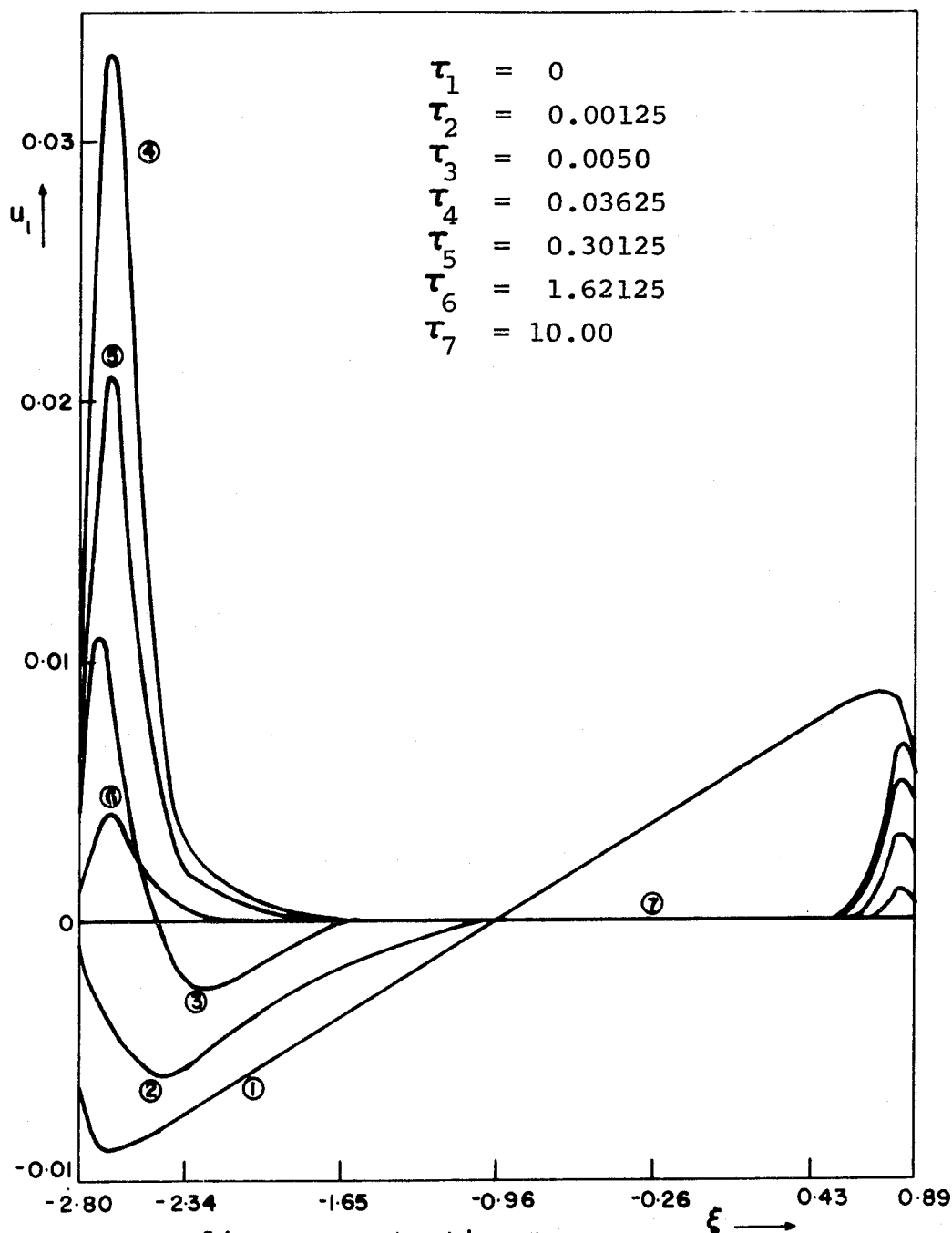


FIGURE 34: Concentration Response to a Disturbance of the h1 Asymmetric Steady State (Point 2, $\alpha_2 = 0.09$)

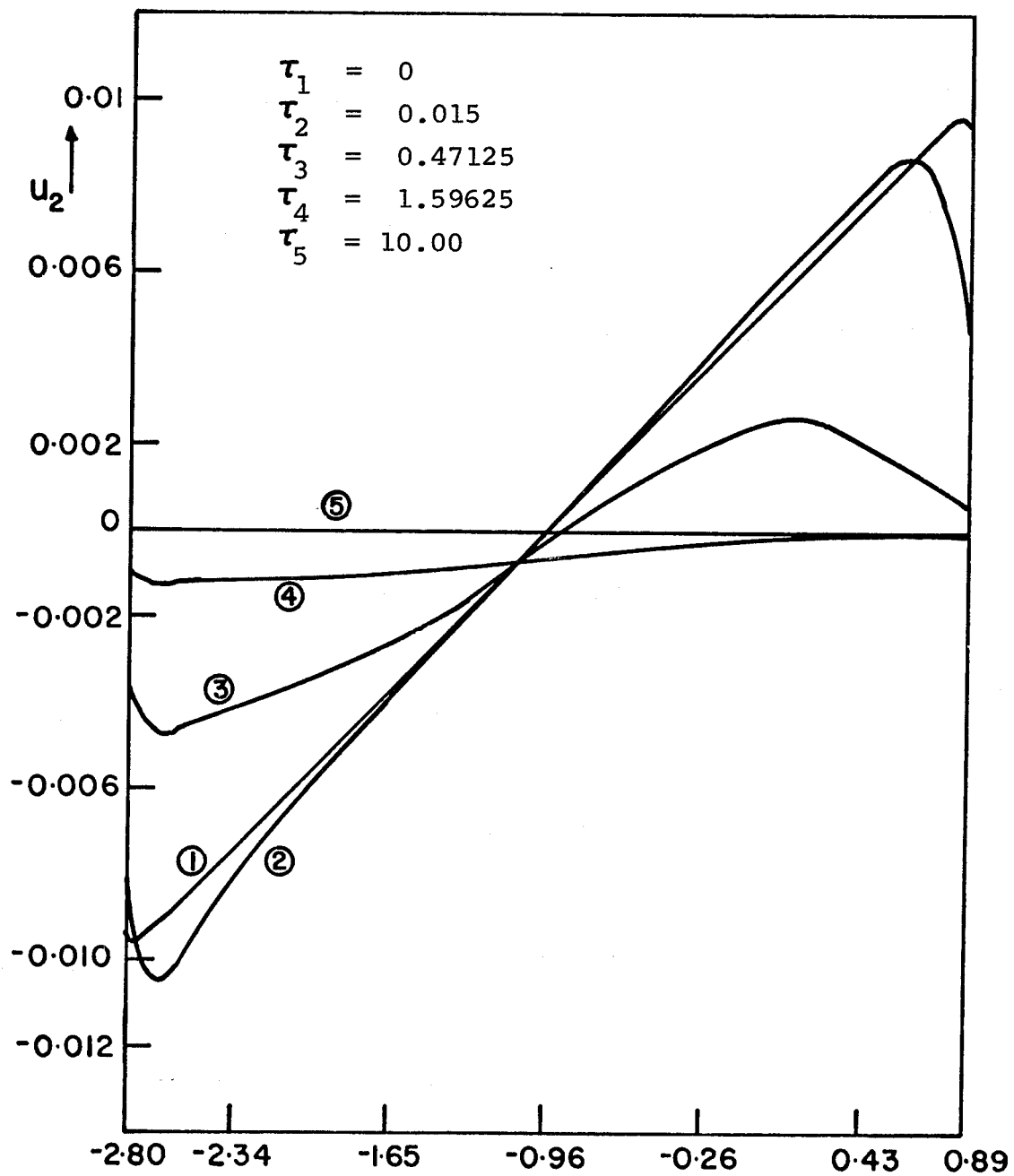


FIGURE 35: Temperature Response to a Disturbance of the h1 Asymmetric Steady State (Point 2, $\alpha_2 = 0.09$)

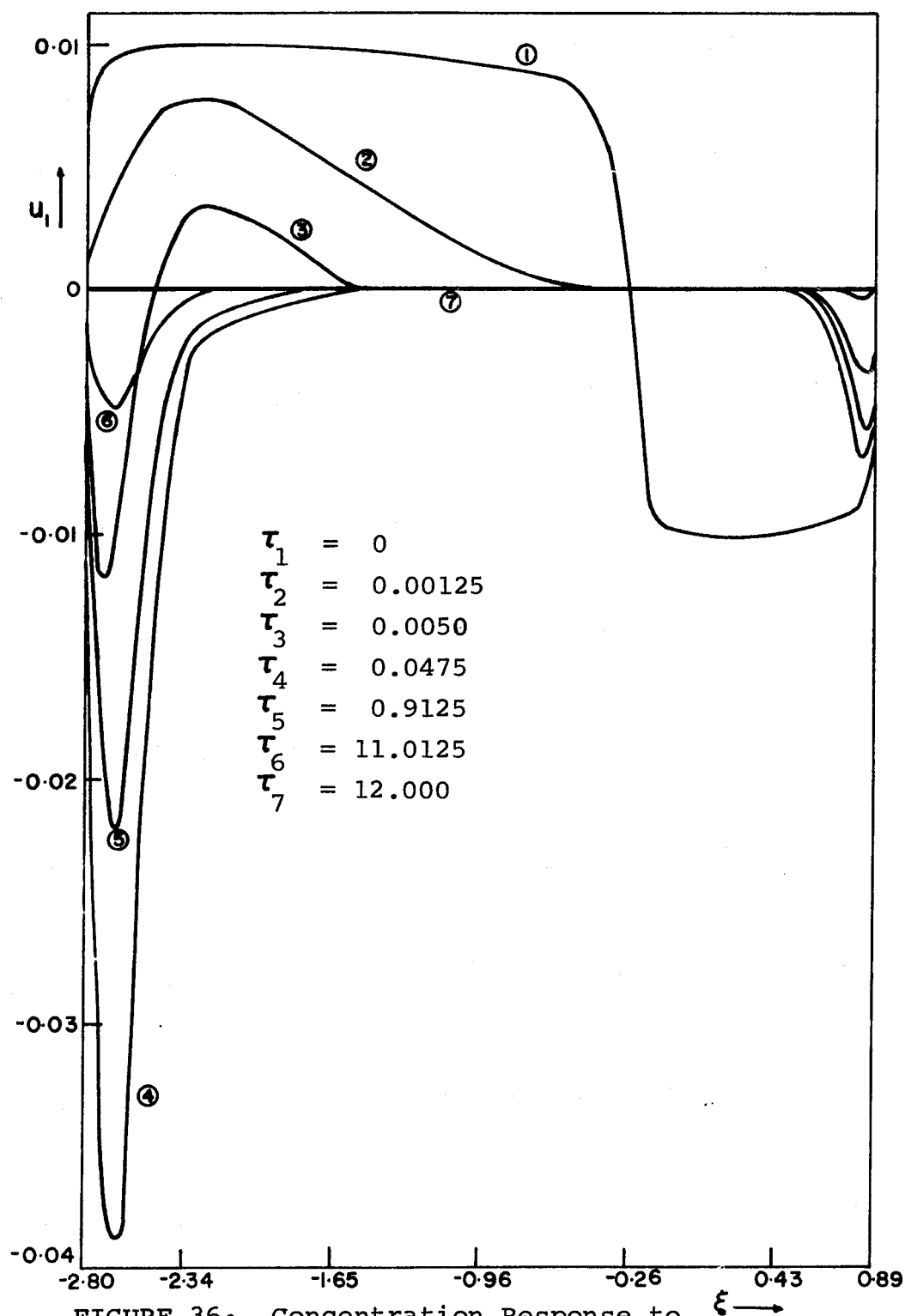


FIGURE 36: Concentration Response to a Disturbance of the h_1 Asymmetric Steady State (Point 2, $\alpha_2 = 0.09$)

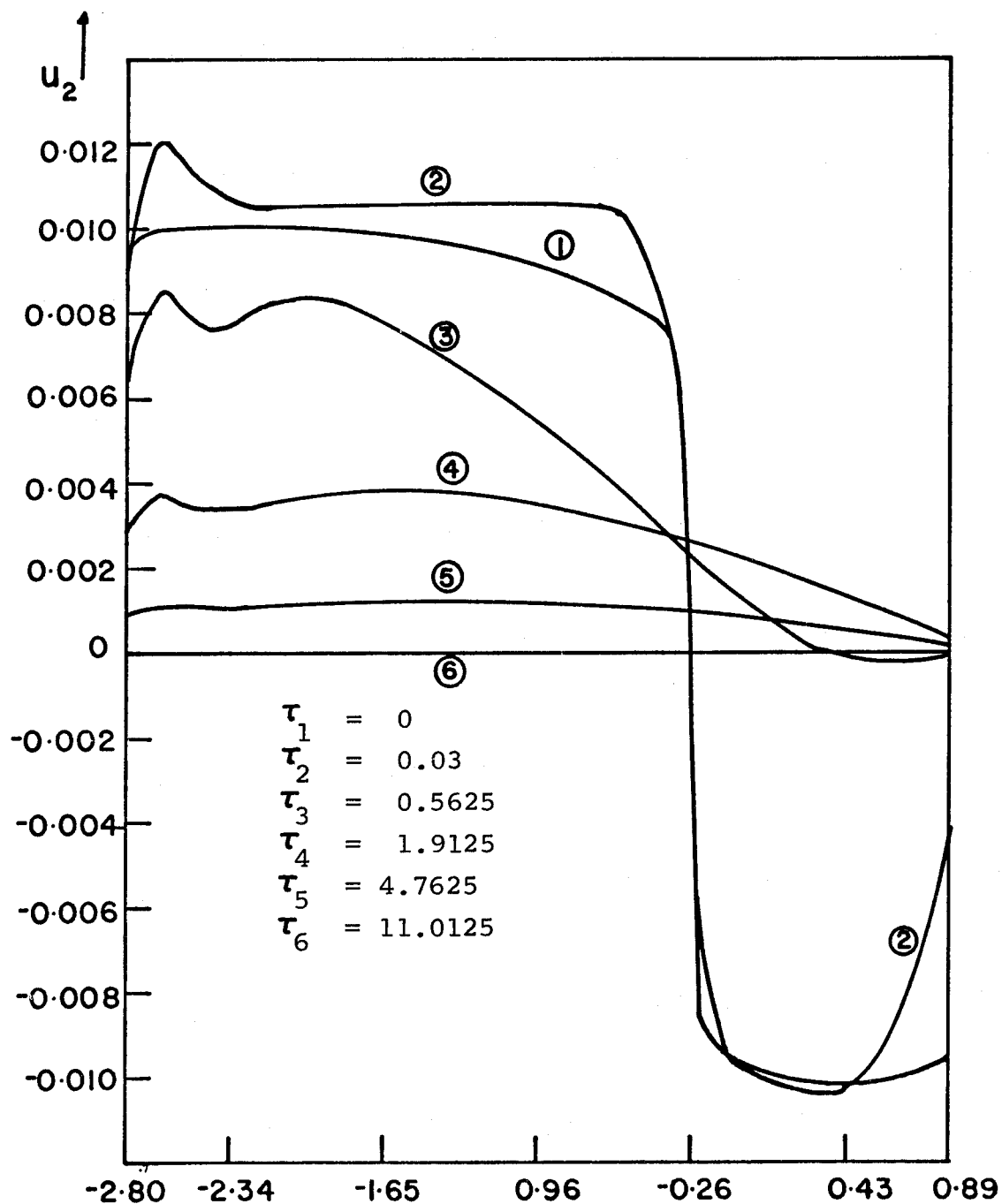


FIGURE 37: Temperature Response to a Disturbance of the h1 Asymmetric Steady State (Point 2, $\alpha_2 = 0.09$)

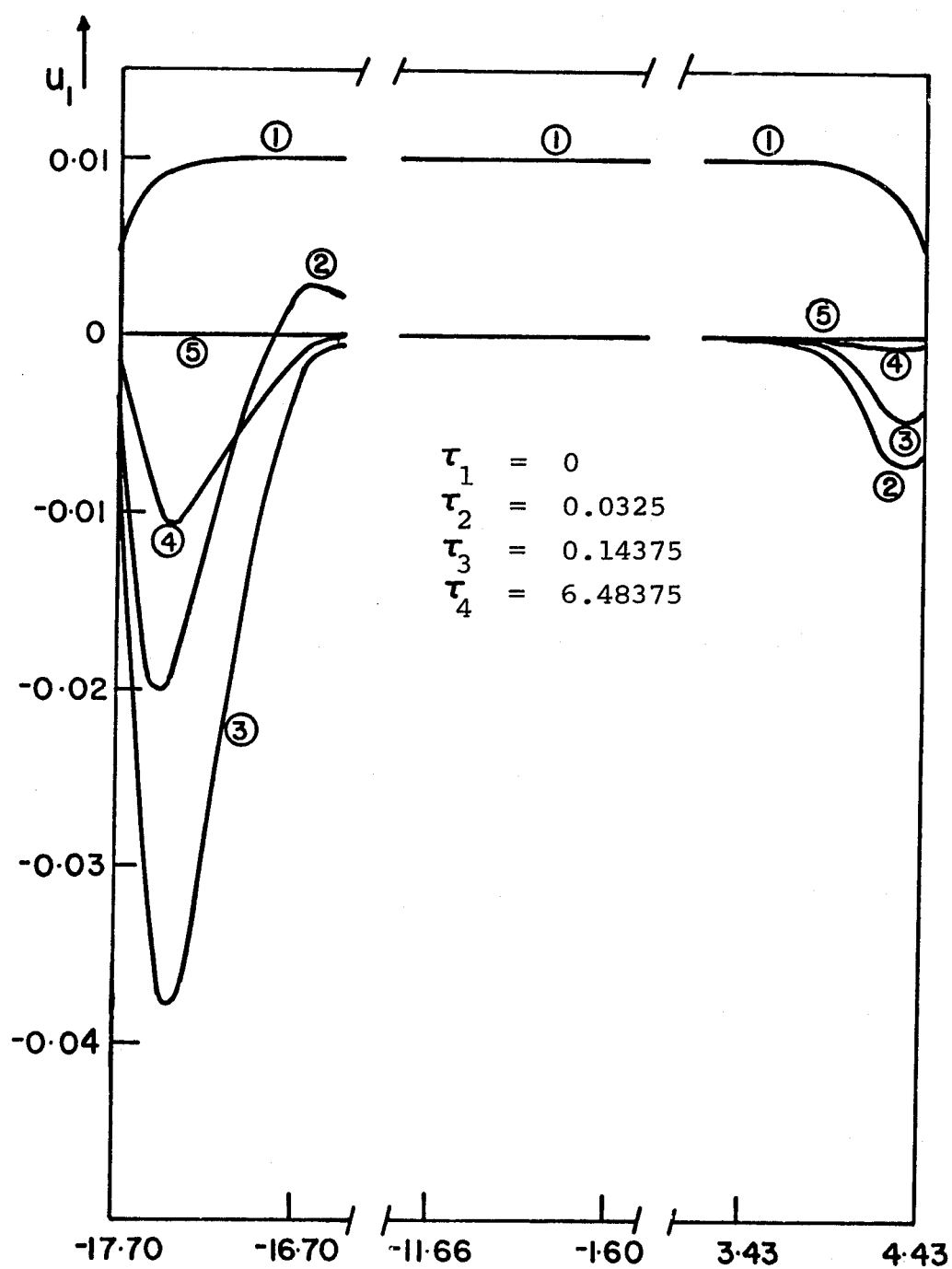


FIGURE 38: Concentration Response to $\xi \longrightarrow$ a Disturbance of the h1 Asymmetric Steady State (Point 2, $\alpha_2 = 0.02$)

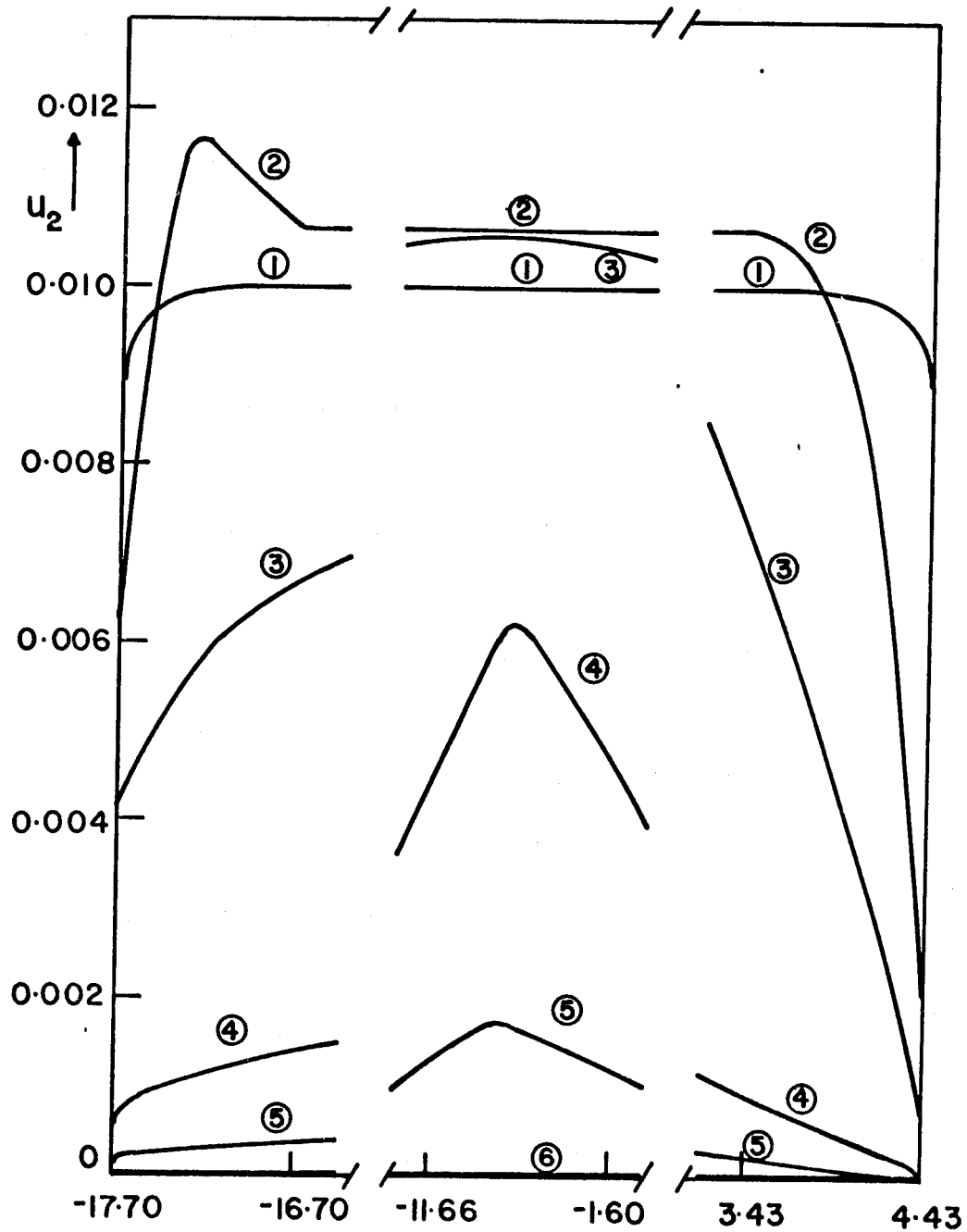


FIGURE 39: Temperature Response to a $\xi \rightarrow$
Disturbance of the hl Asymmetric
Steady State (Point 2, $\alpha_2 = 0.02$)

$$\tau_1 = 0, \quad \tau_2 = 0.06375, \quad \tau_3 = 0.63375, \quad \tau_4 = 42.00, \quad \tau_5 = 110.00$$

$$\tau_6 = 150.00$$

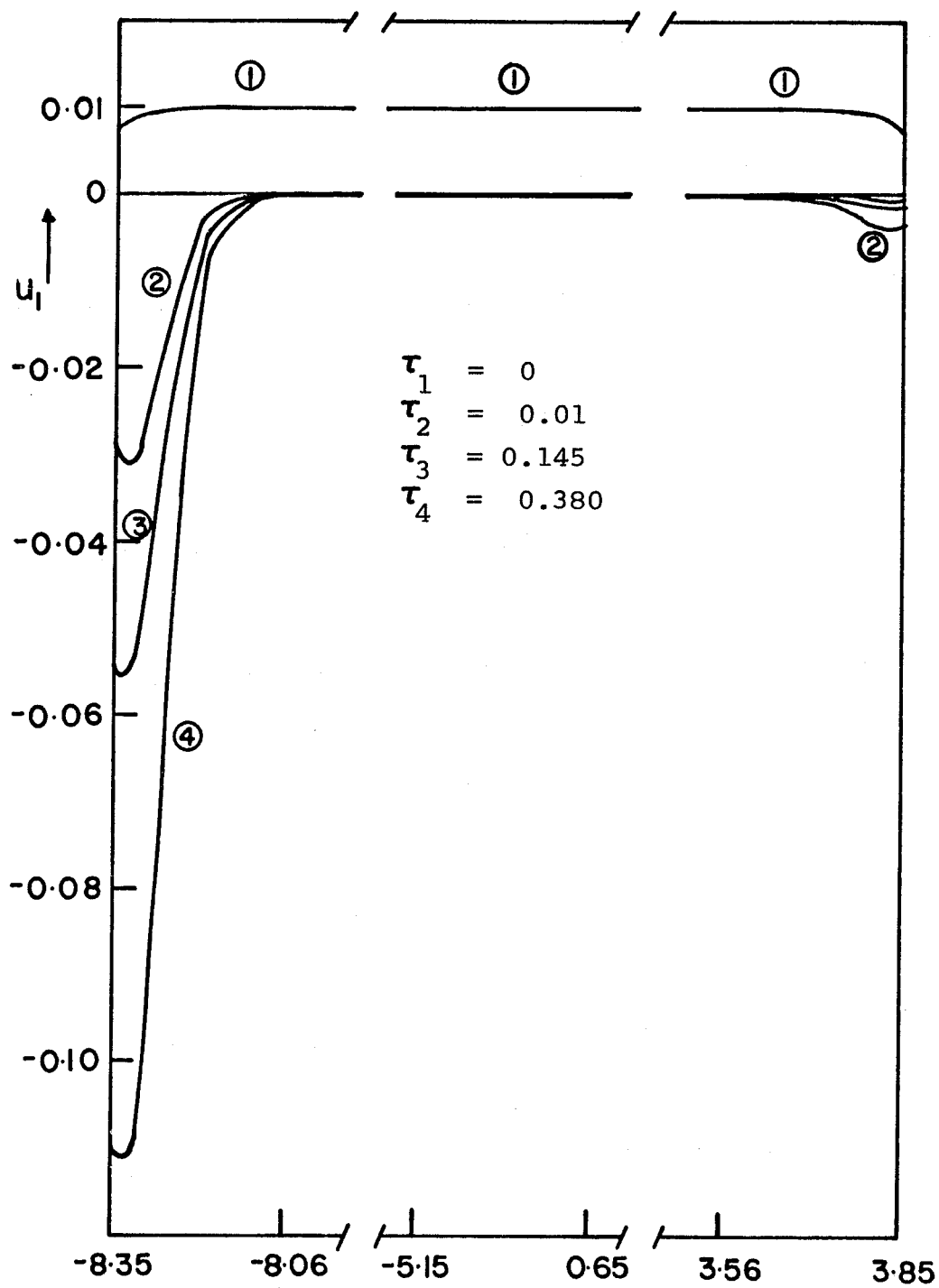


FIGURE 40: Concentration Response $\xi \longrightarrow$ to a Disturbance of the hm Asymmetric Steady State (Point 4, $\alpha_2 = 0.02$)

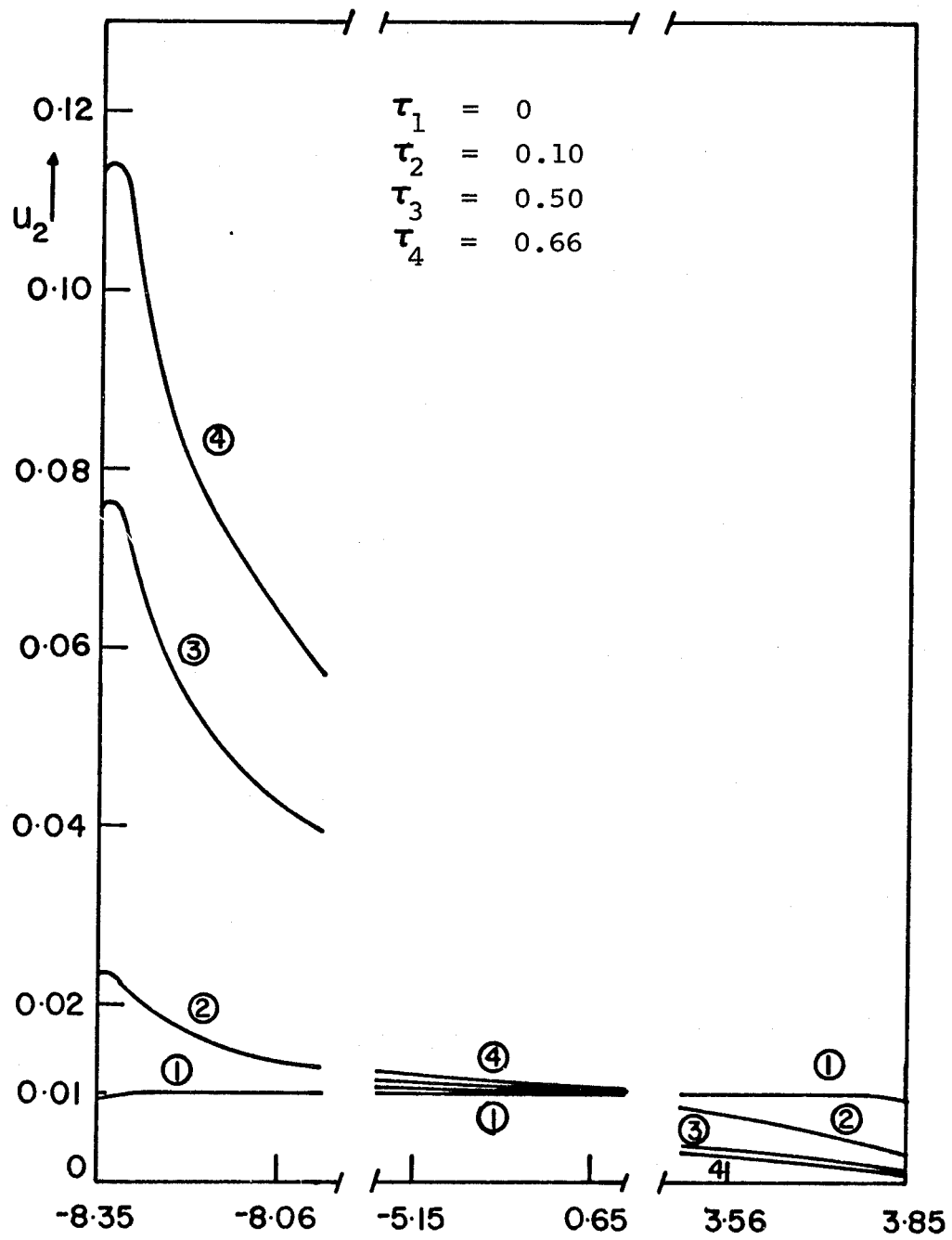


FIGURE 41: Temperature Response $\xi \rightarrow$ to a Disturbance of the hm Asymmetric Steady State (Point 4, $\alpha_2 = 0.02$)

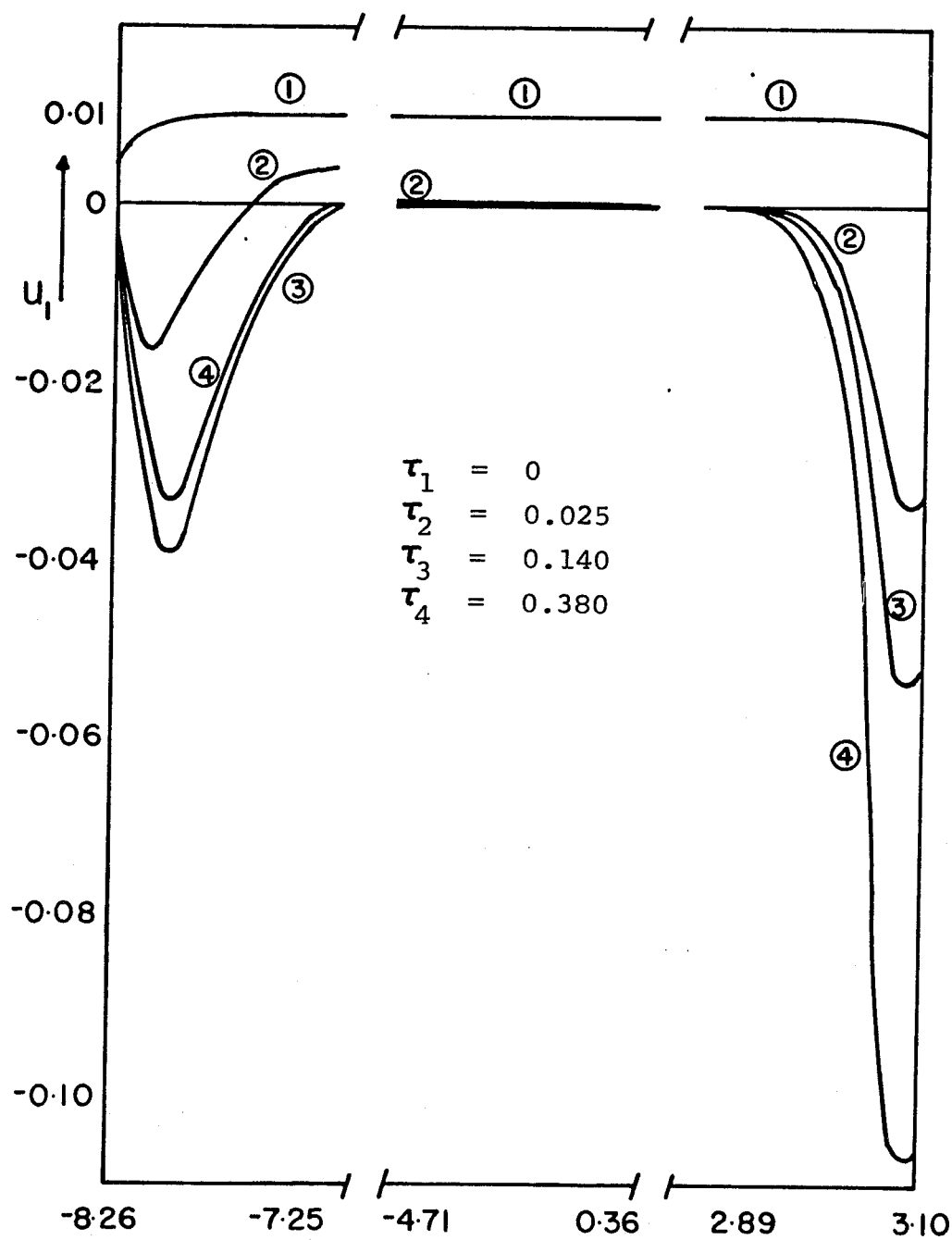


FIGURE 42: Concentration Response $\xi \longrightarrow$
to a Disturbance of the ml Asymmetric
Steady State (Point 1, $\alpha_2 = 0.02$)

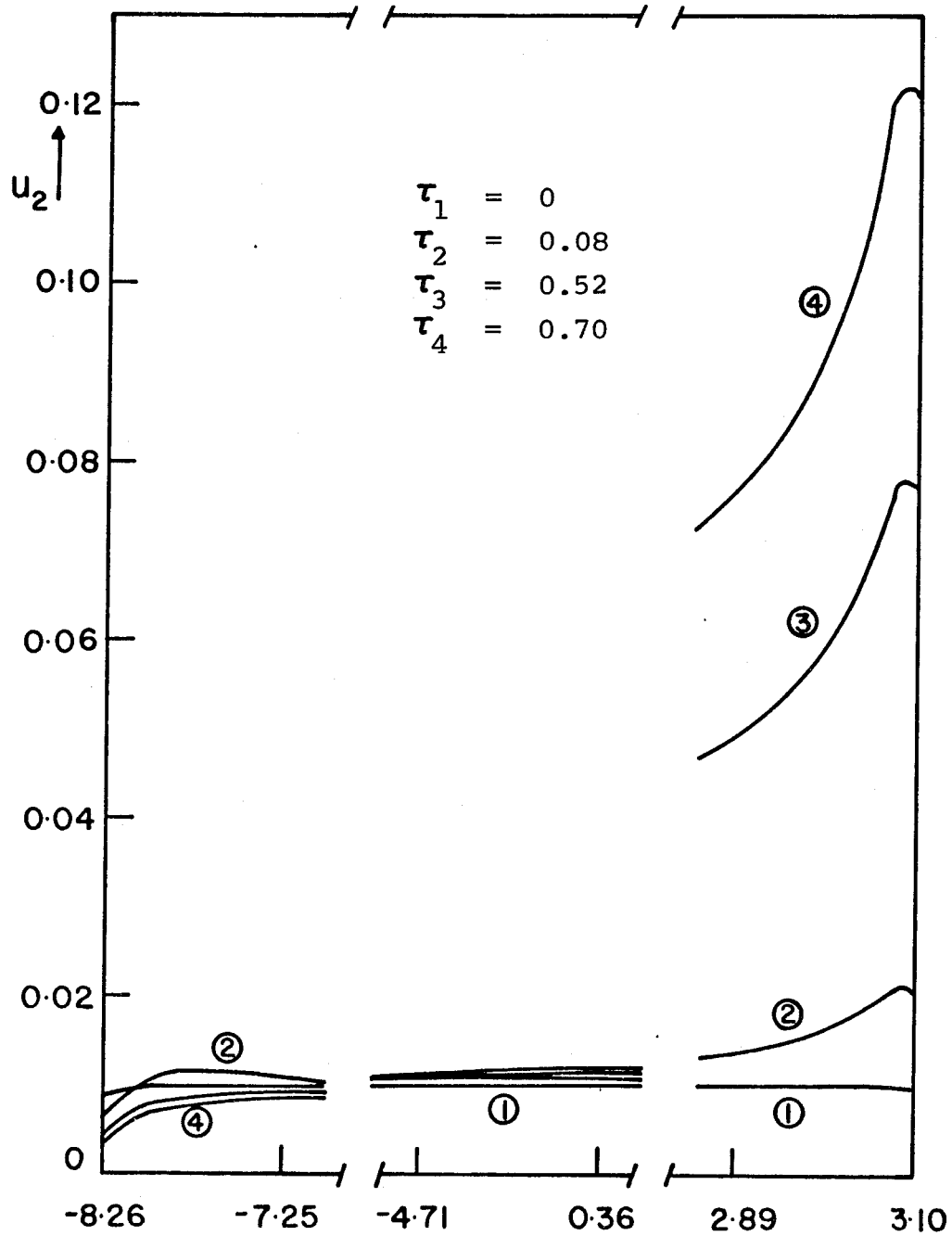


FIGURE 43: Temperature Response ξ to a Disturbance of the m1 Asymmetric Steady State (Point 1, $\alpha_2 = 0.02$)

responses at the ends of the slab more clearly. The behavior of the small positive initial disturbances in time is analogous to that encountered above. Figures 38 and 39 show responses to the disturbances of the high-low steady state that decay in time, while Figures 40 to 43 show responses to the disturbance of the high-medium and medium-low steady states that grow in time.

The machine time required for each set of these transient responses varied from about 15 minutes to 45 minutes on a Burroughs B5500 computer.

Initially, when the changes in u_1 and u_2 were rapid, small time increments $\Delta\tau$ (of the order of 10^{-4}) were used. As the dimensionless time increased, the changes in u_1 and u_2 became less rapid and this permitted larger $\Delta\tau$'s to be used without affecting the accuracy of the numerical solutions. The Crank-Nicolson-Galerkin approximation method used here appears to be very versatile in its ability to approximate the sharp peaks obtained in the concentration responses. The slight drawback of the method is that it is more difficult to program than finite difference methods but the higher order of convergence and the smaller number of grid points required more than offset this difficulty. The method could also be used to solve non-linear parabolic equations by the use of the predictor-corrector approximation as suggested by Douglas and Dupont.¹²

It can thus be concluded that both the high-medium and the medium-low asymmetric steady states are unstable with respect to small perturbations. The high-low steady state was shown to be stable with respect to three different initial disturbances, and it is therefore reasonable to suppose that it is, in fact, a stable steady state.

V. CONCLUSIONS

The results and conclusions stated in the preceding chapter may conveniently be divided into two groups: those related to solutions not invariant under lateral translations, and those related to solutions not invariant under reflection.

Solutions whose symmetry operation is translation parallel to slab faces take the form of standing waves, and exist whenever multiple uniform temperature steady state solutions occur. These have, however, been shown to be unstable against small perturbations for a single exothermic reaction. Frank-Kamenetskii¹⁵ mentions the existence of biological rhythms in living organisms and suggests that this may be connected with periodic chemical processes. He also considers the appearance of self-excited oscillations in industrial systems which involve exothermic chemical processes. In both considerations the possibility of the existence of non-uniform states arises and stable standing waves may exist. In a recent book, Glansdorff and Prigogine¹⁷ discuss systems of complex chemical reactions which describe metabolic processes and demonstrate that symmetric steady states in these systems may become unstable against small perturbations in the form of exponentially growing standing waves. The existence of non-uniform steady states, which they call dissipative space structures, is then assumed.

They speculate that this type of instability might be responsible for the periodic structure of cellular biological material.

The existence of steady states that are asymmetric with respect to reflection across the center plane was demonstrated in an infinite slab of catalyst of finite thickness. A word about the model used is, perhaps, in order. No real slab is infinite in two directions and finite in the third. The only case that can be described by the model is one where four sides of the catalyst are sealed with a chemically inert, perfectly insulating material. The main reason for considering this model is mathematical simplicity.

A complete set of asymmetric steady states in a symmetric catalyst particle is presented. The relations between these asymmetric steady states and the symmetric states are established and new branches that they contribute to the Thiele modulus effectiveness factor plot are mapped for one particular example. The high-medium and medium-low states are shown to be unstable with respect to small perturbations, while there is good indication that the high-low state is stable to small perturbations.

As this is an early work dealing with asymmetric profiles, a small part of the topic has been covered and much work remains to be done. Only the slab type of geometry has been considered. Catalyst particles of cylindrical and spherical geometries are more realistic and the possibility

of asymmetric steady states in these geometries needs to be considered. Methods of estimating lower bounds of slab thicknesses for existence of asymmetric steady state need to be looked at. Systems with finite boundary resistances which can be reduced only to non-self adjoint eigenvalue problems present special difficulties when the question of stability arises, since general theories do not exist for this type of problem. A very important step in the stability analysis of real systems would be to formulate these general theories. In practice, the mass and thermal diffusivities exhibit a temperature dependence and the effect of this on the steady states would be of interest. In this study only unit Lewis number was used and so another area of investigation would be the effect of Lewis number on the stability of the asymmetric steady states. Lee and Luss³⁰ have carried out an extensive numerical study to determine the effect of Lewis number on the stability of the symmetric steady state in a porous catalyst. They discovered some interesting phenomena including the occurrence of a unique unstable steady state with a periodic appearance of a very hot spot during a limit cycle.

The major objectives of this work, which were to demonstrate the existence of asymmetric steady states and to make comments on the stability of these, have been fulfilled. In addition, a Galerkin integration method, which has not been used previously for problems of this type, has been tested and shows much promise.

NOMENCLATURE

a	catalyst slab half-thickness
a_{ij}	$\langle A_{w_i}, w_j \rangle$
A	k_o/α
$A(\xi)$	$(\partial f / \partial z)_e$
$\bar{A}(\xi)$	approximation of $A(\xi)$, defined by Equation (4.69)
b	mass transfer coefficient at wire boundary
b_{ij}	$\langle B_{w_i}, w_j \rangle$
B	$b/\sqrt{k\mu}$
$B(\xi)$	$(\partial f / \partial y)_e$
c	concentration of reactant
c_1	constant defined by Equation (2.16)
c_b	concentration of reactant outside catalyst particle
c_p	specific heat of catalyst slab
C	thermal capacity of wire per unit length
D	effective diffusion coefficient in catalyst slab

E	activation energy
$f(z, y)$	function defined by Equation (4.3)
\bar{f}	$f(\bar{z}, \bar{y})$
$\left(\frac{\partial f}{\partial y}\right)_e$	$\frac{\partial f}{\partial y}(\bar{z}, \bar{y})$
$\left(\frac{\partial f}{\partial z}\right)_e$	$\frac{\partial f}{\partial z}(\bar{z}, \bar{y})$
$F(\theta)$	function defined by Equation (2.8)
G	constant defined by Equation (2.45)
h	space increment
H	$-\left(\frac{dF}{d\bar{\theta}}\right)\bar{\theta} = \theta_2$
I	identity matrix
k	thermal conductivity
k_0	pre-exponential factor in velocity constant
K	effective thermal conductivity in catalyst slab
ℓ	mass transfer coefficient at slab surface
L	length of wire
Le	$\frac{\rho c_p D}{K}$

m	heat transfer coefficient at slab surface
M	defined by Equation (3.30)
\mathcal{M}	subspace spanned by Hermite cubic polynomials
N	defined by Equation (3.28)
p	$\ell / \sqrt{Dk_0 e^{-\gamma}}$
Q	matrix defined by Equation (4.18)
\hat{Q}	$1/2(Q^T + Q)$
r	number of grid points
R	gas constant
s	dimensionless distance = $x \sqrt{\mu / \kappa S}$
s_0	$x_0 \sqrt{\mu / \kappa S}$
s_1	$x_1 \sqrt{\mu / \kappa S}$
S	cross sectional area of wire
S_1	matrix defined by Equation (4.19)
S_2	matrix defined by Equation (4.20)
t	time
T	absolute temperature
T_b	absolute temperature outside catalyst particle

u_1	small perturbation of the steady state dimensionless concentration for the slab problem
u_2	small perturbation of the steady state dimensionless temperature for the slab problem
U	approximation of u_1 defined by Equation (4.31)
\underline{U}	column vector defined by Equation (4.21)
v	auxiliary function defined by Equations (2.41) and (2.42)
V	function defined by Equations (4.20) to (4.25)
w_i	Hermite cubic polynomials defined by Equations (4.28) and (4.29)
W	approximation of u_2 defined by Equation (4.32)
x	co-ordinate measured along wire for the wire problem; co-ordinate normal to slab faces for the slab problem
x_0, x_1	terminal points of Ω
Y	T/T_b
\bar{Y}	steady state dimensionless temperature
z	c/c_b
\bar{z}	steady state dimensionless concentration

Greek Letters

α	mass transfer coefficient per unit length of wire
α_1	integration constant
α_2	integration constant determining asymmetry of solution
$\alpha^i(\tau)$	coefficients defined by Equation (4.31)
α_n^i	$\alpha^i(\tau_n)$
$\underline{\alpha}^n$	column vector defined by Equation (4.89)
β	QDc_b/KT_b
$\beta^i(\tau)$	coefficients defined by Equation (4.32)
β_n^i	$\beta^i(\tau_n)$
γ	E/RT_b
δ_{kij}	$\int_{\xi_0}^{\xi_1} w_k(x) w_i(x) w_j(x) dx$
$\Delta\tau$	time step
ϵ	$E\mu/R\alpha Qc_b$
ϵ_{ij}	$\langle w_i', w_j' \rangle$
ζ_{ij}	$\langle w_i, w_j \rangle$
η	effectiveness factor

η_o, η_1	one-sided effectiveness factor
η_n^i	defined by Equation (4.84)
θ	$T\mu / \alpha_Q c_p$
$\bar{\theta}$	steady state dimensionless temperature
κ	thermal conductivity
λ	Thiele modulus
$\bar{\lambda}$	eigenvalue, defined by Equation (2.37)
μ	heat transfer coefficient per unit length of wire
ξ	$\left(\frac{k_0 e^{-\gamma}}{D} \right)^{\frac{1}{2}} x$
ξ_0	$\left(\frac{k_0 e^{-\gamma}}{D} \right)^{\frac{1}{2}} x_0$
ξ_1	$\left(\frac{k_0 e^{-\gamma}}{D} \right)^{\frac{1}{2}} x_1$
ρ	density of catalyst particle
σ	small perturbation of steady state dimensionless temperature for the wire problem
τ	dimensionless time ($\mu t / C$ for wire problem; $k_0 e^{-\gamma} t$ for slab problem)

τ_n	$n \Delta \tau$
ϕ	$d\bar{\theta}/ds$
ϕ_n^i	defined by Equation (4.83)
$\underline{\phi}^n$	column vector defined by Equation (4.90)
χ_i	defined by Equation (4.71)
ψ	spatial factor of σ
ψ_i	defined by Equation (4.76)
ω	temporal factor of σ
Ω	x interval occupied by catalyst

Mathematical Notation

$\langle \cdot \ , \ \cdot \rangle$	inner product defined by Equation (4.35)
-------------------------------------	--

REFERENCES

1. Amundson, N. R., Canadian J. of Chem. Eng. 43, 49 (1965).
2. Amundson, N. R., and Raymond, L. R., AIChE J. 11, 339 (1965).
3. Bailey, J. E., "Asymmetric States in Porous Catalyst Slabs with Symmetric Non-Uniform Catalytic Activity," Chem. Eng. Science, to be published.
4. Berger, A. J., and Lapidus, L., AIChE J. 14, 558 (1968).
5. Bischoff, K. B., Chem. Eng. Science 22, 525 (1967).
6. Bowdler, H. J., Martin, R. S., Peters, G. and Wilkinson, J. H., Numer. Math. 8, 217 (1966).
7. Collatz, L., "The Numerical Treatment of Differential Equations," 3rd edition, Springer-Verlag, Berlin (1960).
8. Copelowitz, I., and Aris, R., Chem. Eng. Science 25, 906 (1970).
9. Courant, R., and Hilbert, D., "Methods of Mathematical Physics," Vol. 1, Interscience, New York (1953).
10. Cresswell, D. L., Chem. Eng. Science 25, 267 (1970).
11. Douglas, J., Jr., unpublished notes on "Modern Treatment of Non-Linear Transient Problems," May, 1971.
12. Douglas, J., Jr., and Dupont, T., SIAM J. Numer. Anal. 7, 575 (1970).
13. Drott, D. W., and Aris, R., Chem. Eng. Science 24, 541 (1969).
14. Erwin, M. A., and Luss, D., Chem. Eng. Science, 27, 315 (1972).
15. Frank-Kamenetskii, D. A., "Diffusion and Heat Transfer in Chemical Kinetics," 2nd edition, Plenum Press (1969).
16. Gavalas, G. R., Chem. Eng. Science 21, 477 (1966).

17. Glansdorff, P., and Prigogine, I., "Thermodynamic Theory of Structure, Stability and Fluctuations," Wiley-Interscience (1971).
18. Hatfield, B., and Aris, R., Chem. Eng. Science 24, 1213 (1969).
19. Henrici, P., "Discrete Variable Methods in Ordinary Differential Equations," Wiley and Sons (1962).
20. Hlavacek, V., and Marek, M., Chem. Eng. Science 23, 865 (1968).
21. Hlavacek, V., Marek, M., and Kubicek, M., Chem. Eng. Science 23, 1083 (1968).
22. Horn, F. J. M., Jackson, R., Martel, E., and Patel, C., Chem. Eng. J. 1, 79 (1970).
23. Ince, E. L., "Ordinary Differential Equations," Dover (1956).
24. Jackson R., "Some Uniqueness Conditions for the Steady State of a Catalyst Particle with Surface Resistances," to be published in Chem. Eng. Science.
25. Jackson, R., "The Stability of Standing Waves on a Catalytic Wire," to be published in Chem. Eng. Science.
26. Jackson, R., and Horn, F. J. M., "Necessary Conditions for the Existence of Asymmetric Composition and Temperature Profiles in Catalyst Pellets," to be published in Chem. Eng. J.
27. Kantorovich, L. A., and Krylov, V. D., "Approximate Methods of Higher Analysis," Interscience Inc., New York (1958).
28. Kuo, J. C. W., and Amundson, N. R., Chem. Eng. Science 22, 1185 (1967).
29. Lance, G. N., "Numerical Methods for High Speed Computers," Iliffe and Sons, London (1960).
30. Lee, J. C. M., and Luss, D., AIChE J. 16, 620 (1970).
31. Luss, D., Chem. Eng. Science 23, 1249 (1968).
32. Luss, D., and Amundson, N. R., Canadian J. of Chem. Eng. 45, 341 (1967).

33. Luss, D., and Amundson, N. R., Chem. Eng. Science 22, 253 (1967).
34. Luss, D., and Lee, J. C. M., Chem. Eng. Science 23, 1237 (1968).
35. Martin, R. S., and Wilkinson, J. H., Numer. Math. 9, 279 (1967).
36. McGreavy, C., and Cresswell, D. L., Chem. Eng. Science 24, 608 (1968).
37. McGreavy, C., and Cresswell, D. L., Canadian J. of Chem. Eng. 47, 583 (1969).
38. Mercer, M. C., and Aris, R., Lat. Amer. J. of Chem Eng. and Appl. Chem. 2, 149 (1971).
39. Nishimura, Y., and Matsubara, M., Chem. Eng. Science 24, 1427 (1969).
40. Patel, C., and Jackson, R., "Asymmetric Steady States of a Catalyst Particle in a Uniform Environment," to be presented at the 5th European Symposium on Reaction Engineering, Amsterdam, May, 1972.
41. Pis'men, L. M., and Kharkats, Yu I., Dokl. Acad. Nauk. SSSR. 178, 901 (1968).
42. Rachford, H. H., Private Communication, September, 1971.
43. Roberts, G. W., and Satterfield, C. N., I & EC Fund. 5, 317 (1966).
44. Sagan, H., "Boundary and Eigenvalue Problems in Mathematical Physics," Wiley (1961).
45. Wei, J., Chem. Eng. Science 20, 729 (1965).
46. Weisz, P. B., and Hicks, J. S., Chem. Eng. Science 17, 265 (1962).
47. Wheeler, M., Ph.D. Dissertation, Rice University, Houston, Texas (1971).

APPENDIX I

INTEGRALS INVOLVING THE HERMITE CUBIC POLYNOMIALS

$$\zeta_{ij} = \langle w_i, w_j \rangle = \int_{\xi_0}^{\xi_1} w_i(x) w_j(x) dx \quad (A.1)$$

For each i , ζ_{ij} has at most six non-zero elements. Note that $\zeta_{ij} = \zeta_{ji}$.

The non-zero elements are tabulated below, where r is the number of grid points.

(i,j)	ζ_{ij}	(i,j)	ζ_{ij}
1,1	$13h/35$	$2r-1, 2r-3$	$9h/70$
1,2	$11h^2/210$	$2r-1, 2r-2$	$13h^2/420$
1,3	$9h/70$	$2r-1, 2r-1$	$13h/35$
1,4	$-13h^2/420$	$2r-1, 2r$	$-11h^2/210$
2,1	$11h^2/210$	$2r, 2r-3$	$-13h^2/420$
2,2	$h^3/105$	$2r, 2r-2$	$-h^3/140$
2,3	$13h^2/420$	$2r, 2r-1$	$-11h^2/210$
2,4	$-h^3/140$	$2r, 2r$	$h^3/105$

The other non-zero elements can be expressed in terms of the above integrals and are evaluated by the use of the following relations:

$$\zeta_{2i-1,2i-3} = \zeta_{2r-1,2r-3} \quad (\text{A.2})$$

$$\zeta_{2i-1,2i-2} = \zeta_{2r-1,2r-2} \quad (\text{A.3})$$

$$\zeta_{2i-1,2i-1} = \zeta_{2r-1,2r-1} + \zeta_{11} \quad (\text{A.4})$$

$$\zeta_{2i-1,2i} = \zeta_{2r-1,2r} + \zeta_{12} \quad (\text{A.5})$$

$$\zeta_{2i-1,2i+1} = \zeta_{13} \quad (\text{A.6})$$

$$\zeta_{2i-1,2i+2} = \zeta_{14} \quad (\text{A.7})$$

$$\zeta_{2i,2i-3} = \zeta_{2r,2r-3} \quad (\text{A.8})$$

$$\zeta_{2i,2i-2} = \zeta_{2r,2r-2} \quad (\text{A.9})$$

$$\zeta_{2i,2i-1} = \zeta_{2r,2r-1} + \zeta_{21} \quad (\text{A.10})$$

$$\zeta_{2i,2i} = \zeta_{2r,2r} + \zeta_{22} \quad (\text{A.11})$$

$$\zeta_{2i,2i+1} = \zeta_{23} \quad (\text{A.12})$$

$$\zeta_{2i,2i+2} = \zeta_{24} \quad (\text{A.13})$$

The relations (A.2) to (A.13) are valid for $i=2,3,\dots,r-1$.

$$\epsilon_{ij} = \left\langle \frac{dw_i}{dx}, \frac{dw_j}{dx} \right\rangle = \int_{\xi_0}^{\xi_1} \frac{dw_i}{dx} \frac{dw_j}{dx} dx \quad (\text{A.14})$$

For each i , ϵ_{ij} also has at most six non-zero elements.

Also, $\epsilon_{ij} = \epsilon_{ji}$. The non-zero ϵ_{ij} are tabulated below.

(i,j)	ϵ_{ij}	(i,j)	ϵ_{ij}
1,1	6/5h	2r-1,2r-3	-6/5h
1,2	1/10	2r-1,2r-2	-1/10
1,3	-6/5h	2r-1,2r-1	6/5h
1,4	1/10	2r-1,2r	-1/10
2,1	1/10	2r,2r-3	1/10
2,2	2h/15	2r,2r-2	-h/30
2,3	-1/10	2r,2r-1	-1/10
2,4	-h/30	2r,2r	2h/15

$$\epsilon_{2i-1,2i-3} = \epsilon_{2r-1,2r-3} \quad (\text{A.15})$$

$$\epsilon_{2i-1,2i-2} = \epsilon_{2r-1,2r-2} \quad (\text{A.16})$$

$$\epsilon_{2i-1,2i-1} = \epsilon_{2r-1,2r-1} + \epsilon_{11} \quad (\text{A.17})$$

$$\epsilon_{2i-1,2i} = \epsilon_{2r-1,2r} + \epsilon_{12} \quad (\text{A.18})$$

$$\epsilon_{2i-1,2i+1} = \epsilon_{13} \quad (\text{A.19})$$

$$\epsilon_{2i-1,2i+2} = \epsilon_{14} \quad (\text{A.20})$$

$$\epsilon_{2i,2i-3} = \epsilon_{2r,2r-3} \quad (\text{A.21})$$

$$\epsilon_{2i,2i-2} = \epsilon_{2r,2r-2} \quad (\text{A.22})$$

$$\epsilon_{2i,2i-1} = \epsilon_{2r,2r-1} + \epsilon_{21} \quad (\text{A.23})$$

$$\epsilon_{2i,2i} = \epsilon_{2r,2r} + \epsilon_{22} \quad (\text{A.24})$$

$$\epsilon_{2i,2i+1} = \epsilon_{23} \quad (\text{A.25})$$

$$\epsilon_{2i,2i+2} = \epsilon_{24} \quad (\text{A.26})$$

The relations (A.15) to (A.26) are valid for $i=2,3,\dots,r-1$.

$$\delta_{kij} = \int_{\xi_0}^{\xi_1} w_k(x) w_i(x) w_j(x) dx \quad (\text{A.27})$$

For each (i,j) , δ_{kij} has at least six non-zero elements. These are tabulated below, where r is the number of grid points.

(i,j)	k	δ_{kij}
1,1	1	$43h/140$
1,1	2	$97h^2/2520$
1,1	3	$9h/140$
1,1	4	$-43h^2/2520$
1,2	1	$97h^2/2520$
1,2	2	$2h^3/315$
1,2	3	$h^2/72$
1,2	4	$-h^3/280$
1,3	1	$9h/140$
1,3	2	$h^2/72$
1,3	3	$9h/140$
1,3	4	$-h^2/72$

(i, j)	k	δ_{kij}
1,4	1	$-43h^2/2520$
1,4	2	$-h^3/280$
1,4	3	$-h^2/72$
1,4	4	$h^3/315$
2,1	1	$97h^2/2520$
2,1	2	$2h^3/315$
2,1	3	$h^2/72$
2,1	4	$-h^3/280$
2,2	1	$2h^3/315$
2,2	2	$h^4/840$
2,2	3	$h^3/315$
2,2	4	$-h^4/1260$
2,3	1	$h^2/72$
2,3	2	$h^3/315$
2,3	3	$43h^2/2520$
2,3	4	$-h^3/280$
2,4	1	$-h^3/280$
2,4	2	$-h^4/1260$
2,4	3	$-h^3/280$
2,4	4	$h^4/1260$
2r-1,2r-3	2r-3	$9h/140$
2r-1,2r-3	2r-2	$h^2/72$
2r-1,2r-3	2r-1	$9h/140$
2r-1,2r-3	2r	$-h^2/72$
2r-1,2r-2	2r-3	$h^2/72$
2r-1,2r-2	2r-2	$h^3/315$
2r-1,2r-2	2r-1	$43h^2/2520$
2r-1,2r-2	2r	$-h^3/280$

(i, j)	k	δ_{kij}
$2r-1, 2r-1$	$2r-3$	$9h/140$
$2r-1, 2r-1$	$2r-2$	$43h^2/2520$
$2r-1, 2r-1$	$2r-1$	$43h/140$
$2r-1, 2r-1$	$2r$	$-97h^2/2520$
$2r-1, 2r$	$2r-3$	$-h^2/72$
$2r-1, 2r$	$2r-2$	$-h^3/280$
$2r-1, 2r$	$2r-1$	$-97h^2/2520$
$2r-1, 2r$	$2r$	$2h^3/315$
$2r, 2r-3$	$2r-3$	$-43h^2/2520$
$2r, 2r-3$	$2r-2$	$-h^3/280$
$2r, 2r-3$	$2r-1$	$-h^2/72$
$2r, 2r-3$	$2r$	$h^3/315$
$2r, 2r-2$	$2r-3$	$-h^3/280$
$2r, 2r-2$	$2r-2$	$-h^4/1260$
$2r, 2r-2$	$2r-1$	$-h^3/280$
$2r, 2r-2$	$2r$	$h^4/1260$
$2r, 2r-1$	$2r-3$	$-h^2/72$
$2r, 2r-1$	$2r-2$	$-h^3/280$
$2r, 2r-1$	$2r-1$	$-97h^2/2520$
$2r, 2r-1$	$2r$	$2h^3/315$
$2r, 2r$	$2r-3$	$h^3/315$
$2r, 2r$	$2r-2$	$h^4/1260$
$2r, 2r$	$2r-1$	$2h^3/315$
$2r, 2r$	$2r$	$-h^4/840$

The other non-zero δ_{kij} can be evaluated from the above using the following equations

$$\delta_{2i-3,2i-1,2i-3} = \delta_{2r-3,2r-1,2r-3} \quad (\text{A.28})$$

$$\delta_{2i-2,2i-1,2i-3} = \delta_{2r-2,2r-1,2r-3} \quad (\text{A.29})$$

$$\delta_{2i-1,2i-1,2i-3} = \delta_{2r-1,2r-1,2r-3} \quad (\text{A.30})$$

$$\delta_{2i,2i-1,2i-3} = \delta_{2r,2r-1,2r-3} \quad (\text{A.31})$$

$$\delta_{2i-3,2i-1,2i-2} = \delta_{2r-3,2r-1,2r-2} \quad (\text{A.32})$$

$$\delta_{2i-2,2i-1,2i-2} = \delta_{2r-2,2r-1,2r-2} \quad (\text{A.33})$$

$$\delta_{2i-1,2i-1,2i-2} = \delta_{2r-1,2r-1,2r-2} \quad (\text{A.34})$$

$$\delta_{2i,2i-1,2i-2} = \delta_{2r,2r-1,2r-2} \quad (\text{A.35})$$

$$\delta_{2i-3,2i-1,2i-1} = \delta_{2r-3,2r-1,2r-1} \quad (\text{A.36})$$

$$\delta_{2i-2,2i-1,2i-1} = \delta_{2r-2,2r-1,2r-1} \quad (\text{A.37})$$

$$\delta_{2i-1,2i-1,2i-1} = \delta_{2r-1,2r-1,2r-1} + \delta_{111} \quad (\text{A.38})$$

$$\delta_{2i,2i-1,2i-1} = \delta_{2r,2r-1,2r-1} + \delta_{211} \quad (\text{A.39})$$

$$\delta_{2i+1,2i-1,2i-1} = \delta_{311} \quad (\text{A.40})$$

$$\delta_{2i+2,2i-1,2i-1} = \delta_{411} \quad (\text{A.41})$$

$$\delta_{2i-3,2i-1,2i} = \delta_{2r-3,2r-1,2r} \quad (\text{A.42})$$

$$\delta_{2i-2,2i-1,2i} = \delta_{2r-2,2r-1,2r} \quad (\text{A.43})$$

$$\delta_{2i-1,2i-1,2i} = \delta_{2r-1,2r-1,2r} + \delta_{112} \quad (\text{A.44})$$

$$\delta_{2i,2i-1,2i} = \delta_{2r,2r-1,2r} + \delta_{212} \quad (\text{A.45})$$

$$\delta_{2i+1,2i-1,2i} = \delta_{312} \quad (\text{A.46})$$

$$\delta_{2i+2,2i-1,2i} = \delta_{412} \quad (\text{A.47})$$

$$\delta_{2i-1,2i-1,2i+1} = \delta_{113} \quad (\text{A.48})$$

$$\delta_{2i,2i-1,2i+1} = \delta_{213} \quad (\text{A.49})$$

$$\delta_{2i+1,2i-1,2i+1} = \delta_{313} \quad (\text{A.50})$$

$$\delta_{2i+2,2i-1,2i+1} = \delta_{413} \quad (\text{A.51})$$

$$\delta_{2i-1,2i-1,2i+2} = \delta_{114} \quad (\text{A.52})$$

$$\delta_{2i,2i-1,2i+2} = \delta_{214} \quad (\text{A.53})$$

$$\delta_{2i+1,2i-1,2i+2} = \delta_{314} \quad (\text{A.54})$$

$$\delta_{2i+2,2i-1,2i+2} = \delta_{414} \quad (\text{A.55})$$

$$\delta_{2i-3,2i,2i-3} = \delta_{2r-3,2r,2r-3} \quad (\text{A.56})$$

$$\delta_{2i-2,2i,2i-3} = \delta_{2r-2,2r,2r-3} \quad (\text{A.57})$$

$$\delta_{2i-1,2i,2i-3} = \delta_{2r-1,2r,2r-3} \quad (\text{A.58})$$

$$\delta_{2i,2i,2i-3} = \delta_{2r,2r,2r-3} \quad (\text{A.59})$$

$$\delta_{2i-3,2i,2i-2} = \delta_{2r-3,2r,2r-2} \quad (\text{A.60})$$

$$\delta_{2i-2,2i,2i-2} = \delta_{2r-2,2r,2r-2} \quad (\text{A.61})$$

$$\delta_{2i-1,2i,2i-2} = \delta_{2r-1,2r,2r-2} \quad (\text{A.62})$$

$$\delta_{2i,2i,2i-2} = \delta_{2r,2r,2r-2} \quad (\text{A.63})$$

$$\delta_{2i-3,2i,2i-1} = \delta_{2r-3,2r,2r-1} \quad (\text{A.64})$$

$$\delta_{2i-2,2i,2i-1} = \delta_{2r-2,2r,2r-1} \quad (\text{A.65})$$

$$\delta_{2i-1,2i,2i-1} = \delta_{2r-1,2r,2r-1} + \delta_{121} \quad (\text{A.66})$$

$$\delta_{2i,2i,2i-1} = \delta_{2r,2r,2r-1} + \delta_{221} \quad (\text{A.67})$$

$$\delta_{2i+1,2i,2i-1} = \delta_{321} \quad (\text{A.68})$$

$$\delta_{2i+2,2i,2i-1} = \delta_{421} \quad (\text{A.69})$$

$$\delta_{2i-3,2i,2i} = \delta_{2r-3,2r,2r} \quad (\text{A.70})$$

$$\delta_{2i-2,2i,2i} = \delta_{2r-2,2r,2r} \quad (\text{A.71})$$

$$\delta_{2i-1,2i,2i} = \delta_{2r-1,2r,2r} + \delta_{122} \quad (\text{A.72})$$

$$\delta_{2i,2i,2i} = \delta_{2r,2r,2r} + \delta_{222} \quad (\text{A.73})$$

$$\delta_{2i+1,2i,2i} = \delta_{322} \quad (\text{A.74})$$

$$\delta_{2i+2,2i,2i} = \delta_{422} \quad (\text{A.75})$$

$$\delta_{2i-1,2i,2i+1} = \delta_{123} \quad (\text{A.76})$$

$$\delta_{2i,2i,2i+1} = \delta_{223} \quad (\text{A.77})$$

$$\delta_{2i+1,2i,2i+1} = \delta_{323} \quad (\text{A.78})$$

$$\delta_{2i+2,2i,2i+1} = \delta_{423} \quad (\text{A.79})$$

$$\delta_{2i-1,2i,2i+2} = \delta_{124} \quad (\text{A.80})$$

$$\delta_{2i,2i,2i+2} = \delta_{224} \quad (\text{A.81})$$

$$\delta_{2i+1,2i,2i+2} = \delta_{324} \quad (\text{A.82})$$

$$\delta_{2i+2,2i,2i+2} = \delta_{424} \quad (\text{A.83})$$

APPENDIX II

SPACE GRIDS FOR TRANSIENT PROBLEM

Steady State	Step Size		
	First Four Steps	Intermediate Four Steps	Final Four Steps
low symmetric	h	6h	h
medium symmetric	h	8h	h
high symmetric	h	8h	h
ml; $\alpha_2 = 0.09$	h	6h	h
hm; $\alpha_2 = 0.09$	h	6h	h
hl; $\alpha_2 = 0.09$	h	6h	h
ml; $\alpha_2 = 0.02$	h	10h	h/5
hm; $\alpha_2 = 0.02$	h	40h	h
hl; $\alpha_2 = 0.02$	h	20h	h